An Abstract for the Thesis of

Darren L. Williams for the degree of Doctor of Philosophy in Chemistry presented on July 28, 1997.

Title: **High Resolution Infrared and *Ab Initio* Studies of Aluminum and Beryllium Borohydrides**

Abstract approved: Redacted for Privacy

Joseph W. Nibler

Methods for using *ab initio* calculations as an aid in experimental physical chemistry were implemented in the undergraduate chemistry curriculum at Oregon State University and published in the *Journal of Chemical Education*, Volume 73, 1996, 608-611. Similar calculations were used in our analysis of the spectral data obtained for aluminum and beryllium borohydride.

High resolution spectra of $Al(BH_4)_3$, $Al(BD_4)_3$, and $Be(BH_4)_2$ were recorded for low pressure samples at 300 K using FTIR spectroscopy (0.01 cm^{-1} to 0.0015 cm^{-1} resolution). Tunable infrared diode laser spectra (0.001 cm^{-1} resolution) of the BH bridge stretching regions and the BH_2 deformation region are also presented for $Al(BH_4)_3$ samples cooled to ~10 K in a multi-pass, slit expansion apparatus. Both room temperature and 10 K spectra show much more congestion than predicted by non-rigid rotor simulations. In $Al(BH_4)_3$, the potential energy surface for the relevant conrotary torsional coordinate is examined at the CCSD/6-311G**//MP2/6-311G** level, yielding a prismatic barrier height of 490 cm^{-1} and v=0 and 1 level splittings of 0.052 and 2.7 cm^{-1} respectively. The same treatment for the three-fold torsion of the D_{3d} structure of $Be(BH_4)_2$ yields a barrier height of 680 cm^{-1} and v=0 and 1 level splittings of 0.0001 cm^{-1} and 0.005 cm^{-1} respectively.

Resolved vibration rotational lines were observed only in the $Be(BH_4)_2$ jet spectra, and a list of the 1246 spectral lines measured in 7.7 cm^{-1} of the BH bridge stretch region is included. Two band assignments ($^RQ_0$ and $^RQ_1$) were proposed, giving $\nu(K=0) = 2194.55715(60)$ and $\alpha_B = -0.000938(13)$ cm^{-1} and $\nu(K=1) = 2197.2648(15)$ cm^{-1} and $\alpha_B = -0.000819(36)$ cm^{-1}, respectively. The K differences between the bands gave a separation $\nu_{sub} = 2.7074(8)$ cm^{-1} and a centrifugal distortion constant $D_{JK}'' = 0.000066(9)$ cm^{-1}. This sub-band separation, combined with the *ab initio* D_{3d} geometry, was used to deduce coriolis coupling constant and band origin values of $\zeta = 0.291$ and $\nu_0 = 2193.8$ cm^{-1}. The *ab initio* energetics of the low energy forms of $Be(BH_4)_2$ is also discussed. For both $Al(BH_4)_3$ and $Be(BH_4)_2$ the extreme spectral congestion is attributed to level splittings due to BH_4 torsional and tumbling motions.

High Resolution Infrared and *Ab Initio* Studies of Aluminum and Beryllium Borohydrides

by

Darren L. Williams

A THESIS
submitted to
Oregon State University

in partial fulfillment of
the requirements for the
degree of

Doctor of Philosophy

Presented July 28, 1997
Commencement June 1998

Doctor of Philosophy thesis of Darren L. Williams presented on July 28, 1997

APPROVED:

Redacted for Privacy

Major Professor, representing Chemistry

Redacted for Privacy

Chair of Department of Chemistry

Redacted for Privacy

Dean of Graduate School

I understand that my thesis will become part of the permanent collection of Oregon State University libraries. My signature below authorizes release of my thesis to any reader upon request.

Redacted for Privacy

Darren L. Williams, Author

Acknowledgments

Thanks must first and foremost go to God for bringing me here and guiding me through via Proverbs 3:5 and 6. Jennifer's encouragement and character (Proverbs 31:10-31) was a source of strength and purpose, also. These two, in addition to my family, have always been there reminding me that the time of celebration would come soon enough. It is here and the sense of accomplishment has little to do with science.

Two professors stand out in my experience as examples of integrity in teaching and research. They are Dr. Joe Nibler and Dr. Glen Evans. Both have shown a desire to do their best in everything while keeping a keen sense of humor. They also took the time to talk about life. They made chemistry human, and I will endeavor to do the same.

The friends one makes in graduate school are special, and there could scarcely be a stronger bond than that between me and all those who worked in the Asymmetric Nibler Group. Science only made us colleagues; it was the tests, trials, and trips that made us friends.

Contribution of Authors

Dr. J. W. Nibler was involved in the design, analysis, and writing of each manuscript. Dr. Phil Minarik was responsible for some of the *ab initio* calculations in chapter 1 done on the Pentium platform. A great deal of the background of borohydrides was compiled by Dr. Abdullah Al-Kahtani as well as the initial analyses of the FTIR spectra in each manuscript. The initial FTIR results were published in his thesis along with the NMR of $Be(BH_4)_2$. All of the high resolution spectra were obtained at Pacific Northwest Laboratories in collaboration with Dr. Steve W. Sharpe.

Table of Contents

Table of Contents (Continued)

List of Figures

List of Tables

List of Appendix Figures

High Resolution Infrared and *Ab Initio* Studies of Aluminum and Beryllium Borohydrides

1. Overview

1.1 Computational Chemistry

The past five years have seen great changes in the way computational chemistry is done. In 1992 when I arrived at OSU, I was given a university mainframe account and a stack of white papers on how to use it to do chemistry. There was a long learning curve associated with doing *ab initio* calculations on UNIX workstations that had nothing to do with chemistry. This technical learning curve has nearly disappeared with the arrival of Windows versions of electronic structure calculation packages . This was evidenced by the addition of various exercises to the undergraduate curriculum three years ago where the students calculated various parameters of molecules that they had analyzed experimentally. As teaching assistant, I had the primary responsibility for the development of these exercises and chapter two contains a note published in the *Journal of Chemical Education* describing this implementation of computational chemistry in the senior integrated laboratory here at OSU. It is included in chapter two of this thesis because the same methods were applied to the work in chapters three and four.

More and more scientists are using fast, inexpensive PCs to do research-level *ab initio* calculations that until recently were only feasible on supercomputers. Such is the case for the aluminum and beryllium borohydride computations reported in chapter three and four. Some of the initial results were obtained on the university computing services platform, but the majority of the *ab initio* calculations were done on a PC. These calculations were used extensively in our attempts to understand, interpret, and predict the spectral data obtained for the borohydrides.

1.2 High Resolution Infrared Spectroscopy

We have utilized the highest resolution available in our use of a six-meter FTIR spectrometer (0.002 cm^{-1}) and infrared diode laser sources (0.001 cm^{-1}). This resolution allows one to see the complex vibration rotational structure in molecules, yielding the most accurate structural information obtainable. Metal borohydrides have been studied extensively by spectroscopists because they are relatively easy to synthesize, they are volatile, and they have novel three-center two-electron bonds that show a variety of coordination. Their structural determination has been difficult and here we report two of the toughest

cases—aluminum and beryllium borohydride. The format used is that intended for submission for publication. In addition, some programming details and an extensive compilation of spectral line positions for $Be(BH_4)_2$ are included as appendices.

2. PC Calculations Using Gaussian for Windows - a Complement to Laboratory Measurements on HCl

Darren L. Williams, Philip R. Minarik, and Joseph W. Nibler
Department of Chemistry
Oregon State University
Corvallis, OR 97331

Published in the *Journal of Chemical Education*,
Volume 73, Number 7, July 1996, 608-611.

2. PC Calculations Using Gaussian for Windows - a Complement to Laboratory Measurements on HCl

2.1 Introduction

Several articles in this Computer Series have illustrated the increasingly important role of computational chemistry in the undergraduate curriculum. For example, Pietro recently described the use of the program SPARTAN on a workstation to compute at the semiempirical AM1 level solvation effects on the deprotonation of nitromethane[1]. Duke and O'Leary have discussed *ab initio* calculations on molecular hydrogen using the program Gaussian on a microVAX computer[2] and give explicit examples of the input statements necessary to run this program for a range of basis sets. Further examples of chemical applications of Gaussian are contained in the books by Foresman and Frisch[3] and by Hehre et al.[4].

The increased speed and memory capabilities of desktop PC's and the availability of sophisticated PC software at reasonable cost now allow even broader use of quantum mechanical programs. The purpose of this note is to show an application of the Gaussian for Windows program to a calculation of the structural and electronic properties of the diatomic molecule HCl. This molecule is particularly relevant to most physical chemistry laboratory courses, since these commonly include an experiment in which the vibrational-rotational infrared spectra of HCl and DCl are analyzed to obtain vibrational frequencies and the bond length[5]. In addition, experiments are often done on HCl to obtain the dipole moment from a dielectric constant measurement and the polarizability from a refractive index measurement using a simple interferometer and a helium neon laser[5,6]. We have found that a combination of these measurements with a theoretical calculation of the same quantities using Gaussian works exceptionally well in illustrating the strengths (and weaknesses) of *ab initio* computations. The direct relation to laboratory measurements heightens the student interest and motivation to learn more about the "innards" of the calculation. The fact that the exercise can now be done in reasonable times on local PC computers with which students are familiar (rather than on a remote mainframe computer or expensive work station) makes the experience even more meaningful.

These calculations were done as a group student project this past year in our Junior / Senior integrated laboratory sequence at Oregon State University. The students synthesized DCl and analyzed its spectrum and combined the results with a similar analysis of HCl to obtain the equilibrium structural parameters R_e and w_e. The analysis also gave the anharmonicity parameter w_ex_e, from which an estimate of the bond dissociation energy was made ($D_e = ¼\ w_e^2/w_ex_e$). Separate dielectric constant and refractive index measurements on HCl gave the dipole moment m and the mean polarizability a_o. Although the latter quantities are really averages over a thermal distribution of states, rather than the equilibrium

values obtained in the theoretical calculations, this difference is small and can be ignored in making comparisons.

Fifteen different calculations (table 1.1) were done to explore possible improvement in calculated values of R_e, ω_e, μ_e, and α_o as the basis set size and level of the calculation were increased. The notation used for the Gaussian basis sets is "standard" and is defined in references 3 and 4. Briefly, the terminology STO-3G for the minimal basis set means that each of the hydrogenic Slater Type Orbitals (1s, 2s, $2p_x$, etc) is replaced by 3 gaussian functions. The latter have the advantage that the many integrations necessary in calculating molecular properties are done much faster for gaussian functions of the form $\exp(-r^2)$ than is the case for Slater type orbitals of the form $\exp(-r)$.

Table 2.1: Gaussian 92 times (hours) to calculate R_e, ω_e, μ_e, and α_o for HCl.

Basis Set	Comments	# Func-tions	Level of Calculation HF	MP2	MP3	QCISD(T)
STO-3G	Single zeta orbitals	10	0.4			
3-21G	Double zeta orbitals	15	15	0.4		
6-31G(d) 6-31G*	Adds d polarization to Cl	21	0.9	1.1		
6-311G(d,p) 6-311G**	Triple zeta, adds p polarization to H	32	1.5	2.9	2.5	
6-311+ G(2d,2p)	More polarization, diffuse Cl orbitals	44	2.8	5.6	3.9	15.5
6-311++ G(3df,3pd)	More polarization, diffuse Cl, H orbitals	65	8.7	33.8	11.9	74.7

To obtain an improved representation of the size of the electron distribution in the valence (outermost) orbitals, additional gaussians with a different effective charge (zeta) can be added. The 3-21G notation indicates 2 zeta values (2s, 2s', $2p_x$, $2p_x$', etc.) while the 6-31G label corresponds to 6 gaussians for the 1s orbital and triple zeta values for the valence orbitals. Even larger (diffuse) orbitals are useful for systems with lone pair electrons, anions, and excited states; a + denotes addition of these orbitals to heavy atoms and ++ means that diffuse functions have been added to hydrogen atoms as well.

Finally the shape of an orbital can be changed by adding orbitals of higher angular momentum, a procedure said to "polarize" the orbital. To illustrate the notation, addition of two d and one f functions to heavy atom orbitals and two p and one d orbitals to hydrogen would be indicated by the (2df, 2pd) extension on the basis set description. The concept of polarization is analogous to mixing of orbitals to form sp^3 hybrids from s and p orbitals in Valence Bond Theory; both procedures result in a

better description of the electron distributions and in a lowering of energy. The polarized basis set 6-31G(d), also known as 6-31G*, has become a common standard for calculations on medium-sized systems.

More details on basis set usage and notation can be found in refs. 3 and 4. Also discussed there, and in other sources, are the levels of calculation. The most basic of these, the Hartree-Fock (HF) computation at the Self Consistent Field (SCF) level gives the best possible orbital representation in which electrons are assigned individual orbitals. This gives reasonably good structures but its neglect of electron interactions (correlation) makes it inadequate for the accurate calculation of bond energies and many other properties. Configuration interaction (CI) methods endeavor to include the effect of electron correlation by adding excited orbital descriptions. As the basis set size becomes infinite, CI gives the exact solution to the non-relativistic Schrödinger equation. In practical calculations, combinations of singly, doubly, and triply excited states are used and one common approach for this is termed the QCISD(T) method. Finally, another approach to adding higher excitations to Hartree-Fock functions is Møller-Plesset theory. This involves the use of many-body perturbation theory to calculate second (MP2) and even higher order (MP3, MP4) corrections to the HF energies. MP methods are generally faster than CI calculations but, since they are not variational, can lead to ground state energies lower than the true value.

2.2 Discussion

In our study of basis set and level choices, student pairs did three calculations each on HCl, with some redundancy to serve as a check. The results were then pooled for use in class discussion and in individual reports. Indicated in table 1.1 are approximate times (in hours) for the calculations done on a 50 MHz 486 PC with 20 Mbytes of RAM memory and 100 Mbytes of hard disk scratch space. Comparison calculations on a 90 MHz Pentium computer gave times shorter by a factor of about four. All times depend somewhat on the sequence of steps in the calculation and also upon whether analytical or numerical derivatives of the energy are utilized in the calculations. The latter accounts for the apparent time anomaly between MP2 and MP3 calculations. The times also depend upon the number of iterations necessary to find the minimum energy from the starting point for the calculation (initial guess at R_e) which, for consistency, was chosen to be the experimental value[7] of 1.2747.

The Gaussian input requirements to define a calculation are quite simple and consist of several sections, as shown below for a calculation of a potential energy curve displayed in figure 1.1.

Route Section:	# UQCISD(T) 6-31G* SCAN
	<blank line>
Title Section:	POTENTIAL ENERGY SCAN OF HCl
	<blank line>
Charge & Multiplicity:	0 1
Molecule Specification Section:	H
	Cl 1 R
	<blank line>
	R=0.75 70 0.1
	<blank line>

The first line selects the calculation level (UQCISD(T)) and basis set (6-31G*), and SCAN indicates that the bond length variable will be scanned. The U on the level selection means that the calculation is unrestricted (open-shell), i.e. it is not required that the electrons remain paired in orbitals since this can lead to ionic, rather than neutral, products at dissociation. The next line is a title for the output and the third line gives the charge and spin multiplicity for the ground electronic state. Line 6 indicates atom 1 is H and line 7 identifies atom 2 as Cl attached to atom 1 at a bond distance R, and the last line defines the starting value of R, the number of steps, and the increment for the scan. Each section may occupy several lines, so the blanks lines are necessary as section terminators. These parameters are readily entered in the Windows menu format of Gaussian or they can be separately prepared as an ASCII file.

The potential energy curves displayed for HCl in figure 1.1 were obtained using the basis set 6-31G* at three different levels of calculation for both restricted (dashed curves) and unrestricted (solid curves) cases. The MP2 and QCISD(T) levels, which include electron correlation corrections, yield curves significantly lower in energy than those obtained at the HF level. The predicted HF values of R_e and the bond energy D_e are also in poorer accord with the experimental values of 1.2747 and 446 kJ mol^{-1}, respectively. For D_e, computed as E(H) + E(Cl) - E(HCl) from separate calculations for isolated species, values of 298, 370, and 373 kJ mol^{-1} were obtained for UHF, UMP2, and UQCISD(T), respectively. Values closer to the experimental result are obtained if larger basis sets are used. The large disparity in the RHF and UHF curves occurs because the former extrapolates to H^- + Cl^+ dissociation products whereas the latter correctly yields neutral atoms. Note also that, since the MP2 calculation is a perturbation treatment, it is not subject to the variational constraint and the energy curves at large separations are not well represented.

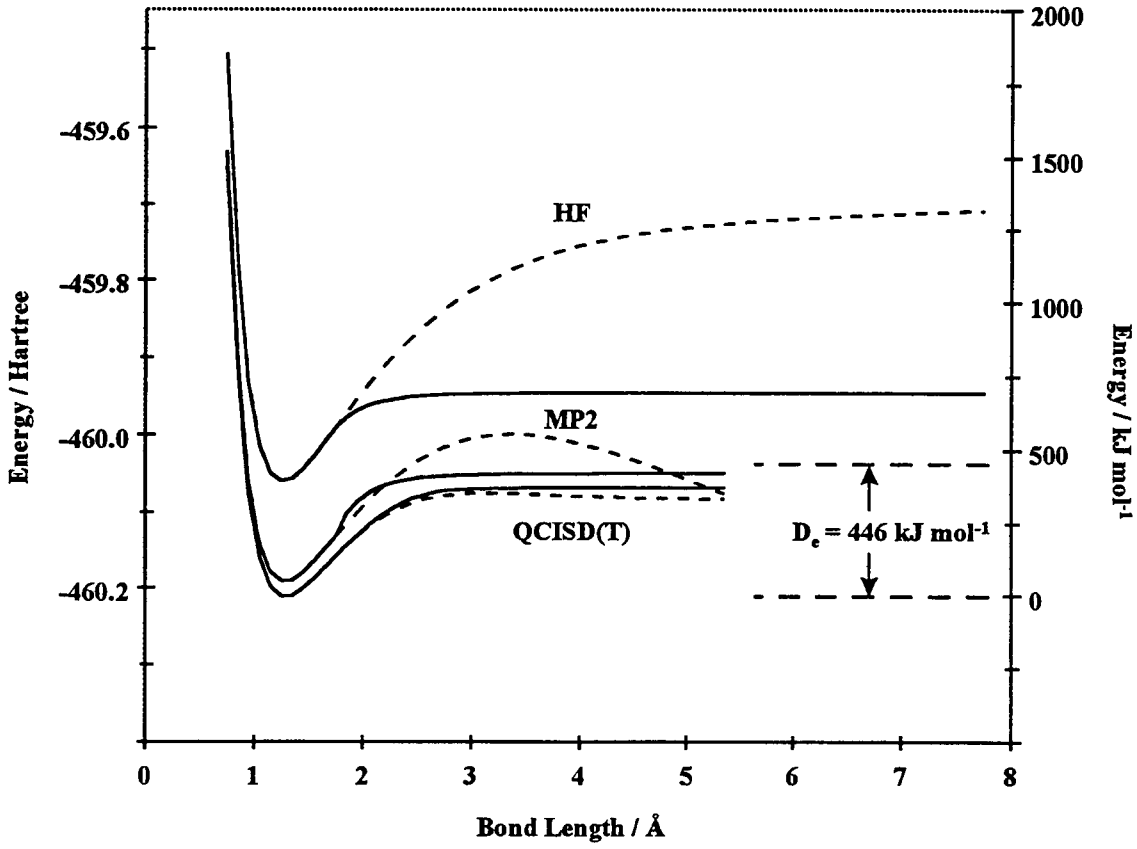

Figure 2.1: Gaussian 92 for Windows calculation of the HCl potential energy as a function of bond length using a 6-31G* basis set at the HF, MP2, and QCISD(T) levels. The solid curves are the open-shell, unrestricted results, the dashed curves are the closed-shell, restricted results.

A detailed display of the effect of basis set size and calculation level on the R_e, w_e, m_e, and a_o parameters is offered in figure 1.2, with experimental values indicated with the horizontal lines. Since the interest was in properties at the minimum energy configuration, where the electrons are paired, the calculations were at the restricted level. In these computations, three steps were performed: a. geometry optimization (keyword = FOPT, in place of SCAN in the above example), b. frequency determination (keyword = FREQ), and c. dipole moment and polarizability determination (keyword = POLAR). More details on the specifics of these commands are given in the Gaussian guide (Ref. 3). The three steps were generally linked to form one job and the times indicated in table 1.1 are totals for all three jobs. The Gaussian output typically contains a large amount of detailed information about each iteration of the calculation, but the final optimized values of interest are readily extracted from a convenient archive summary at the end of the output. It should be noted that the individual polarizability tensor elements α_{xx}, α_{yy}, and α_{zz} are given in the output and the students must calculate the mean of these, $\alpha_o = (\alpha_{xx} + \alpha_{yy} + \alpha_{zz})$, since it is this mean polarizability that is determined in the refractive index experiment.

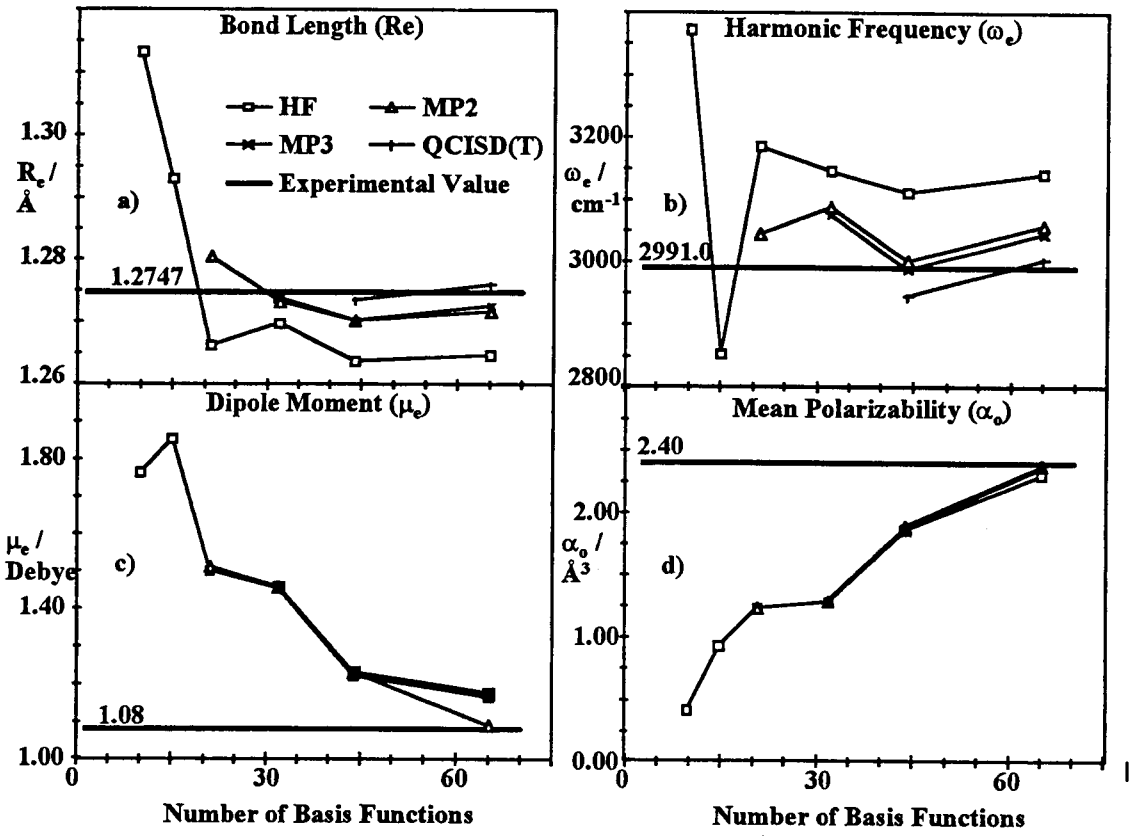

Figure 2.2: Calculated properties of HCl versus the number of basis functions at various calculational levels. The experimental values are indicated with the solid line. a. Equilibrium bond length b. Harmonic vibrational frequency c. Dipole moment d. Mean polarizability

The results shown in the figures serve as a basis for student discussion and an assessment of the quality of the calculations as a function of time (= cost). Comparisons can also be made with the quality of their lab measurements. It is seen that for basis sizes of about 20 or larger, R_e can be calculated to an accuracy nearly comparable to that achieved in the lab. This is not true for w_e, although the QCISD(T) values are within 2% of the experimental result.

In contrast to the trends observed for R_e and w_e, for m_e and a_o the basis set size (rather than calculation level) is seen to be most critical in obtaining accurate values. For the highest basis set size, the agreement with experiment is comparable to that typically obtained by students in the laboratory determination of these quantities (5-10%). Characterization of the basis sets solely by size is a simplification of course. Particular improvement occurs for the last two basis sets, which have p-, d-, and f-type "polarization" orbitals added to the basic valence sets, along with functional changes (+ and ++) which make the orbitals larger (diffuse) to better approximate the lone pair electrons, and thereby to give a more accurate charge distribution description. In discussion of such trends, the instructor will find

references 3 and 4 useful. In particular, generalizations and extensions to larger molecules can be made using the many tables and graphs of Ref. 4.

We have found that the easy access to such calculations on a laboratory PC encourages students to explore further the effects of different orbital choices and calculational level, and to apply Gaussian to other laboratory experiments. The Windows interface of Gaussian is familiar to students and there is no need to set up a university computing account, learn UNIX, VMS, or FTP as is often the case in using Gaussian on a campus mainframe computer. Moreover the shorter calculation times of such large computers are frequently offset by the long batch que that exists if many users are requesting service. With Pentium and faster computer processor units to come, calculations such as those described here can be expected to become common and an integral part of the undergraduate training of chemistry majors.

2.3 Acknowledgments

We thank Gaussian, Inc. for providing a copy of Gaussian 92 for Windows which was used in these calculations.

3. High Resolution Infrared Studies of $Al(BH_4)_3$ and $Al(BD_4)_3$

Darren L. Williams, Abdullah Al-Kahtani, and Joseph W. Nibler*
Department of Chemistry
Oregon State University
Corvallis, OR 97331

Steve W. Sharpe
Molecular Science Laboratory
Pacific Northwest Laboratory
Richland, WA 99352

Prepared for submission to the *Journal of Physical Chemistry*

3. High Resolution Infrared Studies of $Al(BH_4)_3$

3.1 Introduction

Metal borohydrides are fascinating compounds because they show a remarkable variety in bonding characteristics, ranging from ionic salts of the alkali metals (e.g. $LiBH_4$ and $NaBH_4$) to volatile covalent compounds in which hydrogen bridge bonds bind boron to the metal. Among the covalent compounds, $Al(BH_4)_3$, is believed to have a planar trigonal skeletal structure with double hydrogen bridges[8,9] while $Zr(BH_4)_4$, $U(BH_4)_4$, and $Hf(BH_4)_4$ are all thought to have tetrahedral T_d structures with triple bridges.[10] The borohydrides are among the most volatile compounds of the latter heavy metals, a fact sometimes used in their commercial purification.

Aluminum borohydride, synthesized by Schlesinger and coworkers in 1940, was the first covalent metal borohydride molecule to be characterized structurally.[11] An electron diffraction study of the

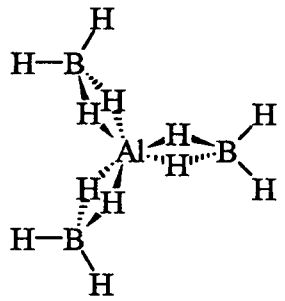

Figure 3.1: The D_{3h} molecular structure of aluminum borohydride, $Al(BH_4)_3$. In the D_3 structure, deduced from electron diffraction data[1], the BH_4 units are rotated by 17°.

compound in the same year demonstrated that the aluminum atom was linked symmetrically to all three boron atoms, all B-Al-B angles close to 120°.[12] The position of the hydrogen atoms remained unclear. Two NMR studies[13,14] of liquid $Al(BH_4)_3$ showed that all the protons were equivalent, i.e., the exchange between bridging and terminal hydrogen positions is fast (on the NMR time scale), as has been the case for all other metal borohydrides subsequently examined. The first infrared spectrum was reported in 1949[15] and, because of the great similarity to the spectrum of diborane, it was interpreted in favor of the

molecular structure shown in figure 3.1. Each boron atom is bonded to four hydrogen atoms, located at roughly the corners of a tetrahedron, and is connected to the aluminum atom through two hydrogen bridge bonds. The infrared study was consistent with a proposed prismatic D_{3h} structure in which the terminal hydrogen atoms lie in the plane of AlB_3 and the line joining the bridge hydrogen atoms is perpendicular to the plane. The same conclusion was also reached in a Raman study in 1960[16] on $Al(^{11}BH_4)_3$, $Al(^{10}BH_4)_3$, $Al(^{11}BD_4)_3$, and $Al(^{10}BD_4)_3$. In this study, a partial vibrational assignment was made based on a D_{3h} structure.

In 1968 another electron diffraction investigation of gaseous $Al(BH_4)_3$ was reported.[8] This study also showed that the aluminum and boron atoms are coplanar, with each BH_4 group double-bridged to the aluminum atom. However, the data could not determine conclusively the overall symmetry of the molecule. It was hypothesized that the molecule could be either of D_{3h} symmetry or of D_3 symmetry (obtained from D_{3h} by conrotation of the three BH_2 bridging planes). To fit the data to the last case, the rotation angle was found to be close to 17°.

The most recent vibrational investigation, reported in 1973[9] involved detailed infrared and Raman results on gaseous, solid, and matrix isolated $Al(BH_4)_3$ and $Al(BD_4)_3$. It was found that there was no evidence for any significant structural change in going from the gas to solid to matrix states. Based on symmetry/selection rules, the data were found to be consistent with a D_{3h} prismatic structure and an assignment of 23 optically-allowed fundamental transitions was proposed. The isotopic frequency shifts were found to be in a satisfactory agreement with the Product Rule and a number of modifications were made of the previous partial fundamental assignment.

Besides the experimental work summarized above, two *ab initio* investigations have been reported on the structure of $Al(BH_4)_3$. In one study at the Hartree-Fock level by Bock *et al.*[17] , the D_{3h} and D_3 structures proposed previously were considered. A vibrational frequency analysis was performed on the prismatic D_{3h} structure to determine if it was indeed a local potential minimum. The appearance of a single imaginary frequency showed that the D_{3h} configuration corresponded to a first-order transition state. Reducing the imposed symmetry to D_3, by allowing the BH_4 units to rotate in a conrotary fashion, lowered the energy by about 5.9 kJ mol^{-1}. A subsequent frequency analysis at the same level showed the antiprismatic D_3 structure to be a stable configuration (i.e. all vibrational frequencies were real). It was suggested that the rotation lowered the energy by reducing the coulombic repulsion between hydridic hydrogens in each of the upper and lower prismatic planes, but the rotation angle was not given.

In a later study at a higher level of *ab initio* theory, Demachy *et al.* included electron correlation using second-order perturbation theory (MP2) and configuration interaction (CIPSI).[18] The rotational barrier associated with the conrotation of the three BH_4 groups around the Al-B bond in the bidentate structure of $Al(BH_4)_3$ was found to be reduced from the Hartree-Fock result of 5.9 kJ mol^{-1} to 0.8 $kJmol^{-1}$. The rotation angle (θ = 23.2°) and other structural parameters of this minimum are given in table 3.1,

Table 3.1: Geometrical parameters of $Al(BH_4)_3$, in Å, degrees, and cm^{-1}.

$Al(BH_4)_3$ Parameter	Experiment[8]	HF/6-31G*[18]	HF/6-311G**[a]	MP2/6-311G**[a]
Al-B	2.143	2.177	2.176	2.155
B-Hb	1.283	1.285	1.288	1.273
B-Ht	1.196	1.189	1.189	1.192
Hb-B-Hb	114.0	106.3	106.5	108.4
Ht-B-Ht	116.2	121.6	121.5	121.6
θ	17.2	23.2	23.3	23.2
$B(^{11}B_3)$	0.1475	0.1435	0.1442	0.1464
$C(^{11}B_3)$	0.0786	0.0758	0.0763	0.0775

[a] This work

along with the electron diffraction results.[8] It was found also that changing the coordination mode of one borohydride group from bidentate to tridentate leads to a structure which is the transition state for the exchange of bridging and terminal hydrogens. This BH_4 "tumbling" barrier was found to have a relatively low energy (9.2 kJ mol^{-1}), a result consistent with the lack of distinction between bridging and terminal hydrogens in the proton NMR spectrum. In contrast a transition barrier of 103.8 kJ mol^{-1} was found for the change in coordination of one borohydride group from bidentate to monodentate.

Whereas both theoretical studies support a stable D_3 geometry for $Al(BH_4)_3$ with facile BH_4 motion about the Al-B axes, the existing experimental data cannot distinguish between D_3 and D_{3h} forms. The calculated rotational constants (table 3.1) suggest that the 2B line separation in the infrared P and R branches should be about 0.3 cm^{-1}, not resolvable at the resolution of previous studies but well within the capability of current instruments. Of course, because the structural change from D_{3h} to D_3 is slight, it is not likely that measurements of the rotational constants would distinguish between these forms. However in principle a distinction might be possible from rotationally resolved K=0 line intensities and one might also expect some subtle splittings of lines due to torsional and tumbling rotations of the BH_4 units. If measurable, the latter splittings are of special interest because they are governed by the transition barriers for motions on the potential energy surface. Recent theoretical[19] and experimental[20] studies of $LiBH_4$ and the other alkali metal borohydrides indicate that such barriers are high enough that no appreciable splitting occurs in the ground state, but that they are low enough that such effects could be expected in upper vibrational levels. To our knowledge, no such vibrational spectra have been obtained for the alkali metal borohydrides, probably because of their very low vapor pressure. Considerably more volatile are the $Be(BH_4)_2$ and $Al(BH_4)_3$ compounds that we have recently examined. The present work describes efforts to obtain vibration-rotational fine structure for $Al(BH4)_3$ and $Al(BD_4)_3$ using FTIR and IR diode laser spectroscopy at a resolution down to 0.001 cm^{-1}, along with some further *ab initio* calculations.

3.2 Experimental

$Al(BH_4)_3$ was prepared via the solid-state metathetic reaction of aluminum chloride and sodium borohydride, following the method of Schlesinger *et al.*[21] Because of the pyrophoric nature of the molecule, all reactants were handled in a dry bag and the reaction was carried out in a hood using a greaseless vacuum system. In the dry bag, one gram of anhydrous $AlCl_3$ (99.5% Aldrich Inc.) and four grams of anhydrous sodium borohydride (95% Alfa) were mixed in a reaction tube. This was then attached to a vacuum line, evacuated, and then slowly heated over eight hours to 140° C while pumping volatile $Al(BH_4)_3$ and B_2H_6 products through a condensation trap at 77 K. The diborane was subsequently removed by warming the trap to about 200 K while pumping. $Al(BD_4)_3$ was made by the analogous reaction of $AlCl_3$ with $NaBD_4$ and purified by a similar procedure.

Survey infrared spectra were recorded using a Mattson Sirius 100 FTIR spectrometer, which has a resolution of 0.125 cm^{-1}. Samples at 5-10 Torr pressure were placed in 10 or 20 cm cells equipped with KBr windows. No rotationally resolved structure was seen in the spectra so higher resolution infrared spectra (0.01 cm^{-1}) were then recorded at Pacific Northwest Laboratories (PNL) using a Bruker IFS 120 HR FTIR spectrometer. The $Al(BH_4)_3$ region near 2100 cm^{-1} was also examined at 0.001 cm^{-1} resolution using an IR diode laser and a multipass gas cell at PNL.

Finally, infrared diode-laser spectra of $Al(BH_4)_3$ cooled in a jet were collected, using a special spectrometer system developed at PNL.[22] This consists of a Laser Photonics cold head mounted on an optical table and containing up to four laser diodes. The output of a selected diode is collimated and directed into a 0.5 meter monochromator, the output of which is intercepted by a rotating gold-coated aluminum sector. The sector intercepts and directs the laser light 1/3 of the time to a reference cell, 1/3 of the time to a 0.25 meter confocal etalon, and the rest of the time into the vacuum chamber where it intercepts the effluent of a pulsed slit nozzle of 100 mm length. Laser light entering the vacuum chamber through BaF_2 windows is multi-passed up to 32 times through the supersonic jet, using a White cell optical configuration. The signals from the three InSb detectors are fed into three parallel digitizers that sample 4096 points at 200 ns intervals, yielding a spectral scan of about 0.4 cm^{-1}. The pulsed valve and the three digitizers are synchronized with the angular position of the rotating sector using a microprocessor, and signal averaging is done by real-time, co-addition of individual spectra over many gas pulses.

3.3 Results And Discussion

3.3.1 FTIR Spectra of $Al(BH_4)_3$ and $Al(BD_4)_3$

A spectrum recorded at 0.010 cm^{-1} resolution for 6 Torr of $Al(BH_4)_3$ in a 10 cm cell is shown in the top trace of figure 3.2. Broad regions of absorption by $Al(BH_4)_3$ are seen in these single-beam

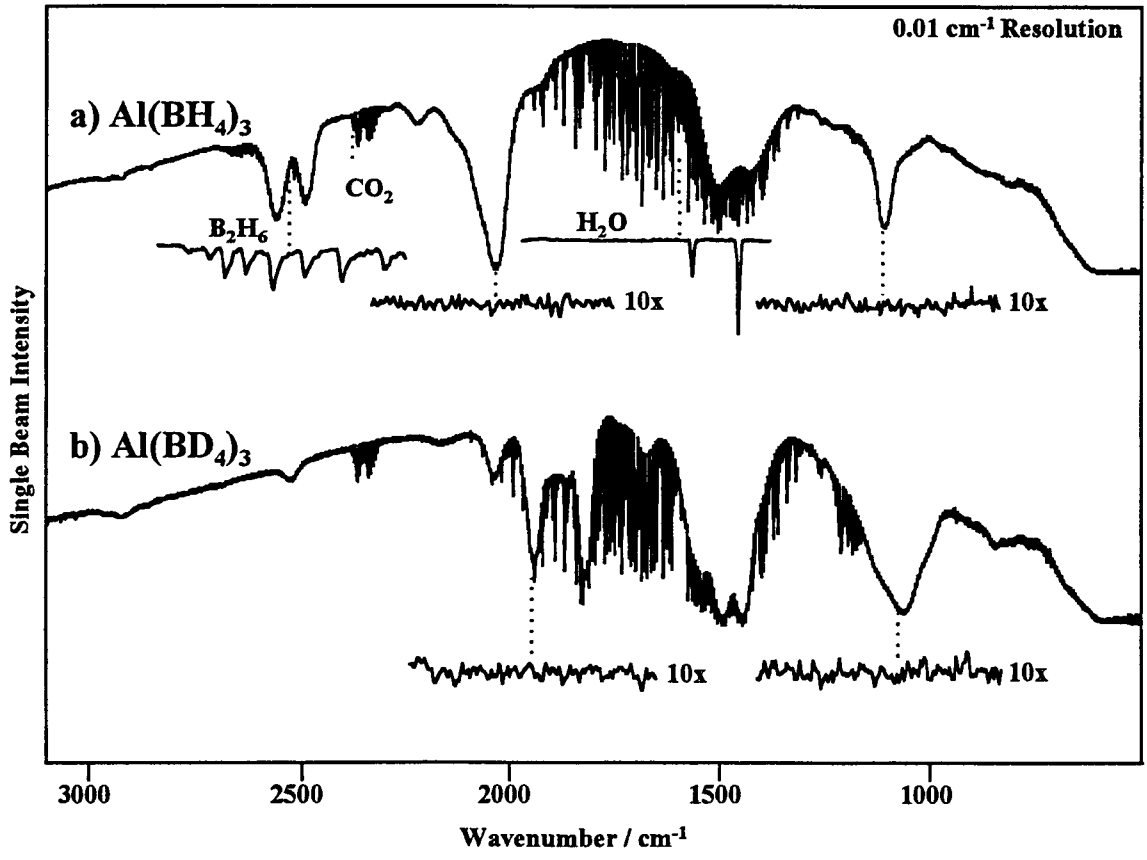

Figure 3.2: FTIR spectra of a) $Al(BH_4)_3$ and b) $Al(BD_4)_3$ at 0.01 cm^{-1} resolution. The 1 cm^{-1} expanded regions show resolved rovibrational structure for background H_2O and B_2H_6 contaminant. No such structure was seen for $Al(BH_4)_3$ or $Al(BD_4)_3$, even at 10x ordinate expansion.

spectra, along with sharp features of diborane contaminant in the sample and of residual CO_2 and H_2O in the evacuated FTIR instrument. One cm^{-1} expanded portions of several of the major features are given as inserts in the figure. The sharp features in the top trace at 2520 cm^{-1} and the bottom trace at 1200 cm^{-1} can be positively identified as diborane lines. The line width of these (0.016 cm^{-1} FWHM) establishes

the limiting measurement resolution, which is due to the convolution of the instrumental resolution, the Doppler width (about 0.005 cm^{-1}), and the collisional width (estimated to be < 0.002 cm^{-1}). The Doppler width for $Al(BH_4)_3$ is about 0.003 cm^{-1} and the collisional broadening in this nonpolar molecule is likely to be comparable to that in diborane.

At our measurement resolution one would expect to easily resolve P and R rotational lines with spacings of about 0.3 cm^{-1}. The P-Q-R band contours for parallel modes of A_2'' symmetry should be distinguishable, with a P-R maxima separation of about 16 cm^{-1} at room temperature. For E′ perpendicular bands, strong Q branch maxima spaced by 2(C-B) ~ 0.15 cm^{-1} are expected. Some blurring of these rigid rotor predictions will of course result from K splittings and coriolis and centrifugal distortion effects. However the expanded traces at 2020 and 1100 cm^{-1} (top, $Al(BH_4)_3$) and 1990 and 1050 cm^{-1} (bottom, $Al(BD_4)_3$) show no hint whatsoever of resolved rotational structure. Moreover, several diode laser scans at 0.001 cm^{-1} resolution for room temperature $Al(BH_4)_3$ at low pressures confirmed the essentially continuous absorption in the region near 2030 cm^{-1}. The broad features in the traces are the same as those reported for $Al(BH_4)_3$ and $Al(BD_4)_3$ in reference 9 and in none of the spectra are P-Q-R band contours discernible. It should also be noted that the increased mass of the BD_4 did not reduce the spectral congestion, as might have been expected if splittings due to rotational tunneling between potential minima were the major cause of spectral complexity.

3.3.2 Isotopic Contributions to Spectral Congestion

The complete absence of any resolved rotational structure in the vibrational spectra of $Al(BH_4)_3$, even at 0.001 cm^{-1} resolution, was surprising to us but might be a consequence of overlap of bands due to the different boron isotopic forms and to hot bands involving low lying vibrational levels. The isotopic forms for $Al(BH_4)_3$ are $^{11}B_3$ (51%), $^{11}B_2{}^{10}B$ (38%), $^{11}B^{10}B_2$ (10%), $^{10}B_3$ (1%); we neglected the contribution of the latter two minor forms in the spectral simulations described here. The ^{10}B vibrational shift will vary for different modes and these were predicted from Gaussian calculations done at the Hartree-Fock level with a 6-311G** basis set. Frequencies and intensities for the $^{11}B_3$ form are listed in table 2.2, with the former scaled by about 0.9 according to common practice.[23]

Band spectra were simulated for three vibrational fundamentals predicted by Gaussian to have high infrared intensities. One of these was the E′ terminal BH_2 bending deformation, a perpendicular band near 1110 cm^{-1} assigned by Coe et al.[9] as ν_{19}. For the $^{11}B_2{}^{10}B$ form, the calculations show that this degenerate E mode yields two uncoupled modes, one at the same wavenumber value as in the $^{11}B_3$ compound and a second ^{10}B mode 4.1 cm^{-1} higher and with equal intensity. A similar uncoupling was calculated for the E′ bridge stretching mode near 2020 cm^{-1}, but with a smaller ^{10}B- ^{11}B shift of 1.1 cm^{-1}.

Table 3.2: Wavenumbers and infrared intensities (km mol^{-1}) calculated for the vibrational fundamentals of $Al(BH_4)_3$ using Gaussian at the HF/6-311G** level.

HF/6-311G**			Experimental[9]		
D_3	ω[a]	IR Int.	ω	D_{3h}	Mode Desc.
A1	2368		2471	A1'	BH_t st sym
E	2364	96	2490	E'	BH_t st sym
A2	2439	52	-	A2'	BH_t st asym
E	2441	145	2555	E'	BH_t st asym
A1	1928		2059	A1'	BH_b st sym
E	**1874**	**561**	**2059[b]**	**E'**	**BH_b st sym[c]**
A2	**1915**	**336**	**2030[b]**	**A2''**	**BH_b st asym[c]**
E	1789	55	2030	E"	BH_b st asym
A1	1544		1511	A1'	AlH_b st sym
E	1353	7	1425	E'	AlH_b st sym
A2	1385	42	1505	A2"	AlH_b st asym
E	1501	616	1565	E"	AlH_b st asym
A1	1112		-	A1"	BH_2 twist
E	1107	3	1155	E"	BH_2 twist
A1	1102		-	A1"	bridge twist
E	994	27	1146	E"	bridge twist
A2	986	5	1113	A1'	BH_2 def
E	**1097**	**129**	**1112**	**E'**	**BH_2 def[c]**
A2	776	6	-	A2'	BH_2 rock xy
E	713	0.2	981	E'	BH_2 rock xy
A1	443		765	A2"	BH_2 wag z
E	550	117	723	E"	BH_2 wag z
A1	228		495	A1'	AlB st sym
E	376	18	605	E'	AlB st asym
A2	167	18	222	A2"	B_3 bend z
E	253	0.04	324	E'	B_3 bend xy
A2	263	6	-	A2'	bridge bend
E	116	10	255	E'	bridge bend

[a] Wavenumber values scaled by 0.8929 as recommended in ref. 23.
[b] The calculated transitions and intensities favor the reversal of these two wavenumber assignments.
[c] **Transitions studied by diode laser in this work.**

The A_2'' symmetric counterpart of this bridge stretch, a parallel band, was predicted by the Gaussian calculation to lie 41 cm^{-1} higher than the E' mode and to have a ^{10}B- ^{11}B shift of 2.6 cm^{-1}. We note that this ordering is a reversal of that chosen by Coe et al.[9], who assigned the intense infrared peaks near 2030 and 2056 cm^{-1} as A_2'' (ν_{11}) and E' (ν_{17}), respectively. The basis for their assignment was not strong however and the match of the calculated intensities to the FTIR data favors the $A_2'' > E'$ ordering adopted in our simulations. In general, the calculated ^{10}B shifts are comparable to those observed experimentally for similar modes in diborane.

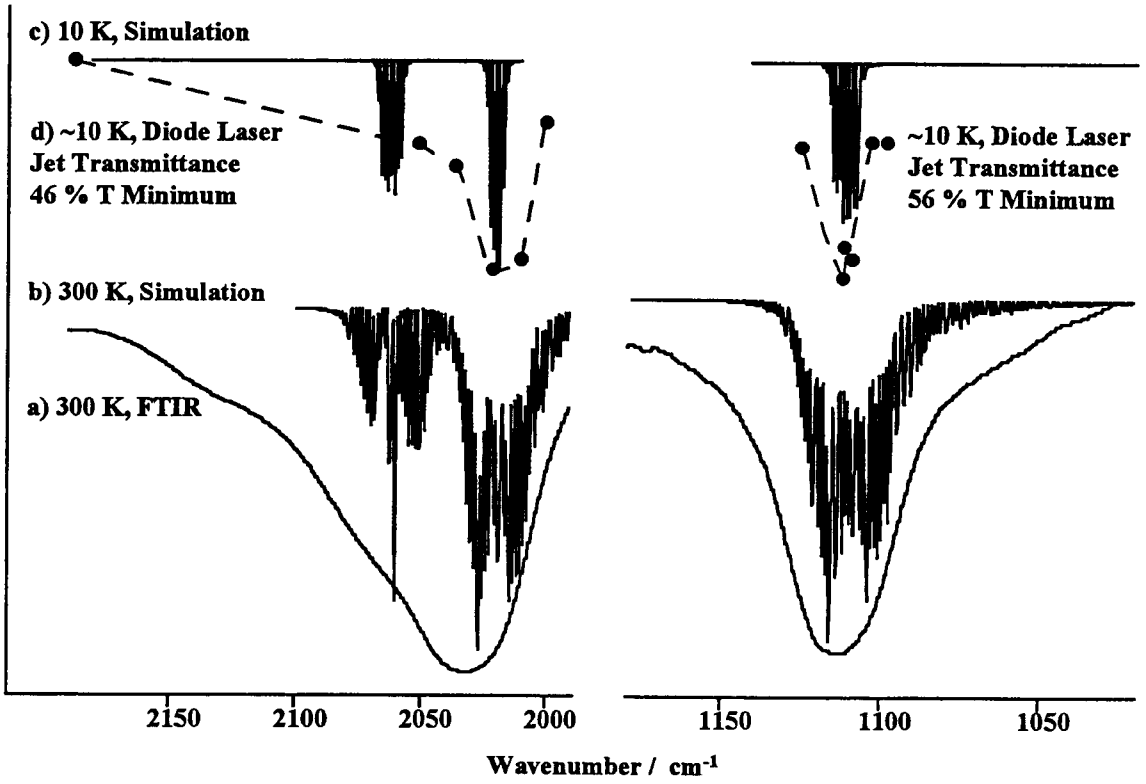

Figure 3.3: The $Al(BH_4)_3$ jet transmittance regions of interest. (a) 300K scan at 0.01 cm^{-1} resolution. (b) simulation for non-rigid rotor at 300 K using parameters in table 2 and Gaussian line shapes with 0.015 FWHM. Simulations include $Al(^{11}BH_4)_3$ (51%) and $Al(^{11}BH_4)_2{}^{10}BH_4$ (38%) and the relative *ab initio* IR intensities. The feature at 2030 cm^{-1} is composed of a parallel band at 2061 cm^{-1}, and a perpendicular band at 2020 cm^{-1}. The band at 1110 cm^{-1} is a perpendicular band. (c) transmittance measurements dotted across each region show a narrowing of the bands in the jet expansion. The temperature is believed to be ~10 K. (d) simulation at 10 K for Gaussian lines with 0.002 cm^{-1} FWHM.

Simulations of both parallel and perpendicular band spectra were done with Grams/32[24] using Array Basic and standard relations given in reference 25; the $^{11}B_2{}^{10}B$ isotopic form was taken to be a near-oblate top with averaged rotational constant (A+B)/2. The band origins of the two E′ modes were adjusted to roughly match the center of the strong absorptions at 1110 and 2020 cm^{-1} while that of the less intense A_2'' transition was situated 41 cm^{-1} higher than the 2020 cm^{-1} band. Centrifugal distortion and first order coriolis parameters were calculated with the Asym40 normal coordinate program of Hedberg and Mills[26], using as input the Cartesian coordinates and force constants obtained from Gaussian at the Hartree-Fock level. The vibration-rotation coupling constants α_i were also calculated for the normal modes but these values are believed to be too small due to neglect of anharmonicity. Accordingly, a single, larger, value of $\alpha_A = \alpha_B = 2\alpha_C = -0.0004$ cm^{-1} was taken as representative for all modes, based on α_i values for comparable modes in the somewhat similar molecule cyclopropane.

Table 3.3: Rotational parameters (cm^{-1}) of the most abundant isotopes of $Al(BH_4)_3$.

Rotational Parameter[a]	$Al^{11}B_3H_{12}$	$Al^{10}B^{11}B_2H_{12}$
A"	0.1443	0.1505
B"	0.1443	0.1443
C"	0.0764	0.0778
D_J"	1.82E-7	1.88E-7
D_{JK}"	-3.36E-7	-3.48E-7
D_K"	9.34E-8	9.30E-8
ζ_{17}	1.79E-2	1.80E-2
ζ_{19}	9.48E-3	8.84E-3

[a] Based on HF/6-311G** results and ASYM40. In addition to these constants a vibration-rotation coupling constant of $\alpha_A = \alpha_B = 2\alpha_C = -0.0004$ cm^{-1} was assumed for all modes for the spectral simulations

The calculated parameters are listed in table 3.3 and in figure 3.3 the simulations for 300 K, 2.3(b), are compared with experiment, 2.3(a). The simulated traces in these figures show that rotational structure in these branches should be easily resolved, a conclusion that is unchanged for reasonable changes in the parameter estimates. Especially, the P-Q-R branch contours are clearly discernible, in marked contradiction to the observations; thus other sources of spectral congestion must be considered.

3.3.3 Hot Band Contributions to Spectral Congestion

The *ab initio* calculations for $Al(BH_4)_3$ predict that five of the vibrational modes lie below 500 cm^{-1} and hence less than 10% of the molecules will be in the ground state at room temperature. In particular, an E′ type bridge-bending mode is predicted at 116 cm^{-1} which, due to its degeneracy, will be more populated than the A_1' ground state. Overtone and combination levels of this mode and other low frequency modes will lead to many overlapping hot bands, each with small, unknown shifts due to anharmonicity. Such hot band transitions could well blur the rotational contours of the vibrational transitions, as would extensive K splitting of high J rotational lines. Both effects would be greatly reduced at low temperatures; accordingly several experiments were done in which aluminum borohydride was expanded in a free jet and probed by high resolution diode laser spectroscopy.

3.3.4 Diode Laser Spectra of $Al(BH_4)_3$ Cooled in a Jet

The samples consisted of a 1% mix prepared by flowing argon at 500 Torr through a glass tube containing liquid $Al(BH_4)_3$ at about -50 °C (5 Torr vapor pressure). From other work with the PNL jet apparatus, such conditions are known to produce mainly monomeric samples with rotational temperatures of about 10 K. At this temperature the collisional width will be negligible, and the Doppler width will be less than 0.001 cm^{-1}, the resolution of the diode sources. A typical line width measured with this apparatus for isolated lines of other molecules is 0.002 cm^{-1} FWHM[22].

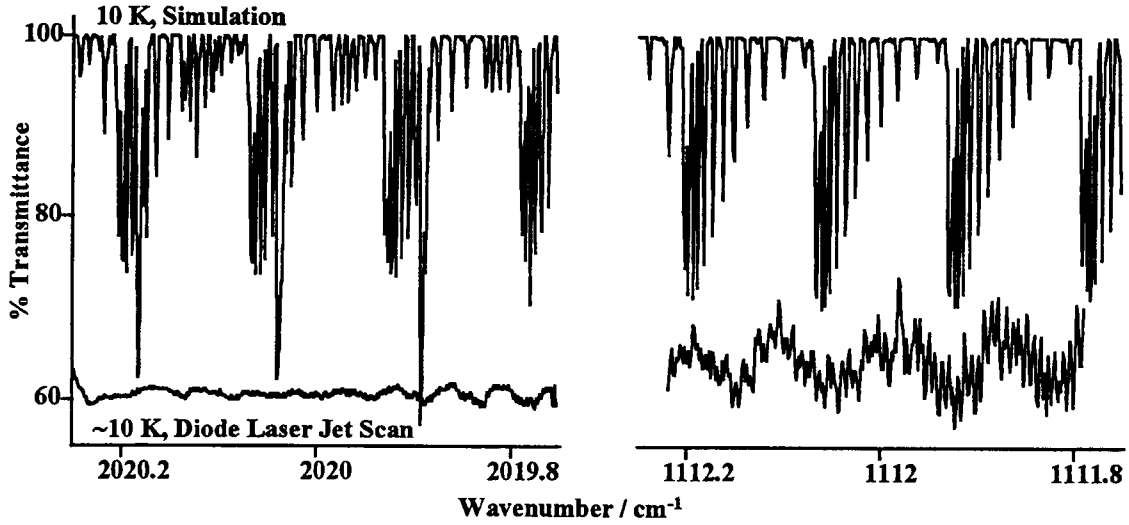

Figure 3.4: Infrared diode laser spectra of $Al(BH_4)_3$ in a supersonic jet expansion are shown in comparison to the simulated pattern of lines for the Q branches of both perpendicular bands. The 100% transmittance level is common for both experimental and simulated spectra for the 1112 cm^{-1} region; in the 2020 cm^{-1} region, the 100% transmittance line for the experimental trace is an estimate.

The strong absorptions located around 2030 cm^{-1} and 1110 cm^{-1} were logical choices for this diode study because they were in regions of available laser sources and there were few overlapping bands of water or diborane that might complicate the spectrum. That appreciable absorption by the $Al(BH_4)_3$ occurred in the jet was confirmed by observing the transmitted laser intensity at 2030 cm^{-1} during the jet pulse and also with it turned off. A sharp dip indicated a transmission drop to about 50%. For comparison, in an expansion of pure argon the drop was only 1-5%; an effect attributed to beam steering by the varying index of refraction caused by the gas pulse. That the dip depends on the laser wavelength is shown by the reduced absorption when the laser was tuned to 2189 cm^{-1}, well off the strong $Al(BH_4)_3$

absorption in the region. Coarse I/Io traces of the absorption profiles at 2030 and 1110 cm^{-1} were generated in this manner and are shown in figure 3.3(c), along with the simulated spectra for 10 K for both regions 3.3(d). A general narrowing of each absorption band is apparent in both jet and simulated spectra. The diode laser was next scanned over selected 0.4 cm^{-1} portions of these absorption profiles and representative traces at 2020 cm^{-1} and 1110 cm^{-1} are shown at the bottom of figure 3.4. It should be noted from the transmission scale of the experimental spectra that the small variations in intensity rest on a broad absorption background. In the 1110 cm^{-1} region, some structure of very regular periodicity is seen which is attributed to an etalon effect in the multipass cell. There is also present in both this spectrum and in the 2020 cm^{-1} scan some evidence of complex overlapping features which are believed to be real. Nonetheless, agreement with the well-resolved, sharp absorptions of the E′ Q-branch spectra simulated for 10 K is remarkably poor and is not improved with modest changes in the spectral parameters or the sample temperature. It is clear that the spectrum is extremely congested, even at this low temperature. Attribution of this to ineffective quenching of the vibrational hot bands is considered unreasonable because many studies support the idea that vibrational relaxation is very effective in jet expansions.[27,28] Rather, we regard this congestion as a strong experimental indication that the large amplitude torsion and tumbling motions of $Al(BH_4)_3$ play an important role in adding to the spectral congestion. That such might be the case is suggested by the low *ab initio* barriers cited earlier and this has led us to explore in more detail the potential energy surface and its effect on the spectrum.

3.3.5 Potential Energy Calculations

Ab initio calculations were done using Gaussian 94[29] on a DEC Alpha OSF/1 workstation and also on an Intel Pentium Pro 200 MHz system, which gave equivalent CPU performance. The computational model[30,31] was CCSD/6-311G**// MP2/6-311G** for all geometries of interest and the harmonic frequencies and Cartesian force constants were calculated at the Hartree-Fock level using the same basis set. The geometry optimizations and analytical frequency calculations were done with no symmetry constraints, and all converged to a D_3 structure. The HF/6-311G** geometrical parameters agreed well with those of Demachy et al.[18], as shown in table 2.1. Tables 2.2 and 2.3 give the vibrational and rotational parameters deduced from these Hartree-Fock calculations and used in the spectral simulations.

For the D_{3h} geometry of $Al(BH_4)_3$, there are $(4x3)^3$ equivalent configurations produced by simple rotation of the BH_4 units and these will produce 576 A and 576 E sublevels for each rigid rotor vibrational state. These will be retained for a distortion to D_3 symmetry but there will now be a doubling of all levels due to the two equivalent minima corresponding to a ± conrotary twist of all three BH_4 units. The extent to which sublevel splittings are discernible for this manifold of states will depend upon the

feasibility of the interchange operation[19]. In the case of $LiBH_4$, microwave rotational spectra[20] show no ground state splittings attributable to mixing of the equivalent states separated by the tumbling barrier. This splitting is estimated at 6.3 x 10^{-5} cm^{-1} by Baronov and Boldrev[32], based on their *ab initio* value of 1053 cm^{-1} for the tumbling barrier. A somewhat lower, but still appreciable, barrier of 770 cm^{-1} has been calculated for$Al(BH_4)_3$ by Demachy et al. so that the splittings in the ground state due to tumbling exchanges would be expected to be very small in this molecule as well. Such need not be true for the sublevels produced by the conrotary torsional motion, however, and we examine the magnitude of these next.

The potential energy of the torsional motion was completely mapped using a z-matrix input to fix all variables while scanning the conrotation angle θ. The other structural parameters were then optimized at the maxima at θ = 0° and 90° via the QST3 transition state searching method.[33] Single point energies were obtained at the minimum and two maxima using a coupled cluster calculation with single and double substitutions (CCSD). The rest of the potential surface points were then scaled to the CCSD maxima with the minimum set to zero, and the resulting surface data was fitted with a Fourier series of cosines by least squares minimization,

$$V(\theta) = \sum_{k=1} \frac{V_k}{2}(1 - \cos(k\theta)) \qquad (3.1)$$

An adequate representation of the shape of this torsional potential was obtained for V_k values of V_0 = 490 cm^{-1}, V_2 = 19700 cm^{-1}, V_4 = -9150 cm^{-1}, V_6 = 1970 cm^{-1}, V_8 = -472 cm^{-1}, and this function is plotted in figure 3.5.

To calculate the effect on the torsional energy levels, the optimized potential function was added as a perturbation to a simple internal rotor Hamiltonian,

$$\hat{H} = \hat{T} + \hat{V} = -\frac{\hbar^2}{2I}\frac{\partial^2}{\partial\theta^2} + \sum_{k=0,2,4} \frac{V_k}{2}\left(1 - \cos(k\theta)\right) \qquad (3.2)$$

where I was taken to be three times the moment of inertia of the BH_4 unit about the Al-B axis. The matrix elements of this Hamiltonian in a free rotor basis are easily calculated[34]. The resultant matrix was diagonalized numerically using Maple V and the basis set size was increased until the lowest twelve energy levels converged to less than 0.0001 cm^{-1}. The energy levels are overlaid with the potential at the bottom of figure 3.5 to show the splitting pattern near the minima. A correlation diagram (figure 3.6) of the torsional energy levels shows the ground and first two excited states as the prismatic barrier increases from zero to our calculated value of 490 cm^{-1} (5.9 kJ mol^{-1}). For the latter case, the ground state splitting

is 0.052 cm^{-1}, a value which increases to 2.7 and 36 cm^{-1} for the next two levels respectively. These splittings of course increase as the prismatic barrier is lowered. For example, a ground state splitting of 9.3 cm^{-1} is predicted for Demachy et al's 70 cm^{-1} (0.8 kJ mol^{-1}) barrier.

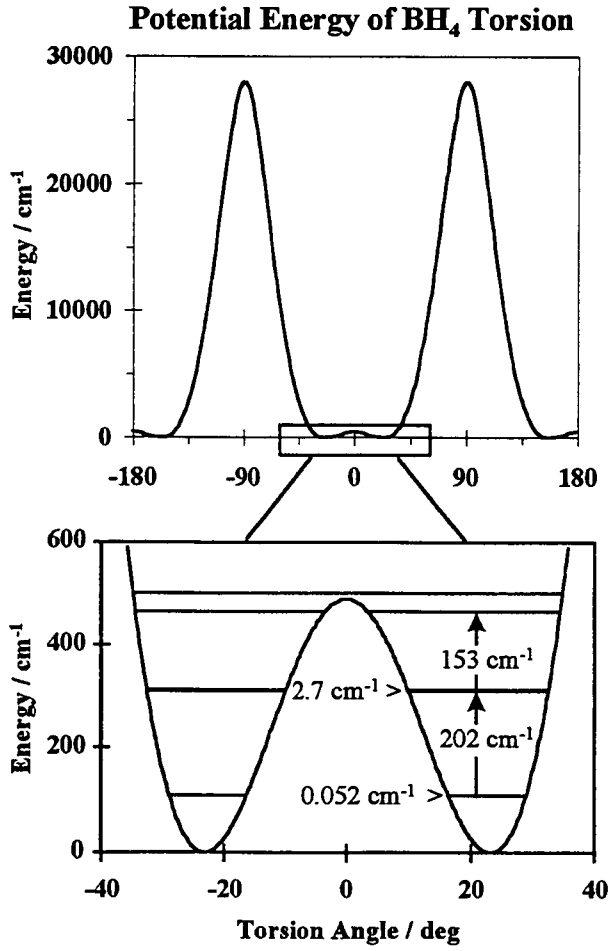

Figure 3.5: The potential energy of the BH_4 torsion (conrotation about the Al-B axes) is periodic with four equivalent minima. The minima separated by the low prismatic barrier (490 cm^{-1}) mix to produce splittings of 0.052 cm^{-1} in the ground state and 2.7 cm^{-1} in the first excited state.

Although the validity of these *ab initio* barrier heights is difficult to assess, it seems clear that the effect of the conrotary torsional motion is enough to cause appreciable splitting of the ground state, thereby producing a doubling of the spectral congestion, even at 10 K. If the tumbling barrier is also lower than the 770 cm^{-1} estimate of Demachy et al., further splittings can be expected from these

motions. More important than this, though, may be additional structure caused by splittings in the upper vibrational states of the modes probed in our measurements. This splitting would be most appreciable for higher vibrational levels involving the BH_4 rocking, wagging, and twisting modes, which combine to produce the tumbling coordinate. Although the three bands examined in our jet measurements are believed to involve primarily BH_2 deformation and BH bridge stretching coordinates, they could be mixed with tumbling modes to some extent. In addition Fermi resonance with overtone and combination levels involving torsional and

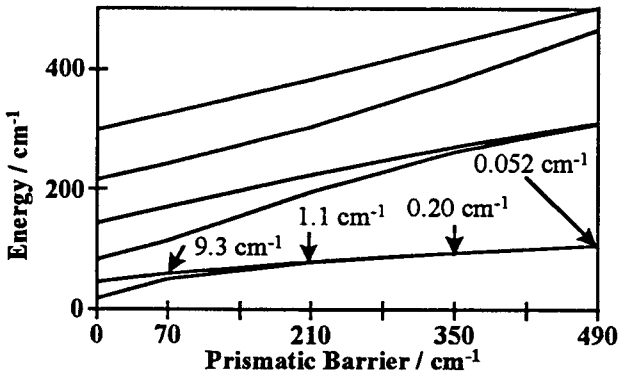

Figure 3.6: The torsional energy level correlation diagram as the prismatic barrier is increased from zero up to our value of 490 cm^{-1}. The ground state splitting is 27 cm^{-1} with no barrier, 9.3 cm^{-1} with Demachy et al.'s value of 70 cm^{-1}, and 0.052 cm^{-1} at 490 cm^{-1}.

tumbling modes could add complexity to the spectrum. Doubtless, all of these effects contribute to the extreme spectral congestion seen, even in the 10 K spectra obtained in this study.

3.4 Conclusions

We have obtained very high resolution IR spectra of $Al(BH_4)_3$ which show no resolved rotation-vibrational structure, even at the low temperatures achieved in a cold jet. *Ab initio* calculations suggest that extreme spectral congestion may arise from small isotopic shifts due to ^{10}B, many low frequency modes below 500 cm^{-1}, and especially, level splittings due to low barriers to internal rotation. The $Al(BH_4)_3$ molecule is a prime example of the complexity introduced by equivalent minima and large amplitude motions, a situation often met in the case of van der Waals complexes, but less common for covalently bonded molecules. The metal borohydrides thus represent an unusual class of compounds in which ionic interactions appear to hold together BH_4^- units which have large librational motion. Such

motions have recently been considered in analyzing the microwave rotational spectra of alkali metal borohydrides and further work on the vibration-rotational spectra of $LiBH_4$ and of $Be(BH_4)_2$ would seem worthwhile, particularly if these samples are cooled in a jet.

3.5 Acknowledgments

Acknowledgment is made to the Donors of the Petroleum Research Fund, administered by the American Chemical Society, for the support of this research. Additional support of the research facilities at OSU by the National Science Foundation and at PNL by the Department of Energy is also appreciated.

4. High Resolution Infrared Studies of $Be(BH_4)_2$

Darren L. Williams, Abdullah Al-Kahtani, and Joseph W. Nibler*
Department of Chemistry
Oregon State University
Corvallis, OR 97331
niblerj@ccmail.orst.edu
FAX: (541) 737-2062

Steve W. Sharpe
Molecular Science Laboratory
Pacific Northwest Laboratory
Richland, WA 99352

Prepared for submission in the *Journal of Physical Chemistry*

4. High Resolution Infrared Studies of $Be(BH_4)_2$

4.1 Introduction

Few classes of compounds show as much variety in their bonding characteristics as metal borohydrides. The hydrogen bridge bonds linking boron to the metal allow ionic bonding as in the solid alkali borohydrides, tridentate covalent bonding as in the large metal borohydrides[10] -- $Zr(BH_4)_4$, $U(BH_4)_4$, and $Hf(BH_4)_4$, and bidentate covalent bonding[8,9] as in $Al(BH_4)_3$. Based on various experiments, many different bonding possibilities have been proposed for $Be(BH_4)_2$, making it "one of the most persistent problems in structural inorganic chemistry."[35] A survey of the fifty-seven year history of $Be(BH_4)_2$ reveals an array of contradictory results.

The molecule was first synthesized in 1940 by Burg and Schlesinger,[11] who made vapor density measurements establishing that the molecule is in monomeric form in the gas phase. They also suggested that the crystalline phase might be polymeric, a feature confirmed later by X-ray diffraction studies[36] which showed that the solid exists as a helical chain and vibrational spectra which suggested that the polymer consisted of coupled $BeBH_4^+ - BH_4^-$ ions.[37] The infrared spectra of the solid and vapor phases of $Be(BH_4)_2$ are quite different, implying a structural change on vaporization. However, the molecular geometry in the gas phase has proved very difficult to establish and a number of unique structures (fig. 4.1) have been considered, most with some kind of purported experimental verification.

The first infrared investigation of $Be(BH_4)_2$ was carried out by Longuet-Higgens and Bell in 1943.[38] They proposed a structure with double hydrogen bridges and D_{2d} symmetry (fig. 4.1 II). A subsequent electron diffraction experiment in 1946 was said to support such a linear B-Be-B arrangement, but with two equivalent sets of triple hydrogen bridges, yielding a D_{3d} molecular symmetry (fig. 4.1 I). However, the electron diffraction data were later reinterpreted and said to be consistent with the double bridged geometry if the bridging hydrogens were appreciably closer to B than Be.[39] In most inorganic texts, this D_{2d} structure became favored and was not questioned for more than fifteen years.

In 1967 the electron diffraction experiment was repeated[40] and, surprisingly, found to be consistent with a C_{2v} structure (fig. 4.1 IV). The radial distribution curve was considerably different and gave no indication of a long boron-boron distance. In 1972, support for this or some other polar structure came from an electric deflection observation[41] and from dielectric measurements,[42] the latter giving a value of about 2 Debye for the dipole moment. These results stimulated another electron diffraction experiment in 1973 by Gundersen *et. al.*,[43] who obtained a radial distribution curve differing from both the 1946 and 1967 results. A fit of the data was found to support a D_{3d} structure or a new structure with C_{3v} symmetry (fig. 4.1 III), which can be derived from the D_{3d} structure by displacing the beryllium along the symmetry axis.

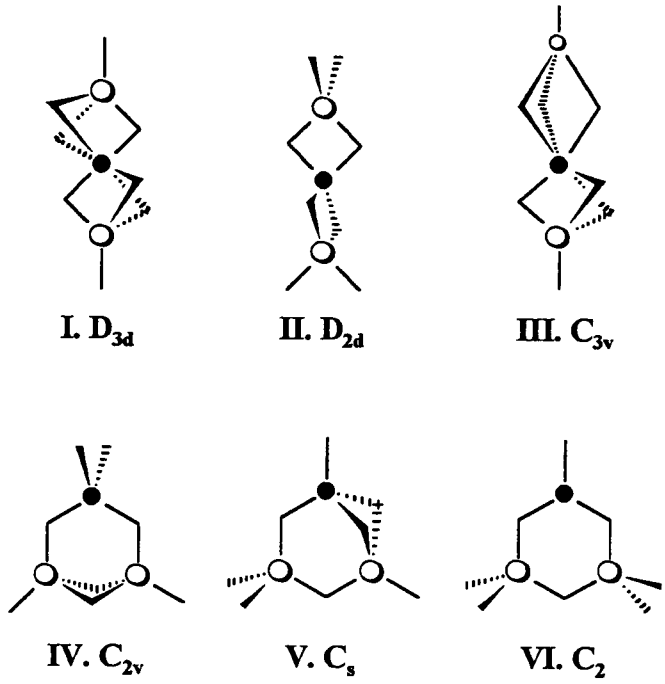

Figure 4.1: Some of the structures proposed in the literature for $Be(BH_4)_2$.

About the same period, two groups published infrared studies of isotopically-substituted beryllium borohydride in the gas phase. Cook and Morgan[44] assumed that the shapes of certain infrared peaks represented rotational contours that they suggested were consistent with a structure having C_{2v} symmetry. About two years later Nibler reported an infrared and Raman study of the gas phase and of the isotopic forms isolated in a matrix.[45] A different spectral interpretation was offered, with all observed peaks treated as separate vibrational transitions. In neither study was any rotational structure resolved in the vibrational spectra. From comparisons between vapor phase and argon matrix spectra, Nibler concluded that two structural forms might exist in the vapor, with a lower energy C_{3v} structure (fig. 4.1 III) favored in the cold matrix. A further indication that the vapor composition might be complex came from a follow-up electron diffraction study[46] in which Haaland's group showed that the diffraction pattern of $Be(BH_4)_2$ depended upon the time of sampling after preparation. This could be due to a nonequilibrium distribution of forms, or could be a result of sample decomposition. Evidence for the latter has been seen in the infrared studies, which showed that the sample undergoes reaction with salt windows and decomposes slowly on metal surfaces. That brings into question the dipole moment deduced from dielectric measurements, since these were made in a capacitance cell with metal electrodes. Several efforts to obtain microwave spectra of $Be(BH_4)_2$ were also unsuccessful, either due to absence of a dipole moment or to sample decomposition in metal waveguides.

Although the structural issue for beryllium borohydride was thus unresolved, the only new experimental work reported in the last two decades was a gas phase NMR study in 1977. In this, the molecule was found to be fluxional and the protons to be equivalent on the NMR time scale.[47] The spectra were said to be consistent with a linear BBeB skeleton, a geometry favored also in several theoretical calculations.

In 1973 Marynick and Lipscomb[48] investigated many different possible structures of $Be(BH_4)_2$ using a minimal basis of Slater type orbitals at the Hartree-Fock and configuration interaction level with single and double valence excitations (CISD). Their calculations predicted that structures I and II of fig 4.1 had relative energies of 31 and 0 kJ mol^{-1}, respectively and the other forms had significantly higher energies (>100 kJ mol^{-1}). During the same year, another theoretical study was reported by Ahlrich,[49] who used Gaussian functions and accounted for correlation with the independent electron pair approximation. He also found that the D_{2d} structure II was lowest in energy at the SCF level but when he included electron correlation, the D_{3d} form I had the lowest energy. A similar trend was observed by Ortiz and Lipscomb, who reported many-body perturbation theory (MBPT) calculations for these structures.[50] In none of these studies were the energy differences judged sufficiently accurate to discriminate between the various "linear" structures.[35]

The most recent theoretical studies were by Stanton *et. al.* in 1988[35] and 1996[51] and Bonaccorsi *et. al.* in 1991.[52] Stanton investigated structures I (D_{3d}) and II (D_{2d}) of Fig. 4.1 using MBPT with a basis set of 85 contracted Gaussian functions. Bonaccorsi et al. also investigated structures I and II for $M(BH_4)_2$ where M was Be, Mg, and Ca. Our *ab initio* calculations for the D_{3d} and D_{2d} structures of $Be(BH_4)_2$ at the MP2/6-311G** level (102 contracted Gaussians) produced geometrical parameters almost identical to those of Stanton and Bonaccorsi and these are listed in table 4.1. Stanton et al's energies at the MBPT(4) level indicated that the D_{3d} structure falls 3.8 kJ mol^{-1} above the D_{2d} structure (before zero point energy corrections) but Bonaccorsi et al.[52] found this difference to vary significantly and even change sign as the level of calculation was changed. We also see this effect with E_{D3d}-E_{D2d} differences (kJ mol^{-1}) of SCF(21.6), MP2(-3.1), MP3(-0.1), MP4D(0.7), MP4DQ(1.9), MP4SDQ(1.8), and CCSD(2.5). Such energy differences are too small to permit a confident conclusion as to which form is most stable but are consistent with the hypothesis of two coexisting structures at room temperature . However, in light of the good structural agreement with the electron diffraction results of Gundersen et al. (table 4.1) and the reasonable correlation of the *ab initio* D_{3d} frequencies with the matrix isolation infrared data (table 4.2), we will use the D_{3d} form in all subsequent simulations shown in this work.

Regarding the polarity of $Be(BH_4)_2$, Stanton et al's investigations of polar forms argued against a dipole as large as 2 Debye, showing that the energy increased significantly with axial displacement of the Be atom, rising to 84 kJ mol^{-1} for a C_{3v} structure distorted sufficiently to reproduce this moment. This energy cost was judged excessive and the authors revisited the problem in 1996[51] looking for a triangular

Table 4.1: Geometrical parameters for $Be(BH_4)_2$ calculated at the MP2/6-311G** level.

$Be(BH_4)_2$ Parameter	This Work D_{3d}	D_{2d}	e^- Diffraction Experiment[43]
r(Be-B)	1.726	1.850	1.790
r(B-H_b)	1.246	1.283	1.303
r(B-H_t)	1.179	1.192	1.16
∠(Be-B-H_b)	64.77	52.25	62.5
∠(Be-B-H_t)	180	119.9	180
A($^{11}B_2$)	2.194	1.992	2.086
B($^{11}B_2$)	.1773	.1556	.1673

Table 4.2: Wavenumbers and infrared intensities (km mol^{-1}) calculated for the D_{3d} form of $Be(BH_4)_2$ using Gaussian at the MP2/6-311G** level.

MP2/6-311G**			Experiment[45]			
D3d	ω[a]	IR Int	ω		C_{3v}	Mode Desc.
A_{2u}	2617	71	2645	ν_1	A_{1u}	νBH$_t$ asym
A_{1g}	2617		2643	ν_2	A_{1g}	νBH$_t$ sym
A_{1g}	2207		2255	ν_3	A_{1g}	νBH$_b$ sym
E_u	**2223**	**130**	**2202**	**ν_{11}**	**E_u**	**νBH$_b$ asym**
A_{2u}	**2195**	**219**	**2172**	**ν_4**	**A_{1u}**	**νBH$_b$ asym**
E_g	2188		2241	ν_{10}	E_g	νBH$_b$ asym
E_g	1313		1284	ν_{13}	E_g	δBH$_t$ sym
E_u	1288	6	1298	ν_{12}	E_u	δBH$_t$ asym
A_{1g}	1299		1105	ν_6	A_{1g}	δBH$_b$ sym
A_{2u}	1239	122	1123	ν_5	A_{1u}	δBH$_b$ sym
E_u	1105	21	1245	ν_{14}	E_u	δBH$_b$ asym
E_g	1096		1184	ν_{15}	E_g	δBH$_b$ asym
A_{2u}	1025	764	1051	ν_7	A_{1u}	BBeB st asym
A_{1g}	570		540	ν_8	A_{1g}	BBeB st sym
E_u	432	6	368	ν_{17}	E_u	bridge bend
E_g	423		386	ν_{16}	E_g	bridge bend
E_u	275	25	280	ν_{18}	E_u	BBeB bend
A_{1u}	217		---	ν_9	A_{2u}	torsion

[a] Wavenumber values scaled by 0.9427 as recommended in ref. 23.
Transitions studied in this work.

isomer which might account for the experimental evidence for a polar structure. They found that the C_s triangular structure (fig 4.1 V) was in fact a stationary point on the potential surface with no low energy pathway to the linear forms other than dissociation (65.7 kJ mol $^{-1}$) and reformation. Although this form is about 80 kJ mol^{-1} higher in energy than the linear forms and should be negligible in room temperature measurements it is a plausible sublimation product and could be a significant piece in this structural puzzle. They concluded the 1988 article by indicating that questions remained about the structure(s) of $Be(BH_4)_2$ and expressed the "sincere hope that this report will reawaken the interest of the experimental community, which has ignored this interesting problem for a decade."

Our interest in this intriguing structural problem was thus duly piqued. It is clear that none of the proposed structures has been proven. None of the electron diffraction experiments have been analyzed in terms of a two-structure hypothesis and no rotational structure was resolved in any of the vibrational spectra. Because of the fluxional character of the bonds, NMR spectroscopy gives limited information. The theoretical calculations favor linear skeletal geometries but do not confidently identify the lowest-energy form, although they raise legitimate questions about the polarity of the molecule(s). Since microwave spectroscopy is only feasible for polar structures and is problematic because of the decomposition of $Be(BH_4)_2$ in metal systems, high resolution vibration-rotation spectroscopy would seem to offer the best hope of ascertaining whether two forms coexist and of determining their symmetries and perhaps bond lengths. In fact, infrared and coherent Raman instruments now exist with a sensitivity adequate for study of gas phase samples at pressures of a few Torr, and with 0.001 cm^{-1} resolution, about 3 orders of magnitude better than that available in all earlier vibrational studies. Recent microwave pure rotational[20] studies of $LiBH_4$ and the other alkali metal borohydrides indicate that torsional and tumbling splittings of the ground vibrational states are very small, but theoretical[19] calculations suggest that such splittings in higher vibrational levels might be observed with this resolution. To our knowledge, no such vibrational spectra have been obtained for the alkali metal borohydrides, probably because of their very low vapor pressure. Considerably more volatile are $Be(BH_4)_2$ and $Al(BH_4)_3$, compounds that we have recently reexamined at high resolution. The present work describes efforts to obtain vibration-rotational fine structure for $Be(BH_4)_2$ using FTIR and IR diode laser spectroscopy at a resolution down to 0.001 cm^{-1}, along with some further *ab initio* calculations.

4.2 Experimental

$Be(BH_4)_2$ was prepared via the solid-state metathetic reaction of beryllium chloride and lithium borohydride, following the method of Schlesinger *et. al.*[21] Because of the flammable nature of the molecule, all reactants were handled in a dry bag and the reaction was carried out in a hood using a greaseless vacuum system. In the dry bag, one gram of anhydrous $BeCl_2$ (99.5% Aldrich Inc.) and four

grams of anhydrous lithium borohydride (95% Alfa) were mixed in a reaction tube. This was then attached to a vacuum line, evacuated, and then slowly heated over eight hours to 140° C while pumping. Volatile $Be(BH_4)_2$ and B_2H_6 products were condensed in a trap at 77 K and the diborane was then removed by warming the trap to about 200 K. $Be(BD_4)_2$ was made by the analogous reaction of $BeCl_2$ with $LiBD_4$ and purified by a similar procedure.

Gas phase NMR spectra of 400 Torr B_2H_6 and 8 Torr $Be(BH_4)_2$ were recorded using a Bruker AM-400 FT-NMR spectrometer and a 15 mm diameter gas sample tube. The purpose was to characterize the $Be(BH_4)_2$ compound using ^1H and ^{11}B spectra. The diborane was used to calibrate the chemical shifts in the $Be(BH_4)_2$ spectra, and to test the sensitivity of the instrument.

Survey infrared spectra were recorded using a Mattson Sirius 100 FTIR spectrometer, which has a resolution of 0.125 cm^{-1}. Samples at 5-10 Torr pressure were placed in 10 or 20 cm cells equipped with sapphire windows, a material found to not react with $Be(BH_4)_2$. High resolution infrared spectra were also recorded at Pacific Northwest Laboratories (PNL) using a Bruker IFS 120 HR FTIR spectrometer at a resolution of 0.0015 cm^{-1} and a wavenumber accuracy of 0.001 cm^{-1}.

Infrared laser-diode spectra were also collected at Pacific Northwest Laboratories, using a spectrometer system developed by Steve Sharpe.[22] This consists of a Laser Photonics cold head mounted on an optical table and containing up to four laser diodes. The output of a selected diode is collimated and directed into a 0.5 meter monochromator, the output of which is intercepted by a rotating gold-coated aluminum sector. The sector intercepts and directs the laser light 1/3 of the time to a reference cell, 1/3 of the time to a 0.25 meter confocal etalon, and the rest of the time into the vacuum chamber where it intercepts the effluent of a pulsed, slit nozzle of 100 mm length. Two BaF_2 windows are used to couple the laser light into and out of the expansion chamber where it is multipassed up to 32 times using a White cell configuration. Each InSb detected channel is sampled 4096 times at 200 ns intervals by three parallel digitizers that are interfaced through a CAMAC crate to a PC. The pulsed valve and the three digitizers are synchronized with the angular position of the rotating mirror sector using a microprocessor. Finally, signal averaging is done by the real-time, co-addition of individual spectra over five to ten gas pulses.

4.3 Results And Discussion

4.3.1 NMR Results.

Our diborane spectra closely match the reported NMR results. The terminal and bridging hydrogens were clearly distinguished and the sensitivity of the instrument proved to be excellent for our gas phase studies. The ^1H and ^{11}B NMR gas phase spectra of $Be(BH_4)_2$ also matched the results of an

earlier gas-phase study.[47] The proton spectrum was a 1:1:1:1 quartet, indicating that all four protons about the ^{11}B (I=3/2) nucleus are equivalent on the NMR time scale. The quartet is centered at 0.04 PPM relative to TMS and the coupling constant is J_{BH} = 86 Hz. Also, there is evidence of a weak contribution due to coupling with ^{10}B (I=3) in the sample, which should result in a weaker, overlapping septet. The proton spectrum shows the presence of a small amount of diborane produced as a result of the slow decomposition of $Be(BH_4)_2$ over time. This served to calibrate the chemical shifts.

The ^{11}B spectrum of $Be(BH_4)_2$ consists of a 1:4:6:4:1 quintet as a result of the presence of two equivalent boron nuclei, each coupled to four equivalent protons (J_{BH} = 86 Hz). The ^{11}B spectrum did not show appreciable diborane impurity and the chemical shift of ^{11}B is less certain. However, the proton chemical shift and the coupling constants are the same as those of the previous NMR study, and we assume that the boron chemical shift to be a value of 36.2 PPM (BF_3:OEt_2 = 0) reported by Gaines *et. al.*[47]

The possible presence of two distinct forms of $Be(BH_4)_2$, which was proposed in reference 45, was tested by changing the sample temperature. On heating, the equilibrium between the two forms will be altered and such a change might be apparent in the NMR spectrum. Accordingly, the proton NMR spectrum was recorded at 298, 320, and 330 °C. Other than an improvement in signal-to-noise ratio at the higher temperatures, due to a higher vapor pressure, there was no discernible change in the NMR spectra as a function of temperature. Thus, if two structures exist at comparable concentrations, they are magnetically equivalent on the NMR time scale.

It is interesting that, for both proton and ^{11}B spectra, there was no indication of coupling with ^{9}Be, which has a nuclear spin of 3/2. This absence of Be coupling has also been noted for alkyl beryllium hydrides, where it is attributed to quadrupolar broadening.[47] An attempt was made to record the ^{9}Be NMR spectrum of $Be(BH_4)_2$ at 56.226 MHz, but no peak was observed for the gas phase sample. A very weak peak of ^{9}Be was seen in a solution of $BeCl_2$ dissolved in sulfuric acid. The weakness of this ^{9}Be resonance, even in concentrated solutions, is consistent with not seeing it for $Be(BH_4)_2$.

Based on the NMR results, our conclusion is that the NMR spectra are disappointingly uninformative regarding the possible $Be(BH_4)_2$ structure(s). The spectra indicate magnetically-equivalent borohydride groups so that, within each borohydride group, rapid internal hydrogen exchange must be taking place. No distinction can be seen between bridge and terminal hydrogens, nor between borons in possible asymmetric polar structures such as III and V in figure 1. If these structures exist, the NMR results would require rapid tunneling motion of the heavy Be atom. Also, any mechanism involving rapid transformation from one linear conformation to another (i.e. tridentate to bidentate and back) is consistent with the observed NMR spectra so that the possible coexistence of two structural forms can not be excluded. It was hoped that high resolution infrared spectroscopy, a faster probe of molecular geometry, might be more illuminating.

4.3.2 FTIR Spectra of $Be(BH_4)_2$

The spectra collected at OSU at a resolution of 0.125 cm^{-1} showed no resolved rotational fine structure although this instrument did display such structure for allene, a molecule with similar rotational constants. It is of course possible that congestion due to hot bands and to the different boron isotopic forms of $Be(BH_4)_2$ would blur the spectrum enough that 0.125 cm^{-1} resolution would not be sufficient.

A spectrum recorded on the Bruker IFS 120 HR for 8 Torr of $Be(BH_4)_2$ in a 10 cm cell is shown in figure 4.2. This single beam trace has been "deresolved" to eliminate background H_2O and CO_2 lines and to emphasize the broad $Be(BH_4)_2$ features, which are the same as those reported in reference 45. One cm^{-1} portions of several of the major features at the full 0.0015 cm^{-1} resolution are given as insets in the figure. The sharp features are due to background water (1870 cm^{-1}) in the evacuated spectrometer and diborane (2520 cm^{-1}) from the decomposition of $Be(BH_4)_2$. Other features of B_2H_6 contaminant are shown in figure 4.3. The line width of these lines (0.008 cm^{-1}) establishes the limiting peak resolution, which is due to the convolution of the instrumental resolution, the collisional width (estimated to be <0.002 cm^{-1}), and the Doppler width (about 0.007 cm^{-1} at 1900 cm^{-1} for H_2O and 0.008 cm^{-1} at 2500 cm^{-1} for B_2H_6). The Doppler width for $Be(BH_4)_2$ is about 0.006 cm^{-1} at 2200 cm^{-1} and the collisional broadening in this nonpolar molecule is likely to be comparable to that in diborane. However, the underlying absorption is essentially continuous. The expanded traces at 2200, 2167, and 2070 cm^{-1} are representative of the lack of resolved rovibrational structure throughout the strong $Be(BH_4)_2$ absorptions.

At 0.0015 cm^{-1} resolution one would expect to easily resolve the P and R rotational lines with predicted spacings of about 0.4 cm^{-1} for D_{2d} and D_{3d} forms. For example, for the D_{3d} parallel B-H bridge stretching mode ν_4 of A_{1u} symmetry, P-Q-R branch contours should be observed, with Q at about 2172 cm^{-1} and a separation of ~17 cm^{-1} between P-R maxima. For the E_g perpendicular band ν_{11} one expects dominant Q branch structure at about 2202 cm^{-1} with large spacings of about 2(A-B) ~4 cm^{-1}. These broad predictions should remain valid with the presence of coriolis interactions and centrifugal distortion effects, but the P and R branch regularity would be modified if the values of the vibration rotation interaction constants (α_i) are large. To judge the likely size of these constants an analysis of the ν_{16} parallel band Q branch K structure of diborane (figure 4.3(a), 2525 cm^{-1}) was done which showed that the (α_A-α_B) difference is substantial, 0.0154 cm^{-1}. In the same Q branch region the J splittings (4.3(b)) give a value for α_B = 0.0007 cm^{-1} making α_A=0.0161 cm^{-1}. A similar analysis of J differences in the diborane ν_8 $^RQ_0$ sub-band (figure 4.3(c), 2612 cm^{-1}) gave a larger α_B of 0.0024 cm^{-1}. Reported values[53] for the analogous modes of allene are very similar. (α_A=0.0242 and 0.0156 cm^{-1} and α_B=0.000605 and 0.00036 cm^{-1} for ν_5 and ν_8 respectively) Although, α_B varies substantially, values as large as 0.02 cm^{-1} seem possible for both α_A and α_B. For such large α parameters, less regularity will be seen in the spectra

and band heading may be visible at room temperature. However, as illustrated by the expanded traces in figure 4.2, a careful search of the broad contours revealed no resolved rotational structure for $Be(BH_4)_2$, and hence other sources of spectral congestion must be explored.

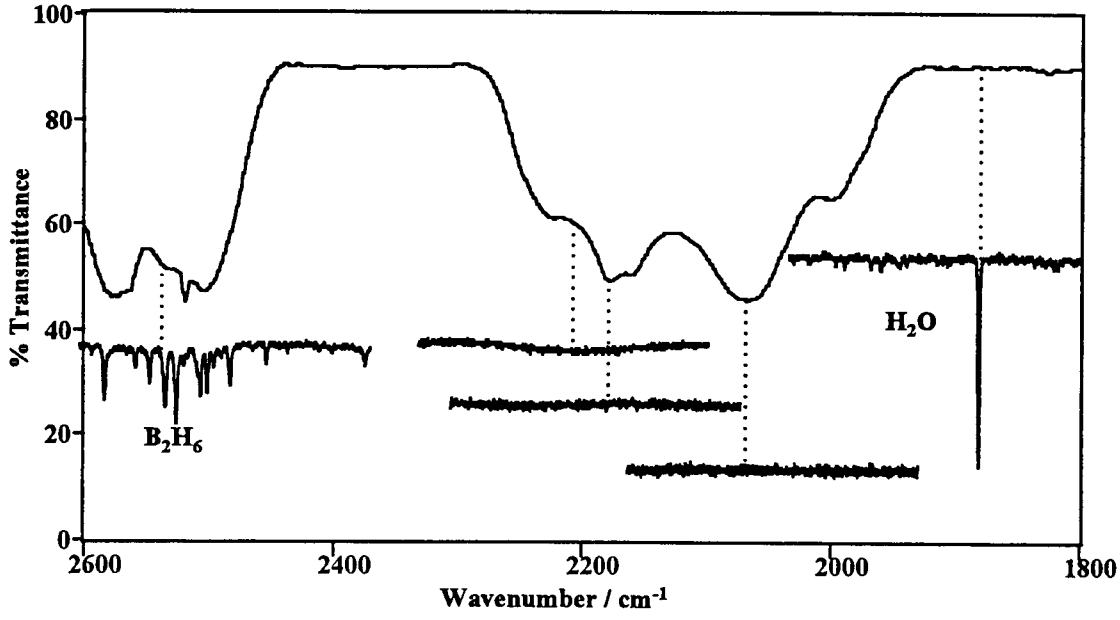

Figure 4.2: Room temperature FTIR spectrum of $Be(BH_4)_2$. The expanded one cm^{-1} regions at 0.0015 cm^{-1} resolution have an ordinate multiplication factor of 100. Rovibrational structure can be easily seen for background water and for the decomposition product B_2H_6. The strong absorptions by $Be(BH_4)_2$ show no rovibrational structure.

4.3.3 Isotopic Contributions to Spectral Congestion

The absence of any resolved ro-vibrational structure is very unusual for a molecule the size of $Be(BH_4)_2$. Some of this congestion of course comes from the three isotopic combinations of boron—$^{11}B_2$ (64%), $^{11}B^{10}B$ (32%), $^{10}B_2$ (4%), each with vibrational shifts that vary for the different modes. The minor $^{10}B_2$ form is neglected in the following. The vibrational frequencies and the ^{10}B vibrational shifts were calculated for the D_{3d} structure at the MP2 level with a 6-311G** basis set. Frequencies and intensities for the $^{11}B_2$ form are listed in table 4.2, with the former scaled by about 0.9 according to common practice.[23] The $Be^{10}BH_4{}^{11}BH_4$ frequencies were 4.7 and 0.45 cm^{-1} higher for the ν_{11} and ν_4 modes respectively. The geometries and the Cartesian forces were used to calculate centrifugal distortion constants and first order coriolis coupling constants via the Asym40 normal coordinate program of

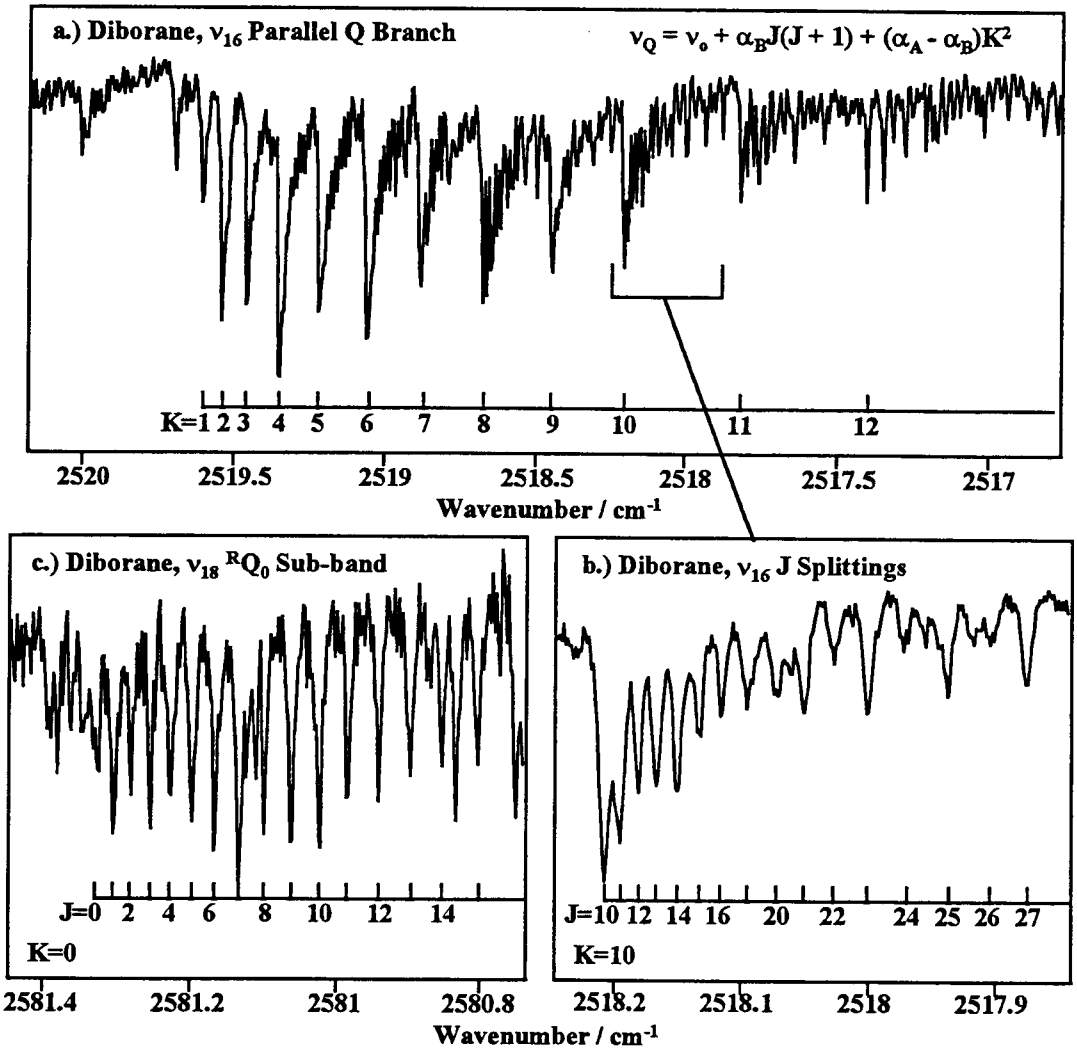

Figure 4.3: Rovibrational structure seen for diborane contaminant in the FTIR spectrum of $Be(BH_4)_2$. The differences in K sub-bands (a) give α_A-α_B = 0.0154 cm^{-1}, and in the same band, J differences give α_B=0.00069 cm^{-1} resulting in α_A=0.0161 cm^{-1}. A similar analysis of the $^RQ_0$ perpendicular sub-band of diborane gives α_B=0.0024 cm^{-1}.

Hedberg and Mills[26]. The vibration-rotation coupling constants α_i were also calculated for the normal modes but these values were an order of magnitude smaller than those for allene and diborane, presumably due to neglect of anharmonicity. Therefore, values representative of those measured for diborane and allene (α_A = 0.02 cm^{-1} and 0.0009 cm^{-1}) were used for the preliminary simulations for the spectra of $Be(BH_4)_2$.

The results of these calculations are listed in table 4.3 and are utilized in the combined simulations for both isotopic forms shown in figure 4.4(b. and c.) in comparison to the experimental

Table 4.3: Rotational parameters (cm^{-1}) of the most abundant isotopes of $Be(BH_4)_2$.

Rotational Parameter[a]	$Be^{11}B_2H_8$ (64%)	$Be^{10}B^{11}BH_8$ (32%)
A"	2.194	2.194
B"	0.1773	0.1832
D_J"	5.69e-8	6.04e-8
D_{JK}"	8.46e-7	8.99e-7
D_K"	8.34e-6	8.29e-6
ζ_{11}	0.0566	0.0482

[a] Based on MP2/6-311G** results and ASYM40.
In addition to these constants vibration-rotation coupling constants of α_A = .02 cm^{-1} and α_B=0.0009 cm^{-1} were assumed for all modes.

region of interest near 2200 cm^{-1}, 4.4 (a.). The simulations show that the P-R contours of ν_4 should be clearly discernible and the overall match to the experimental band contour is remarkable, even though individual lines are not discernible. Part of this spectral congestion must arise from hot bands, and the *ab initio* calculations were also useful in estimating the contributions of these to spectral congestion.

4.3.4 Hot Band Contributions to Spectral Congestion

The *ab initio* calculations for the D_{3d} form of $Be(BH_4)_2$ predict that four of the vibrational modes lie below 500 cm^{-1}, and same is true for the D_{2d} form. From these values, we compute that less than 30 % of the molecules are in the ground state at room temperature. Overtone and combination bands with these low frequency transitions will lead to many overlapping hot bands, each with small, unknown shifts due to anharmonicity. Such hot bands could well blur the P-Q-R contours of the vibrational transitions, as would overlap of high J, K rotational lines at room temperature. Since both effects would be greatly reduced at low temperatures, an experiment was done in which beryllium borohydride was expanded in a free jet and probed by high resolution diode laser spectroscopy.

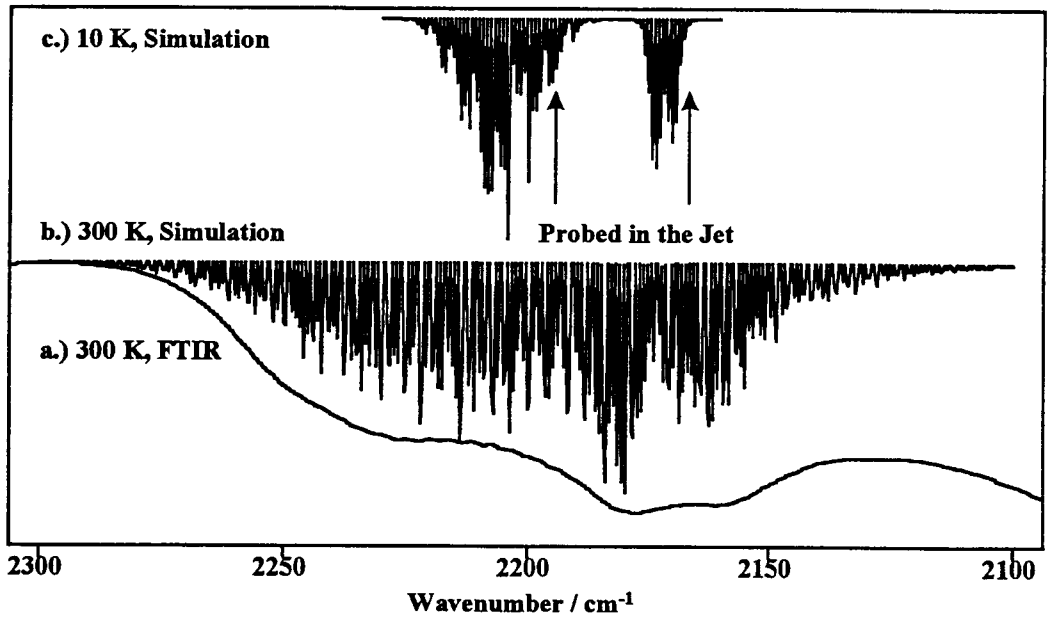

Figure 4.4: FTIR spectrum of $Be(BH_4)_2$ compared to a non-rigid rotor simulation of the E_u band (2202 cm^{-1}) and the A_{2u} band (2172 cm^{-1}). Although no rotational fine structure is resolved, the general rotational contours match those of the simulation. The band centers for the simulations are the reported matrix frequencies, which are typically subject to shifts of 1 to 10 cm^{-1} from gas phase values. Two regions found to give significant absorption in the jet expansion are indicated by arrows and were studied in detail.

4.3.5 Diode Laser Spectra of $Be(BH_4)_2$ Cooled in a Jet

The samples of 1% $Be(BH_4)_2$ in Ar were prepared by flowing 500 Torr of argon through a U-tube containing solid $Be(BH_4)_2$ at 20 °C (5 Torr vapor pressure). From other work with the PNL jet apparatus, such conditions are known to produce mainly monomeric samples with rotational temperatures of about 10 K. At this temperature the collisional width will be negligible, and the Doppler width will be less than 0.001 cm^{-1}, the resolution of the diode sources. A typical line width measured with this apparatus for isolated lines of other molecules is 0.002 cm^{-1} FWHM[22].

The bridge-stretching region around 2200 cm^{-1} was a logical choice for this diode study because it lies in a region accessible by the diode sources and it is free from overlapping bands of water or diborane. The diode laser was coarsely tuned over the region 2160 to 2240 cm^{-1} and was then scanned over selected 0.4 cm^{-1} portions, which showed beautiful but complex rotation vibrational structure. The absorptions were easily visible on the oscilloscope screen and the data collected for a typical scan are illustrated in figure 4.5. Scans with the jet off (4.5(a)) confirmed that the lines were due to sample

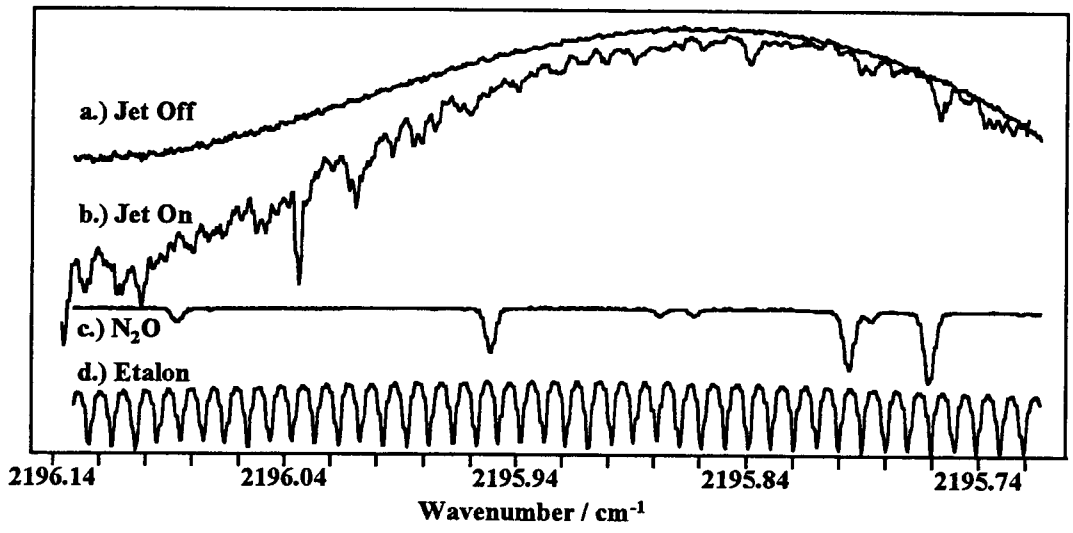

Figure 4.5: Sample data scan of $Be(BH_4)_2$ in a jet expansion after linearization to the etalon trace (d) and calibration to the N_2O (c). The top trace (a) was taken with the jet off to ensure that the strong absorptions (b) were due to the sample.

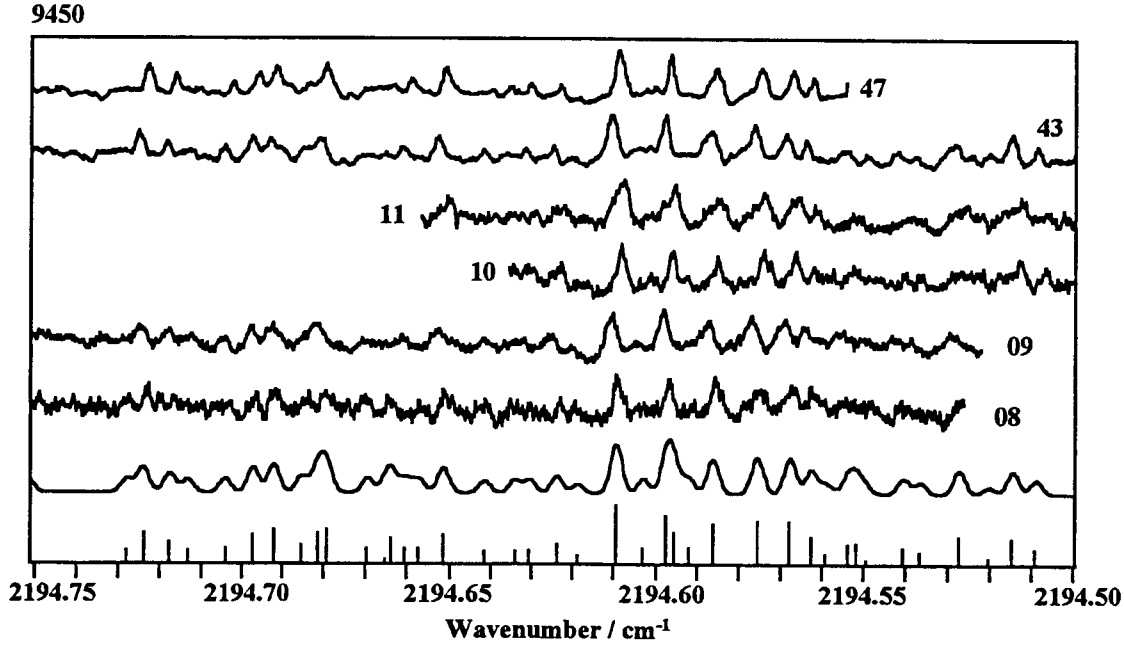

Figure 4.6: Panel 9450, taken from the spectral atlas in appendix B, shows the reproducibility of the jet spectra of $Be(BH_4)_2$ and the richness of the spectrum. The bottom two traces are the peak table stick spectrum and its noise-free convolution (Gaussian, FWHM=0.003 cm^{-1}).

absorption. Each frequency sweep consisted of a sample scan (4.5(b)), an etalon trace (c) for frequency linearization, and an N_2O reference scan (d) for absolute frequency calibration. Only 5 to 10 laser shots were averaged, to prevent degradation of the line widths due to laser drift. Figure 4.6 shows the reproducibility of the scans and demonstrates the richness of the spectrum.

Due to the limited amount of sample and the hazardous nature of the compound, only one experiment was done. In all, forty-seven scans were taken in two regions (2164-2167 cm^{-1} and 2193-2197 cm^{-1}) with ample overlap to aid in the assembly of an overall spectrum (figures 4.7 and 4.8). After linearization and calibration each transition in the sample trace was located by least squares fitting of the line to a Gaussian function. Appendix B contains a table of 1246 frequencies and intensities as well as panels displaying all of the calibrated sample scans.

4.3.5.1 Parallel Band Analysis

From the matrix work in ref. 45 and from our Gaussian calculations, the 2164 cm^{-1} region is expected to contain a parallel band, with definite P and R patterns. One expects clusters of triplets spaced by about 2B (0.35 cm^{-1}) and consisting of the K=0,1,2 lines spaced by $(\alpha_A-\alpha_B)$ and $3(\alpha_A-\alpha_B)$, 0.02 and 0.06 cm^{-1}, respectively. If the band origin is captured one expects a Q branch similar to that shown for ν_{16} in diborane (figure 4.3), but with only the K=1 and 2 sub-bands due to the low temperature (K=0 is forbidden). The sub-bands would contain up to seven J lines each with very small separations, $-\alpha_B(2J+1)$. In an effort to identify any predictable pattern both regions of the jet spectrum were printed in 0.25 cm^{-1} panels and taped together to form two ten foot long displays. This composite spectrum, at a more convenient scale, and the expected trends are shown in figure 4.7. The simulation shows the expected patterns, including the $Be^{10}BH_4{}^{11}BH_4$ contributions, marked with an "*". Neither these patterns nor those of any other familiar band structure could be identified in the parallel band region. The line density (~178 lines/cm^{-1}) was much greater than predicted by the 10 K simulations and the large separation expected in the triplet patterns make their detection impossible. Also, because fewer scans were taken in this region than in the perpendicular band region, the reproducibility of this data was not easily judged.

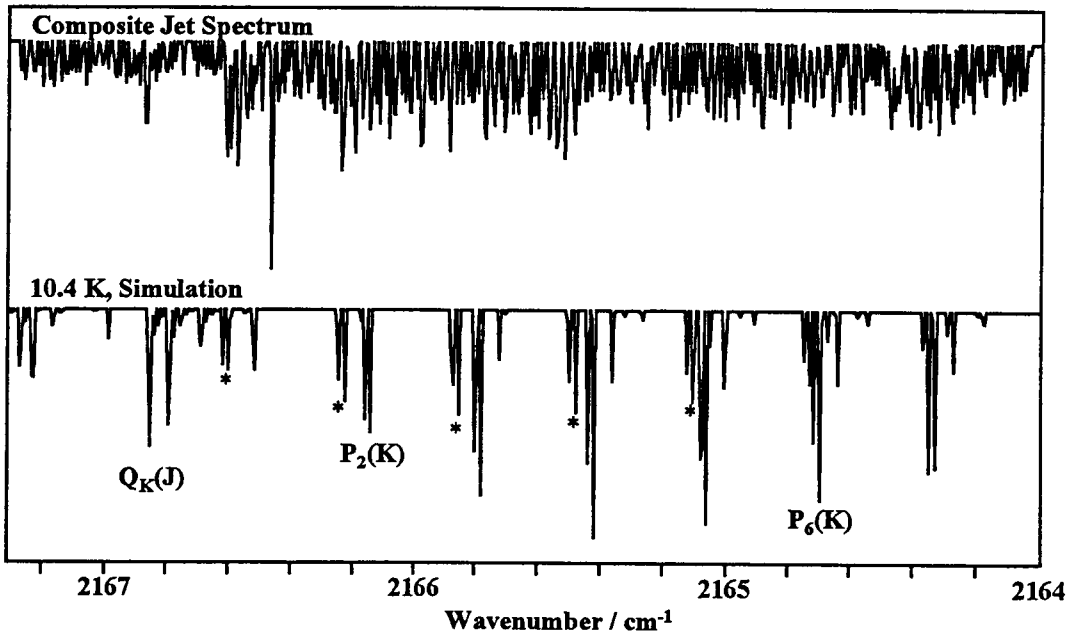

Figure 4.7: Parallel band region of $Be(BH_4)_2$. No recognizable features were found in this region due to the high density of lines. The lower simulated trace shows the patterns expected for a non-rigid rotor in this region, with no meaning to be attached to the absolute positions. The ^{10}B P branch transitions are marked with an * in the simulation and are based on the *ab initio* isotopic shifts.

4.3.5.2 Perpendicular Band Analysis

For the 2194 cm^{-1} perpendicular band, the Q branches for different K values should be spread throughout the whole band, with a spacing of $2(A'(1-\zeta)-B')$ ~4 cm^{-1}. Thus, in the 4.5 cm^{-1} scan region we predict at least one and possibly two perpendicular Q branches, with the same J splittings as that expected in a parallel band Q branch. The perpendicular band P and R branches would give similar spacings as the parallel P and R but without the triplet K structure. These predictions are shown in comparison to the jet data in figure 4.8; the excess density of experimental lines is again obvious. No obvious P or R sequence could be found that fit the regular pattern of the simulations. However, the pattern shown in figure 4.6 kept drawing our eye. This resembled a "backward" Q branch, one which extends toward higher wavenumber values. For this effect one must assume a negative value for α_B meaning the rotational constant **increases** with vibrational excitation, rather than decreases, as seen for B_2H_6. That some contraction of the Be-B distance might occur as the ring B-H stretch is excited does not seem unreasonable. Accepting this as a possibility, the usual equation for a Q branch sub-band was used for the assignment of this feature.

$$^{R}Q_{K}(J) = \nu(K) - \alpha_{B}J(J+1) \qquad (4.1)$$

Linear regressions in -J(J+1) were performed for the five most likely Q branch possibilities, {$^{P}Q_{2}$, $^{P}Q_{1}$, $^{R}Q_{0}$, $^{R}Q_{1}$, $^{R}Q_{2}$}. Here, the K'' value is shown as a subscript and the ΔK = + or - 1 choice is indicated by superscript R or P, respectively. The $^{R}Q_{0}$ assignment had the best statistics (R^2 = 0.99966) and random residuals, giving $\nu(0)$ = 2194.55715 (60) and α_B = -0.000938 (13) cm^{-1}. The errors (2σ) in parentheses increased by an order of magnitude for the other assignments.

The line strength and Boltzman factors for this assignment $^{R}Q_{0}$ were then used to deduce a rotational temperature in the range 10.4 K. to 12.5 K, the former obtained without inclusion of the J = 6 and 7 peaks, which had higher intensities than predicted. In view of the line density, some intensity anomalies could be expected but, regardless the temperatures are in good accord with that expected for the expansion conditions used in this experiment.

It should be noted that the $^{R}Q_{0}$ branch is at the low wavenumber end of this scan region so that, depending on the magnitude of the coriolis coupling constant, one might also expect another Q branch on the high wavenumber end. Also, even though the ab initio results predict an isotopic shift of 5 cm^{-1}, this could be an overestimate so that the ^{10}B Q branch might be present with an intensity half that of the one for ^{11}B. Another Q branch candidate was in fact found at 2197.26 cm^{-1}. This Q branch could be either ^{11}B $^{R}Q_{1}$ or ^{10}B $^{R}Q_{0}$ since the other possible assignments (^{10}B $^{P}Q_{1}$ or ^{10}B $^{P}Q_{2}$) would have much lower intensity at 10 K. One expects an intensity ratio of this Q branch to the one already identified of 0.5 if due to ^{10}B and 0.6 if due to ^{11}B. The measured ratio of the intensities of the bands is 0.6, favoring the latter choice, but the possibility of intensity perturbations such as those seen in the ^{11}B $^{R}Q_{0}$ branch makes us cautious in this comparison. A better basis for choice between these assignments is their fit to equation 4.1. The ^{11}B $^{R}Q_{1}$ assignment with a $\nu(1)$ = 2197.2648 (15) cm^{-1} and an α_B = -0.000819 (36) cm^{-1} were found to reproduce the line spacing much better than the ^{10}B $^{R}Q_{0}$ assignment. Also, the α_B is close to that derived from the other Q branch and slightly smaller, whereas with ^{10}B one expects a larger α_B due to the larger rotational constant. Table 4.4 contains a summary of the assignments and the index numbers used in appendix B.

With the assignment of two Q branches of the same molecule one can take the difference between Q lines with the same J quantum number to get the D_{JK} centrifugal distortion term using the following equation.

$$^{R}Q_{1}(J) - {}^{R}Q_{0}(J) = \nu_{K}^{sub} - 2D_{JK}J(J+1) \qquad (4.2)$$

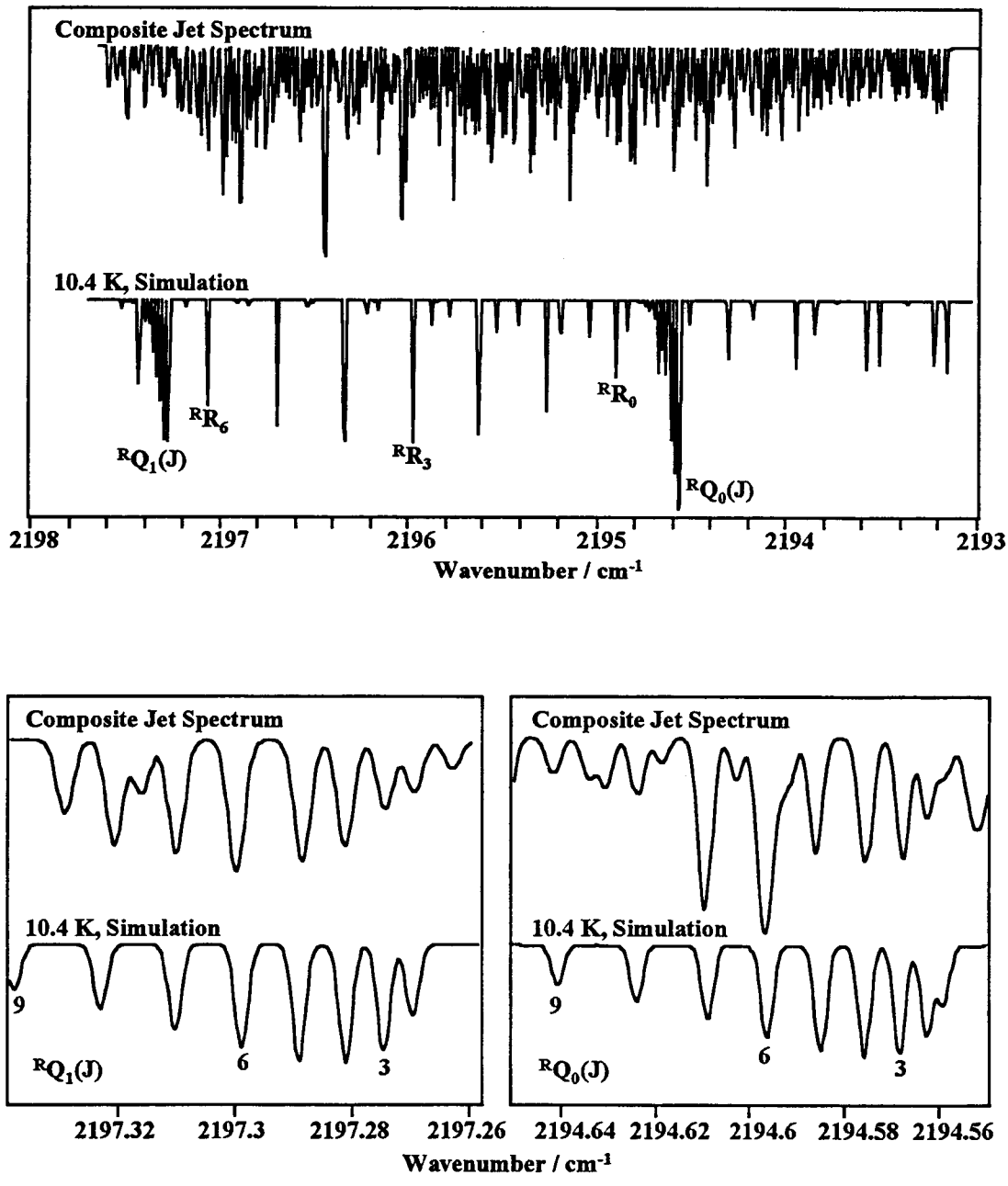

Figure 4.8: Composite jet spectrum of the perpendicular band of $Be(BH_4)_2$. The 10.4 K simulation below shows our assignment of the two Q branches. That above shows the entire band with the expected R branch progression.

where $D_{JK}' = D_{JK}''$ is assumed. The linear regression of the differences in -2J(J+1) gives a ν_{sub} = 2.7074 (8) cm^{-1} and a D_{JK} = 0.000066 (9) cm^{-1}. This value of D_{JK} is about one hundred times larger than that estimated by Asym40, but for such a fluxional molecule, reasonably large centrifugal distortion constants may not be unreasonable. The separation between Q branches, ν_{sub}, yields a coriolis coupling constant ζ = 0.291 and a band origin ν_0 = 2193.8 cm^{-1}, assuming our *ab initio* values of A'', B'', and α_A. Use of the electron diffraction rotational constants A'' and B'' give values of ζ = 0.258 and ν_0 = 2193.7 cm^{-1}. This band origin is in good accord with the 2202 cm^{-1} peak assigned for this mode for $Be(BH_4)_2$ in an argon matrix[45].

With these features identified we began looking for related trends, such as regular $^RR_0$ structure that originates at 2194.55715 cm^{-1} and walks up the spectrum in 2B increments of 0.33 to 0.36 cm^{-1} the former predicted by the electron diffraction results and the latter from our calculations (table 4.1). With this density of lines there were many candidates, but none of the progressions matched the intensity profile shown in figure 4.8 well enough to permit a confident assignment.

The high density of lines and irregular structure is not surprising in light of the recent work by Ohashi et al.[19] and Hirota[54] on molecules with loosely-bound tetrahedra like Ar-SiF_4. Ohashi et al. concluded that the traditional method of assigning a new spectrum by grouping rotational lines into branches characterized by effective B values in the upper and lower state will have limited usefulness for molecules with low barriers to internal motion. The analysis in such cases is formidable and is strongly dependent upon the potential function. As a partial step toward understanding this function, an analysis of the magnitude of torsional and tumbling barriers was undertaken.

Table 4.4: Q branch assignments for the $Be(BH_4)_2$ ν_{11} BHb bridge stretch perpendicular band. The index column contains the line number used in appendix B. The residuals (obs. - cal.)are reported in parenthesis.

	K''=0			K''=1	
J''	Index	ω	J''	Index	ω
1	678	2194.55904(1)			
2	679	2194.56277(-1)	2	1201	2197.26972(-5)
3	680	2194.56777(-64)	3	1202	2197.27459(-9)
4	681	2194.57558(-34)	4	1203	2197.28152(29)
5	682	2194.58617(87)	5	1204	2197.28878(-64)
6	685	2194.59731(75)	6	1205	2197.30014(90)
7	687	2194.60956(-14)	7	1206	2197.31030(-41)
8	689	2194.62412(-59)			
9	692	2194.64168(8)			

4.3.6 Potential Energy Calculations

Ab initio calculations were done on a DEC Alpha workstation and also on an Intel Pentium Pro 200 MHz system utilizing the Gaussian model[30,31] CCSD/6-311G**//MP2/6-311G** for all geometries, frequencies, and Cartesian forces. The geometry optimizations and analytical frequency calculations were done with no symmetry constraints on structures I and II of figure 4.1.

The potential energy of the torsional and tumbling motion was completely mapped using a z-matrix input to fix each BH_4 unit to a reference bridge hydrogen. The torsion angle θ was defined as the dihedral angle (Hb-B-B-Hb) between the reference Hb on each BH_4 unit. All bond lengths and angles were fixed as θ was varied from 0 to 180 . The tumbling coordinate was also mapped by increasing the angle ϕ (Hb-B-Be) of the reference Hb a small amount and scanning the torsional angle through 180 . The bond lengths and angles were scaled linearly for each ϕ increment so the structure would move smoothly from D_{3d} at $\phi = 65$ (fig 4.1 I) to D_{2d} at $\phi = 120$ (fig 4.1 II). The potential energy as a function of both coordinates is shown in figure 4.9. From this analysis we conclude that the lowest potential barrier separating minima of the BH_4 orientations is the three-fold torsion with a barrier of 690 cm^{-1} (8.24 kJ mol^{-1}). All bond lengths and angles were then optimized at the maximum of the three-fold torsion ($\theta = 0°$, $\phi = 65$) via the QST3 transition state searching method.[31] High level single point energies were obtained at $\theta = 0°$ and 60° using a coupled cluster calculation with single and double substitutions (CCSD). The rest of the potential surface points along the torsional path were then scaled to the CCSD maximum with the minimum set to zero, and the resulting surface data was fitted with a Fourier series of cosines by least squares minimization,

$$V(\theta) = \sum_{k=0} \frac{V_k}{2}(1 - \cos(k\theta)) \qquad (4.3)$$

An adequate representation of the shape of this torsional potential was obtained for V_k values of V_0 = 681.85 cm^{-1}, V_3 = -681.85 cm^{-1}, V_6 =-4.0437 cm^{-1}, and this function is plotted in figure 4.9.

To calculate the effect on the torsional energy levels, the optimized potential function was added as a perturbation to a simple internal rotor Hamiltonian,

$$\hat{H} = \hat{T} + \hat{V} = -\frac{\hbar^2}{2I}\frac{\partial^2}{\partial\theta^2} + \sum_{k=0,3,6} \frac{V_k}{2}\left(1 - \cos(k\theta)\right) \qquad (4.4)$$

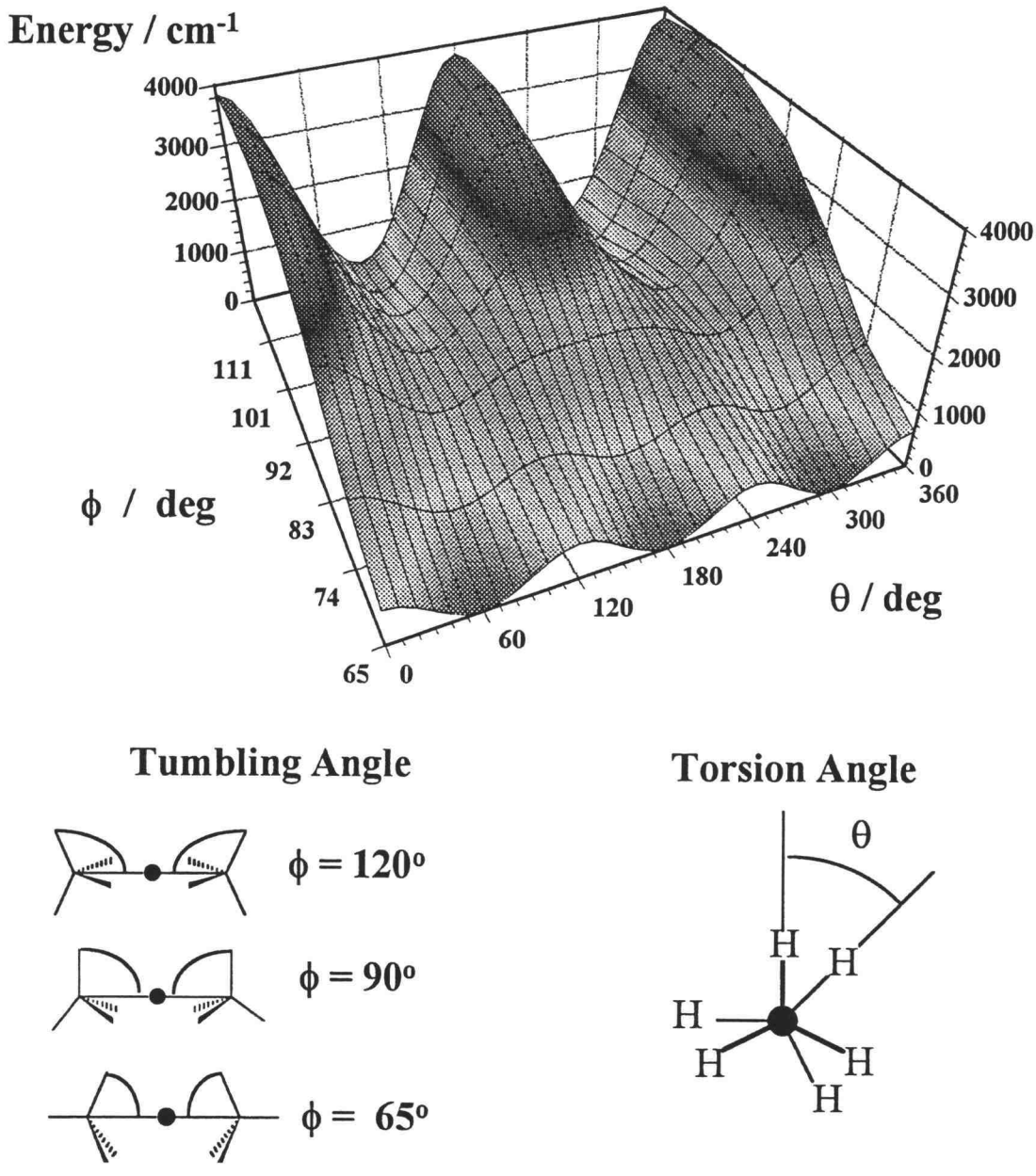

Figure 4.9: The torsional and tumbling potential energy surface for $Be(BH_4)_2$. The energies were calculated at the MP2/6-311G** level. The three-fold torsional barrier is 690 cm^{-1}, the two-fold torsional barrier is 3600 cm^{-1}. The energy difference between the D_{2d} and D_{3d} structures is 260 cm^{-1} and the barrier to interconversion from D_{3d} to D_{2d} is 1150 cm^{-1}.

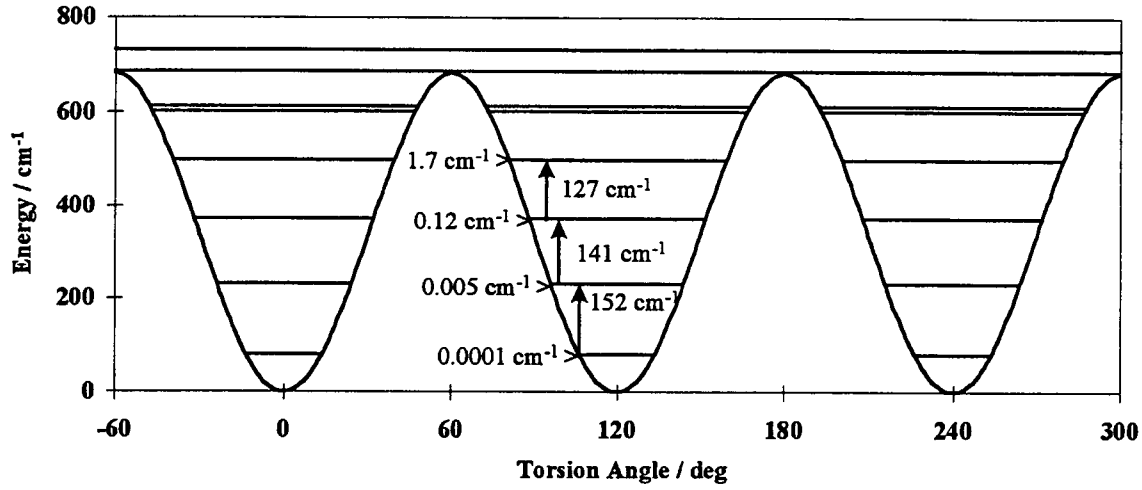

Figure 4.9: The potential energy of the D_{3d} torsion of $Be(BH_4)_2$. The potential was generated from equation 4.1 with $V_0 = 681.85$ cm^{-1}, $V_3 = -681.85$ cm^{-1} , $V_6 = -4.0437$ cm^{-1}.

where the reduced moment of inertia I was taken to be one half the moment of inertia of one BH_4 unit about the Be-B axis. The matrix elements of this Hamiltonian in a free rotor basis are easily calculated[34]. The resultant matrix was diagonalized numerically using Maple V and the basis set size was increased until the lowest twelve energy levels converged to less than 0.0001 cm^{-1}. The energy levels are overlaid with the potential in figure 4.9 to show the splitting pattern near the minima.

Figure 4.9 shows that the torsional ground state splittings are indeed small (0.0001 cm^{-1}) and would not be seen with our resolution. This need not be true for the upper vibrational states of the transitions examined. The apparent J regularity of the Q branches we see for the perpendicular transition, if real, would seem to indicate some cancellation of level shifts in the upper and lower states, a cancellation which is lost when J changes, as for P and R transitions. Unfortunately, modeling of the upper state structure will be difficult. The theory of how the oscillatory potentials affect the higher vibrational modes is still under development especially for tetrahedral moities[19,20,54], and even then only one motion has been considered in the case of MBH_4. Our studies of both $Al(BH_4)_3$ and $Be(BH_4)_2$ show that the spectra are very complex, undoubtedly as a result of these unusual internal motions.

4.4 Conclusions

We have obtained very high resolution FTIR spectra of $Be(BH_4)_2$ which show no resolved rotation-vibrational structure at room temperature. However, when compared to a non-rigid rotor simulation of the bridge stretching bands (ν_4 and ν_{11}) one can see slight evidence of the ν_4 P-R band

contour. This region was probed with infrared diode laser absorption in a free jet and rich vibration rotational structure was seen. Two Q branches in the ν_{11} perpendicular band of $Be(^{11}BH_4)_2$ were assigned giving $\nu(0) = 2194.55715$ (60) and $\alpha_B = -0.000938$ (13) cm^{-1} for $^RQ_0$ and $\nu(1) = 2197.2648$ (15) cm^{-1} and an $\alpha_B = -0.000819$ (36) cm^{-1} for $^RQ_1$. The J dependent differences between these Q branches gave the centrifugal distortion constant $D_{JK} = 0.000066$ (9) cm^{-1} and a sub-band separation $\nu_{sub} = 2.7074$ (8) cm^{-1}. The coriolis coupling constant and the band origin were calculated to be $\zeta = 0.29$ and $\nu_0 = 2193.8$ cm^{-1} (using the D_{3d} *ab initio* rotational constants) and $\zeta = 0.26$ and $\nu_0 = 2193.7$ cm^{-1} (using D_{3d} rotational constants from the electron diffraction structural parameters).

The jet spectrum was too congested (1246 lines in 7.7 wavenumbers) to allow confident assignment of P and R lines. Nevertheless, a spectral line list was compiled and is included in appendix B. *Ab initio* calculations suggest that this extreme spectral congestion may arise from small isotopic shifts due to ^{10}B, many low frequency modes below 500 cm^{-1}, and especially, level splittings due to low barriers to internal rotation. In fact the low three-fold barrier produces many degenerate, low-lying torsional levels which will be appreciably populated even at 10 K. Combination bands associated with higher torsional and tumbling levels are believed to be the main contributor to the complex jet spectrum. The contribution of the D_{2d} minimum of the potential surface to ground state splittings is assumed to be small since the barrier to interconversion is calculated to be 1100 cm^{-1} and mixing will be small compared to that between the three-fold torsional wells. However, upper state splitting due to both of these minima could contribute to the spectral complexity.

4.5 Acknowledgements.

Acknowledgment is made to the Donors of the Petroleum Research Fund, administered by the American Chemical Society, for the support of this research. Additional support of the research facilities at OSU by the National Science Foundation and at PNL by the Department of Energy is also appreciated.

5. Conclusions

In chapter 2, we have described the methods for using *ab initio* geometries, frequencies, dipole moments, and polarizablilities as aids in experimental physical chemistry, and show their implemention in the undergraduate chemistry curriculum at Oregon State University. It was found, in general, that those parameters related to the gradient of the energy (bond lengths and frequencies) are most affected by the level of electron correlation, whereas those parameters related to the spatial distribution of the electron cloud (dipole moment and polarizability) depended mainly on the basis set chioces. These same types of calculations were used extensively in our attempts in chapters 3 and 4 to understand, interpret, and predict the spectral data obtained for the aluminum and beryllium borohydride

High resolution spectra of $Al(BH_4)_3$, $Al(BD_4)_3$, and $Be(BH_4)_2$ were recorded for low pressure samples at 300 K using FTIR spectroscopy (0.01 cm^{-1} to 0.0015 cm^{-1} resolution). Tunable infrared diode laser spectra (0.001 cm^{-1} resolution) of the BH bridge stretching regions and the BH_2 deformation region ($Al(BH_4)_3$ only) are also presented for samples cooled to ~10 K in a multi-pass, slit expansion apparatus. Both room temperature and 10 K spectra show much more congestion than predicted by non-rigid rotor simulations which include boron isotopic shifts and coriolis and centrifugal distortion parameters estimated from *ab initio* calculations. In $Al(BH_4)_3$ the *ab initio* results indicate that a particularly low barrier exists, which separates the prismatic D_{3h} structure from two equivalent D_3 minima in which the BH_4 units are rotated ± 23° about the Al-B axes. The potential energy surface for the relevant conrotary torsional coordinate is examined at the CCSD/6-311G**//MP2/6-311G** level, yielding a prismatic barrier height of 490 cm^{-1} and v=0 and 1 level splittings of 0.052 and 2.7 cm^{-1} respectively. The same treatment for the three-fold torsion of the D_{3d} structure of $Be(BH_4)_2$ yields a barrier height of 680 cm^{-1} and v=0 and 1 level splittings of 0.0001 cm^{-1} and 0.005 cm^{-1} respectively.

Resolved vibration rotational lines were observed only in the beryllium jet spectra and the density of these was much higher than predicted by non-rigid rotor simulations. A list of the 1246 spectral lines measured in 7.7 cm^{-1} of the BH bridge stretch region is included as an appendix. Two band sequences ($^RQ_0$ and $^RQ_1$) were assigned in the ν_{11} perpendicular band, giving $\nu(K=0)$ = 2194.55715 (60) and α_B = -0.000938 (13) cm^{-1} and $\nu(K=1)$ = 2197.2648 (15) cm^{-1} and α_B = -0.000819 (36) cm^{-1}, respectively. The K differences between the bands gave a separation ν_{sub} = 2.7074 (8) cm^{-1} and a centrifugal distortion constant D_{JK} = 0.000066 (9) cm^{-1} where $D_{JK}' = D_{JK}''$ was assumed. This sub-band separation was used to deduce the coriolis coupling constant and the band center, ζ = 0.291 and a band origin ν_0 = 2193.8 cm^{-1} (with *ab initio* A's and B's) and ζ = 0.258 and ν_0 = 2193.7 cm^{-1} (with electron diffraction A's and B's).

The spectral congestion, which prevented any further assignments of P and R lines, is believed to arise from splittings of the upper vibrational levels of modes which couple to the torsional motions and to other tumbling modes of the BH_4 units. The barriers to internal motion in $Be(BH_4)_2$ were calculated to

be 8.2, 10.2, and 3.28 kJ mol^{-1} for the three-fold torsion, the two-fold torsion, and the D_{3d} to D_{2d} interconversion, respectively. These energy differences are greatly affected by the level of electron correlation as is evidenced by our calculations of the relative energies of the D_{3d} form to the D_{2d} form; ,SCF(21.6), MP2(-3.1), MP3(-0.1), MP4D(0.7), MP4DQ(1.9), MP4SDQ(1.8), and CCSD(2.5) (kJ mol^{-1}). The small theoretical differences do not provide a confident basis for predicting whether the D_{3d} or D_{2d} potential minimum is lower. Likewise, the resolved rotational features seen in the 10 K jet spectra do not permit such a distinction, although a D_{3d} configuration is assumed in calculating the ν_{11} band origin.

Bibliography

[1] Pietro, W. J. *J. Chem Educ.* **1994,** *71*, 416.

[2] Duke, B. J. ; O'Leary, B. *J. Chem. Educ.*, **1992,** *69*, 529.

[3] Foresman, J. B.; Frisch, A. *Exploring Chemistry with Electronic Structure Methods: A Guide to Using Gaussian*, Gaussian, Inc., Pittsburgh, Pa. **1993**.

[4] Hehre, W. J.; Radom, L.; Schleyer, P. v.R.; Pople, J. A. *Ab Initio Molecular Orbital Theory*, Wiley, New York, **1986**.

[5] Shoemaker, D. P.; Garland, C. W.; Nibler, J. W. *Experiments in Physical Chemistry*, 5th ed.; McGraw-Hill: New York, NY, **1989**; Expts. 32 and 38.

[6] Coe, D. A.; Nibler, J. W. *J. Chem. Ed.*, **1973,** *50*, 82.

[7] Huber, K. P.; Herzberg, G. *Constants of Diatomic Molecules*, Van Nostrand Reinhold: New York, NY, **1979**.

[8] Almenningen, A.; Gundersen, G.; Haaland, A. *Acta. Chem. Scand.*, **1968**, *22*, 328.

[9] Coe, D. A.; Nibler, J. W. *Spectrochim. Acta*, **1973**, *29A*, 1789.

[10] Plato V.; Hedberg K. *Inorg. Chem.*, **1971**, *10*, 590; James B. D.; Wallbridge, M. G. H. *Progress in Inorganic Chemistry*, **1970**, *11*, 99.

[11] Schlesinger, H. I.; Brown, H. C.; Burg, A. B. *J. Am. Chem. Soc.*, **1940**, *62*, 3421.

[12] Beach, T. Y.; Bauer, S. H. *J. Am. Chem. Soc.*, **1940**, *62*, 3440.

[13] Ogg R. A.; Ray, J. D. *Discussion Faraday Soc.*, **1955**, *19*, 215.

[14] Maybury P. C.; Ahnell, J. E. *Inorg. Chem.*, **1967**, *6*, 1286.

[15] Price, W. C. *J. Chem. Phys.*, **1949**, *17*, 1044.

[16] Emery, A. R.; Taylor, R. C. *Spectrochem. Acta.*, **1960**, *16*, 1455.

[17] Bock, C. W.; Roberts, C.; O'Malley, K.; Trachtman, M.; Mains, G. J. *J. Phys. Chem.*, **1992**, *96*, 4859.

[18] Demachy, I.; Volatron, F. *Inorg. Chem.*, **1994**, *33*, 3965.

[19] Ohashi, N.; Hougen, J. T. *J. Mol. Spec.*, **1992**, *153*, 429.

[20] Hirota, E.; Kawashima, Y. *J. Mol. Spec*, **1997**, *181*, 352.

[21] Schlesinger, H. I.; Brown, H. C.; Hyde, E. K. *J. Am. Chem. Soc.*, **1953**, *75*, 209.

[22] Sharpe, S. W.; Zeng, T. P.; Wittig, C.; Beaudet, R. A. *J. Chem. Phys.*, **1990**, *92*, 943.

[23] Foresman, J. B.; Frisch, Æ. *Exploring Chemistry with Electronic Structure Methods*, 2nd ed.; Gaussian Inc.: Pittsburgh, 1996; p 64.

[24] Grams/32 Spectral Notebase, Galactic Industries Corporation.

[25] Allen, Jr., H. C.; Cross, P. C. *Molecular Vib-Rotors*, John Wiley and Sons, Inc., New York, 1963.

[26] Hedberg, L.; Mills, I. M. *J. Mol. Spec.*, **1993**, *160*, 117.

[27] Al-Kahtani, A.; Montero, S.; Nibler, J. W. *J. Chem. Phys.*, **1993**, *98*, 101.

[28] Van Helvoort, R.; Knippers, W.; Fantoni, R.; Stolte, S. *Chem. Phys.*, **1987**, *111*, 445.

[29] Gaussian 94, Revision E.1, M. J. Frisch, G. W. Trucks, H. B. Schlegel, P. M. W. Gill, B. G. Johnson, M. A. Robb, J. R. Cheeseman, T. Keith, G. A. Petersson, J. A. Montgomery, K. Raghavachari, M. A. Al-Laham, V. G. Zakrzewski, J. V. Ortiz, J. B. Foresman, J. Cioslowski, B. B. Stefanov, A. Nanayakkara, M. Challacombe, C. Y. Peng, P. Y. Ayala, W. Chen, M. W. Wong, J. L. Andres, E. S. Replogle, R. Gomperts, R. L. Martin, D. J. Fox, J. S. Binkley, D. J. Defrees, J. Baker, J. P. Stewart, M. Head-Gordon, C. Gonzalez, and J. A. Pople, Gaussian, Inc., Pittsburgh PA, 1995.

[30] Møller, C.; Plesset, M. S.; *Phys. Rev.*, **1934**, *46*, 678.

[31] Scuseria, G. E.; Schaefer, III, H. F. *J. Chem. Phys*, **1989**, *90*, 3700.

[32] Baranov, L. Ya.; Boldyrev, A. I. *Chem. Phys. Lett.*, **1983**, *96*, 218.

[33] Peng, C.; Schlegel, H. B. *Israel J. Chem,*. **1993**, *33*, 449.

[34] Flygare, W. H. *Molecular Structure and Dynamics*, Prentice-Hall, Inc., New Jersey, 1978; Section 4.2

[35] Stanton, J. F.; Lipscomb, W. N.; Bartlett, R. J. *J. Chem. Phys.*, **1988**, *88*, 5726.

[36] Marynick, D. S.; Lipscomb, W. N. *Inorg. Chem.*, **1972**, *11*, 820.

[37] Nibler, J. W.; Shriver D. F.; Cook T. H. *J. Chem. Phys.*, **1971**, *54*, 5257.

[38] Longuet-Higgens, H. C.; Bell, R. P.; *J. Am. Chem. Soc.*, **1943**, *65*, 250.

[39] Bauer, S. H. *J. Am. Chem. Soc.*, **1950**, *72*, 622.

[40] Almenningen, A.; Gundersen, G.; Haaland, A. *Chem. Commun.*, **1967**, 557.

[41] Nibler, J. W.; Dyke, T. *J. Am. Chem. Soc.*, **1970**, *92*, 2920.

[42] Nibler. J. W.; McNabb, J. *Chem. Commun.*, **1969**, 134.

[43] Gundersen, G.; Hedberg, K.; Hedberg, L. *J. Chem. Phys.*, **1973**, *59*, 3777.

[44] Cook, T. H.; Morgan, G. L. *J. Am. Chem. Soc.*, **1970**, *92*, 6493.

[45] Nibler, J. W. *J. Am. Chem. Soc.*, **1972**, *94*, 3349.

[46] Brendhaugen, K.; Haaland, A.; Novak, D. P. *Acta. Chem. Scand.*, **1975**, *29*, 801.

[47] Gaines, D. F.; Walsh, J. L.; Hillenbrand, K. F. *Chem. Commun.*, **1977**, 224.

[48] Marynick, D. S.; Lipscomb, W. N. *J. Am. Chem. Soc.*, **1973**, *95*, 7244.

[49] Ahlrich, R. *Chem. Phys. Lett.*, **1973**, *19*, 174.

[50] Ortiz, J. V.; Lipscomb, W. N. *AIP Conf. Proc.*, eds. Emin, D.; Aselage, T.; Beckel, C. L.; Hopward, I. A.; Wood, C., Am. Inst. Phys., New York, **1986**.

[51] Saeh, J. C.; Stanton, J. F. in press

[52] Bonaccorsi, R.; Charkin, O. P.; Tomasi, J. *Inorg. Chem.*, **1991**, *30*, 2964.

[53] Maki, A. G.; Pine, A. S.; Dang-Nhu M. *J. Mol. Spec.*, **1985**, *112*, 459.

[54] Hirota, E. *J. Mol. Spec.*, **1992**, *153*, 447.

Appendices

Appendix A

A.1 Array Basic code that produces XY stick spectra of symmetric non-rigid rotors

```
'filename=simulatn.ab
'Generates Stick Spectra for Rigid Rotors with Distortion
'Latest version completed July 13, 1997 by Darren L. Williams
free             'clears all previously defined variables
portout -44,-1  'Turns on error checking with line number values
'Default variable definition section
JMax=200: KMax=200: T=300
'aluminum borohydride
Nu11=2061
Nu17=2020
Nu19=1110
'beryllium borohydride
BNu4=2172
BNu11=2202
threshold=0.05  'intensity cutoff to save time and memory space
IFactor=1       'Infrared Intensity factor from Gaussian94
Boltz=0.695009961       'Boltzman constant in wavenumbers K**-1
dialogon "Initial Parameters"
        dialogask JMax,1,0,200,  "Maximum J Value :"
        dialogask KMax,1,0,200,  "Maximum K Value :"
        dialogask T   ,1,0,600,  "Temperature :"
        dialogask BAND,3+64,0,0, "Band_Type_: Parallel Perpendicular"
        dialogask Top ,3+64,0,0, "Symmetric_Top_: Oblate Prolate"
        dialogask Constants,3+64,0,0,"Rot_Constants_: Al1B3H12
Al(10)B1(11)B2H12 BeB2H8 Be(10)B(11)H8 Manual"
dialogoff
If Constants<2 then top=0       'Prevents a prolate calc. for Al1B3H12
if Constants=2 or constants=3 then top=1 'No oblate calc. for BeB2H8
If KMax>JMax then KMax=JMax     'KMax cannot be > JMax by definition.
gosub (Constants+2)*1000+BAND   'go get specified values
If band=1 then NTrans=6*((KMax*JMax)-((KMax+1)*(KMax)/2)) else
NTrans=3*((KMax*JMax)-((KMax+1)*(KMax)/2))

        'The Difference parameter in calculating the Energy Expression
        'depends on the type of Top and the unique symmetry axis
        'Up is the Unique Rot Constant
        '(If,then,else must be on one line!)
        If Top=0 then Diffp=Cp-Ap:Diffpp=Cpp-App:Up=Cp else Diffp=Ap-
Cp:Diffpp=App-Cpp:Up=Ap

'debug printing dialog box
dialogbeg "NTrans"
        print Ntrans;" transitions"
        print "Consider hitting Cancel if over 2 million."
        'if top=0 then print "2*(C-B)=";2*diffpp else print "2*(A-
B)=";2*diffpp
dialogend


        dim Total(NTrans+1000), TInt(NTrans+1000)
        m=0
        BEEP    'Calculation has begun
```

```
        'Select set of loops for requested band type
        IF BAND=1 THEN GOTO 100

'*************************************************************************
'PARALLEL BAND CALCULATIONS ********************************************
'*************************************************************************
For J = 0 to JMax
    For K=0 to JMax     'positive Ks; degeneracy is in line strength
        if abs(K)>J then goto 90
        if abs(K)>KMax then goto 90
        Ground=Bpp*J*(J+1)+(Diffpp)*squared(K)-
DJpp*squared(J)*squared(J+1)-DJKpp*J*(J+1)*squared(K)-
DKpp*squared(squared(K))
        BFactor=(exp(-Ground/(Boltz*T)))
        Mod2 = (J/2) - INT(J/2)
        Mod3 = (K/3) - INT(K/3)
        GNS=1*IFactor    'IFactor = Isotope abundance * IR Intensity

20      if J=0 then goto 30
        PLS=((squared(J))-(squared(K)))/J
        if K<>0 then PLS=PLS*2  '+/- K degeneracy
        INTENSITY=GNS*PLS*BFactor
        if INTENSITY<threshold then goto 30     'skip if negligible
        LASTJ=J:lastk=K
        TInt(m)  = INTENSITY
        Total(m) = (Bp*(J-1)*((J-1)+1))+((Diffp)*squared(K)-
DJp*squared(J-1)*squared((J-1)+1)-DJKp*(J-1)*((J-1)+1)*squared(K)-
DKp*squared(squared(K)))+Nu-Ground
        m=m+1

30      if K=0 goto 40
        IF J=0 THEN GOTO 40
        QLS=((2*J+1)*(squared(K)))/(J*(J+1))
        if K<>0 then QLS=QLS*2
        INTENSITY=GNS*QLS*BFactor
        if INTENSITY<threshold then goto 40
        LASTJ=J:lastk=K
        TInt(m)  = INTENSITY
        Total(m) = (Bp*J*(J+1))+((Diffp)*squared(K)-
DJp*squared(J)*squared(J+1)-DJKp*(J)*(J+1)*squared(K)-
DKp*squared(squared(K)))+Nu-Ground
        m=m+1

40      RLS=(((J+K)+1)*((J-K)+1))/(J+1)
        if K<>0 then RLS=RLS*2
        INTENSITY=GNS*RLS*BFactor
        if INTENSITY<threshold then goto 50
        LASTJ=J:lastk=K
        TInt(m)  = INTENSITY
        Total(m) = (Bp*(J+1)*((J+1)+1))+((Diffp)*squared(K)-
DJp*squared(J+1)*squared((J+1)+1)-DJKp*(J+1)*((J+1)+1)*squared(K)-
DKp*squared(squared(K)))+Nu-Ground
        m=m+1
50

90  Next K
Next J

goto 1000
```

```
100
'*************************************************************************
'PERPENDICULAR BAND CALCULATIONS ***************************************
'*************************************************************************
For J=0 to JMax
    For K=-JMax to JMax
        if abs(K)>J then goto 900
        if abs(K)>KMax then goto 900
        Ground=Bpp*J*(J+1)+(Diffpp)*squared(K)-
DJpp*squared(J)*squared(J+1)-DJKpp*J*(J+1)*squared(K)-
DKpp*squared(squared(K))
        BFactor=(exp(-Ground/(Boltz*T)))
        Mod2 = (J/2) - INT(J/2)
        Mod3 = (K/3) - INT(K/3)
        GNS=1*IFactor



'DeltaK=-1 PP,PQ,PR Branches-------------------------------------------
200     'goto 300 'skip lines for debugging
        if J=0 then goto 300
        PPLS=((J+K)*((J+K)-1))/J
        INTENSITY=GNS*PPLS*BFactor
        if INTENSITY<threshold then goto 300
        LASTJ=J:lastk=K
        TInt(m)  = INTENSITY
        Total(m) = Bp*(J-1)*((J-1)+1)+(Diffp)*squared(K-1)+2*Up*zeta*(K-
1)-DJp*squared(J-1)*squared((J-1)+1)-DJKp*(J-1)*((J-1)+1)*squared(K-1)-
DKp*squared(squared(K-1))+Nu-Ground
        m=m+1

300     'goto 400 'skip
        if J=0 goto 400
        PQLS=((2*J+1)*(J+K)*(J-K+1))/(J*(J+1))
        INTENSITY=GNS*PQLS*BFactor
        if INTENSITY<threshold then goto 400
        LASTJ=J:lastk=K
        TInt(m)  = INTENSITY
        Total(m) = Bp*J*(J+1)+(Diffp)*squared(K-1)+2*Up*zeta*(K-1)-
DJp*squared(J)*squared(J+1)-DJKp*(J)*(J+1)*squared(K-1)-
DKp*squared(squared(K-1))+Nu-Ground
        m=m+1

400     'goto 600 'skip
        PRLS=((J-K+1)*(J-K+2))/(J+1)
        INTENSITY=GNS*PRLS*BFactor
        if INTENSITY<threshold then goto 500
        LASTJ=J:lastk=K
        TInt(m)  = INTENSITY
        Total(m) = Bp*(J+1)*((J+1)+1)+(Diffp)*squared(K-1)+2*Up*zeta*(K-
1)-DJp*squared(J+1)*squared((J+1)+1)-DJKp*(J+1)*((J+1)+1)*squared(K-1)-
DKp*squared(squared(K-1))+Nu-Ground
        m=m+1
500

'DeltaK=+1 RP,RQ,RR Branches-------------------------------------------
600     'goto 700 'skip
        if J=0 then goto 700
        RPLS=((J-K)*(J-K-1))/J
```

```
        INTENSITY=GNS*RPLS*BFactor
        if INTENSITY<threshold then goto 700
        LASTJ=J:lastk=K
        TInt(m)  = INTENSITY
        Total(m) = Bp*(J-1)*((J-1)+1)+(Diffp)*squared(K+1)-
2*Up*zeta*(K+1)-DJp*squared(J-1)*squared((J-1)+1)-DJKp*(J-1)*((J-
1)+1)*squared(K+1)-DKp*squared(squared(K+1))+Nu-Ground
        m=m+1

700     'goto 800 'skip
        if J=0 then goto 800
        RQLS=((2*J+1)*(J-K)*(J+K+1))/(J*(J+1))
        INTENSITY=GNS*RQLS*BFactor
        if INTENSITY<threshold then goto 800
        LASTJ=J:lastk=K
        TInt(m)  = INTENSITY
        Total(m) = Bp*J*(J+1)+(Diffp)*squared(K+1)-2*Up*zeta*(K+1)-
DJp*squared(J)*squared(J+1)-DJKp*(J)*(J+1)*squared(K+1)-
DKp*squared(squared(K))+Nu-Ground
        m=m+1

800     'goto 900 'skip
        RRLS=((J+K+1)*(J+K+2))/(J+1)
        INTENSITY=GNS*RRLS*BFactor
        if INTENSITY<threshold then goto 900
        LASTJ=J:lastk=K
        TInt(m)  = INTENSITY
        Total(m) = Bp*(J+1)*((J+1)+1)+(Diffp)*squared(K+1)-
2*Up*zeta*(K+1)-DJp*squared(J+1)*squared((J+1)+1)-
DJKp*(J+1)*((J+1)+1)*squared(K+1)-DKp*squared(squared(K+1))+Nu-Ground
        m=m+1
900 Next K
Next J

1000    beep    'Calculation is done
        TEnd = index0(Total)     'TEnd=index of the last nonzero datum
        newspc trace2(TEnd,128) '128 is the x,y trace flag
        setxtype 1               'Wavenumbers
        setytype 2               'Absorbance
        #S.X = Total             'assign arrays
        #S.Y = TInt
        savespc "simulatn"       'write to disk
        'portout -32,2  'DISPLAY MODE OVERLAID(p.219 Array Basic Man)
        'Portout -32,3  'display stacked p.219
        autoscale
'DIALOGBEG "ENDING VALUES"               'debug printing
'       print "Last J=";lastj,"Last K=";lastk
'dialogend
end
'%%%
```

```
2010
    App=0.1443032:      Bpp=0.1443031:          Cpp=0.0763713
    Ap =App-4.0e-4:     Bp =Bpp-4.0e-4:         Cp =Cpp-2.0e-4
    'DJpp=0:            DJKpp=0:                DKpp=0
    DJpp=1.81609e-7:    DJKpp=-3.36129e-7:      DKpp=1.61496e-7
    DJp =DJpp       :   DJKp =DJKpp     :       DKp =DKpp
return
'-------------------------------------
2050
        dialogon "Initial Parameters"
                dialogask NuNum,3+64,0,0,"Which_Band?: Nu19_1110
Nu17_2020"
        dialogoff
return
'-------------------------------------
3000    'boron ten-Aluminum Borohydride
        Nu=Nu11+2.5686: IFactor=128.30
        GOTO 3010
3001    GOSUB 2050
        if NuNum=0 then Nu=Nu19+4.095:zeta=0.008841:IFactor=41.85  else
Nu=Nu17+1.1163:zeta=0.018019:IFactor=214.71
3010App=0.1504628:      Bpp=0.1443032:          Cpp=0.0780626
    Ap =App-4.0e-4:     Bp =Bpp-4.0e-4:         Cp =Cpp-2.0e-4
    'DJpp=0:            DJKpp=0:                DKpp=0
    DJpp=1.88147E-07:   DJKpp=-3.47593E-07:     DKpp=9.29688E-08
    DJp =DJpp       :   DJKp =DJKpp     :       DKp =DKpp
return
'-------------------------------------------------------------------------
4000    'Beryllium Borohydride
        Nu=BNu4 : IFactor=140.59
        goto 4010
4001    Nu=BNu11 : IFactor=83.59: zeta=0.056584
4010App=2.194098:       Bpp=0.177286:           Cpp=0.177286
    Ap =App-6e-4:       Bp =Bpp-3e-4:           Cp=Cpp-3e-4
    'DJpp=0:            DJKpp=0:                DKpp=0
    DJpp=5.69e-8:       DJKpp=8.46e-7:          DKpp=8.34e-6
    DJp =DJpp   :       DJKp =DJKpp  :          DKp =DKpp

return
'---------------------------------------
5000    'Boron ten-Beryllium Borohydride
        Nu=BNu4+.4796 : IFactor=69.88
        goto 5010
5001    Nu=BNu11+4.9619 : IFactor=41.33: zeta=0.04815
5010App=2.194098:       Bpp=0.183153:           Cpp=0.183153
    Ap =2.181658:       Bp =0.183176:           Cp =0.183176
    'DJpp=0:            DJKpp=0:                DKpp=0
    DJpp=6.04e-8:       DJKpp=8.99e-7:          DKpp=8.29e-6
    DJp =DJpp   :       DJKp =DJKpp  :          DKp =DKpp
return
'---------------------------------------

6000    'User defined rotational constants
        'default Values
    App=5.25        :   Bpp=0.85        :       Cpp=Bpp
    Ap=5.18         :   Bp=0.84         :       Cp=Bp
    goto 6010
6001
    App=5.25        :   Bpp=App         :       Cpp=0.85
    Ap=5.18         :   Bp=Ap           :       Cp=0.84
```

```
6010
    DJpp=0:              DJKpp=0:              DKpp=0
    DJp=0:               DJKp=0:               DKp=0
    Nu=0
    zeta=0       'coriolis effects

dialogon "Molecular Parameters"
        Print "Ground State Constants"
        dialogask App,0,0,0,"A'' :"
        dialogask Bpp,0,0,0,"B'' :"
        dialogask Cpp,0,0,0,"C'' :"
        dialogask DJpp,0,0,0,"DJ'' :"
        dialogask DJKpp,0,0,0,"DJK'' :"
        dialogask DKpp,0,0,0,"DK'' :"
        Print "Excited State Constants"
        dialogask Ap,0,0,0, "A'  :"
        dialogask Bp,0,0,0, "B'  :"
        dialogask Cp,0,0,0, "C'  :"
        dialogask DJp,0,0,0,"DJ' :"
        dialogask DJKp,0,0,0,"DJK' :"
        dialogask DKp,0,0,0,"DK' :"
        Print "Vibration Data"
        dialogask Nu,0,0,0, "Nu  :"
        dialogask zeta,0,0,0,"Coriolis :"
dialogoff
return

10000 Print J,K,m
end
```

A.2 Array Basic code for convolving a stick spectrum with a Gaussian function

```
'filename=convolve.ab
'Convolves an XY Trace with a Gaussian
'Latest version completed July 13, 1997 by Darren L. Williams
free
portout -44,-1  'turns on error checking with line numbers
First=getLEFT()
Last=getRIGHT()
density=2000
Baseline=0
W=0.015
dialogbeg "Gaussian Convolution"
         Print "Select an XY Stick Spectrum before running Convolve :"
         dialogask First,0,0,0,     "High Wavenumber Value :"
         dialogask Last,0,0,0,      "Low Wavenumber Value :"
         'dialogask baseline,0,0,0, "Baseline Value :"
         dialogask W,0,0,0,         "Linewidth FWHM :"
dialogend
density=rnd(10/W)       'ten points over each linewidth
points = int(density*abs(last-first))
ntrans=npts(#s)

dim x(ntrans), y(ntrans)
x=#s.x : y=#s.y
newspc trace(points)
setxtype 1      'Wavenumbers
setytype 2      'Absorbance
setffp first,last
beep    'Calculation has begun
trace=Baseline
'
'-------------------------------------------------------------------------
'This loop adds the Y values to the new trace _at_the_closest_point.
'This introduces an error in X of +/-0.5 of the point spacing!
'This may not be suitable for your purposes, but it is fine for ours.
'
'-------------------------------------------------------------------------
for i=0 to ntrans-1
   trace(x(i))=trace(x(i))+y(i)
next i

'portout -32,3   'set to stacked display
savespc "zerofill"
autoscale

dim gaussian(100)
fillbeg 0
fillinc (1/density)
H=1:C=50*(1/density)
'This Gaussian function is not a mistake.See Array Basic Reference.
gaussian = (exp(-(squared((fill(gaussian)-C)/(W*.606)))))*H
'Width is scaled by sqrt(e^-1)
'This is the main statement.  See Array Basic Reference.
        convolve zerofill, gaussian
beep    'Calculation is over.
savespc "Convolve"
end
```

Appendix B Spectral Line List for $Be(BH_4)_2$

B.1 Data Manipulation

High resolution infrared spectroscopy using diode lasers is a great tool especially when used in conjunction with a jet expansion where the Doppler limit is less than or nearly equal to the instrumental line width of 0.001 cm^{-1}. Also, direct absorption has sensitivity advantages over non-linear jet techniques. However, there is no such thing as a free lunch. The data work-up for these diode laser experiments is tedious and sensitive to human error. Eleven megabytes of ascii x,y data were brought back from PNL in January 1996 and one year was spent working on the linearization, calibration, and intensity conversion. The results are described in detail in this thesis and the data is included in this appendix for future reference.

The data files contained three arrays of digitized infrared signals. All three arrays were imported and plotted versus data point number. The etalon trace (FSR $\cong$ 0.01) was peak picked in Grams/32 using the following parameters: Sensitivity = 25, Smooth = 25, Edge = Normal, all other parameters = 0. The peak numbers (typically 1 to 42) were defined to be the new x axis on which each trace is replotted. To do this, the data point x value must be recalculated to be linear between each etalon peak value. The linearized N_2O trace was then peak picked using the same parameters as for the etalon peaks. If there was only one reference peak that matched the NIST N_2O atlas the spectra were shifted to match the peak picked value and the atlas value and the etalon FSR was used to scale the x axis. If there were two reference peaks the x axis was shifted and scaled so that the two peaks matched the atlas values. If there were more than two peaks that matched the atlas the shift and scale were calculated to minimize the sum of the squares of the residuals of the peak picked positions and the atlas values for the N_2O peaks. The resulting x shift and scale were then applied to the sample and etalon traces. From this linearized and calibrated data one can measure the free spectral range of the etalon very accurately (0.00981 (4) cm^{-1}), and one can begin assembling an overall spectrum.

The y axis of the sample trace is collected on a 12 bit digitizer for added dynamic range (1 in 4096). The maximum value of the sample trace is governed by how many scans were averaged and whether there was any additional signal processing such as AC coupling (relative gain of 500). The sample traces are first divided by these gain factors to normalize all y values to the same scale. Also there is a considerable curvature in the sample trace that is not present in the etalon or reference traces. The BaF_2 windows (n = 1.47 and L $\cong$ 6 mm) could cause this fringe effect with a period of about 0.6 cm^{-1}–very close to that observed. A polynomial of degree seven was fit through the data using the method of least squares. This baseline was then subtracted from the trace. Since an estimate of 100 percent transmission was needed sample number 39 was taken with the jet turned off. The maximum of the

baseline polynomial for this trace (687.7) was taken to be 100 % T for the whole data set. With this information the spectrum was converted to transmission. For convenience, however, the 1-T spectrum was curve-fit in Grams/32 since it performs more reliably with peaks that 'go up'. The peak centers and heights were collected in a peak log, sorted according to wavenumber, and compared to an objective criteria to decide which peaks were the same and which were unique. Two adjacent line centers had to match the following criteria before being averaged: a) They had to be from different jet scans. b) They each had to have a line width less than 0.007 cm^{-1}. c) They had to be less than 0.002 cm^{-1} apart. If all three factors were met the peaks were declared to be the same and the average and standard deviation of their centers was taken. Likewise, their heights were averaged, and this revised master list is what is reported here for $Be(BH_4)_2$. A pictorial description of the above scheme is included in the following figures

B.2 Intensity Manipulations

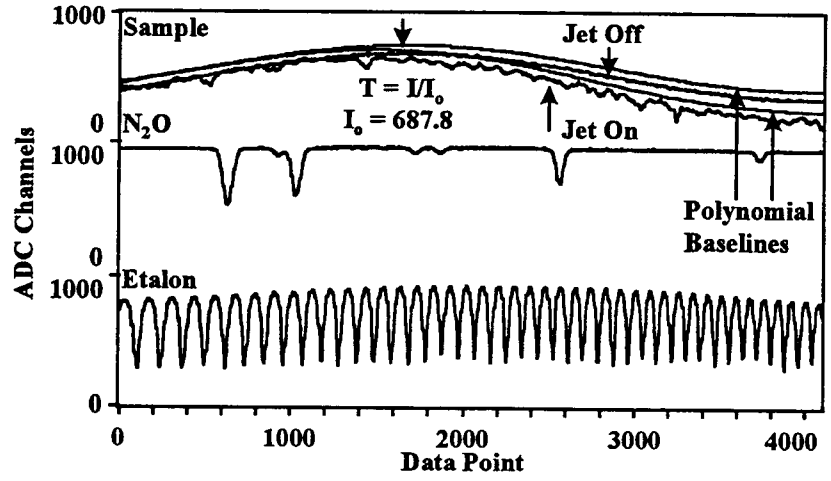

Figure B.1: Raw data for IR diode laser jet study. All three channels are shown as well as two separate sample scans superimposed. (jet on and jet off) The broad fluctuation in the sample traces was removed with the polynomial baselines shown. The maximum of the jet-off trace was taken as I_o.

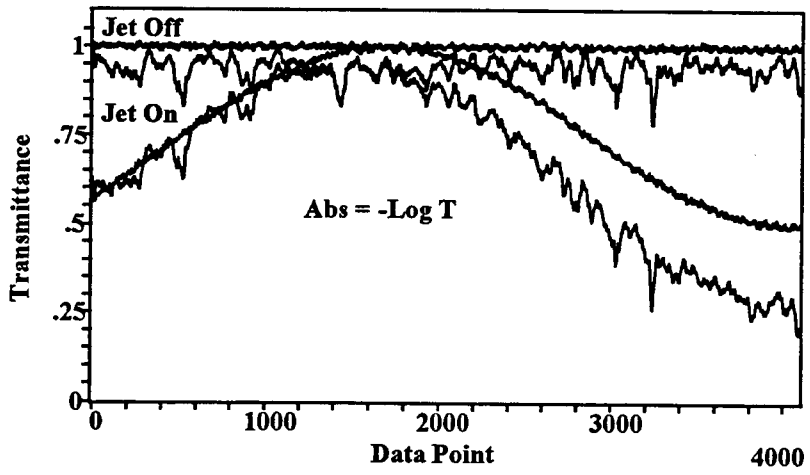

Figure B.2: The transmittance spectra are shown before and after baseline subtraction. For convenience, after calibration the (1-T) spectrum was curvefit to produce the peaklog. Then the peak heights were converted to absorbance.

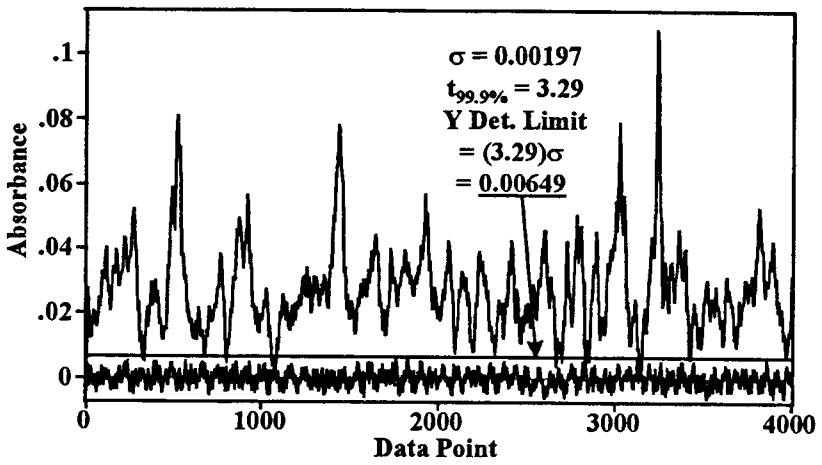

Figure B.3: The absorbance spectrum is shown with the 99.9% confidence detection level. The noise contains a regularity which was not removed making this a conservative estimate.

B.3 Frequency Linearization and Calibration

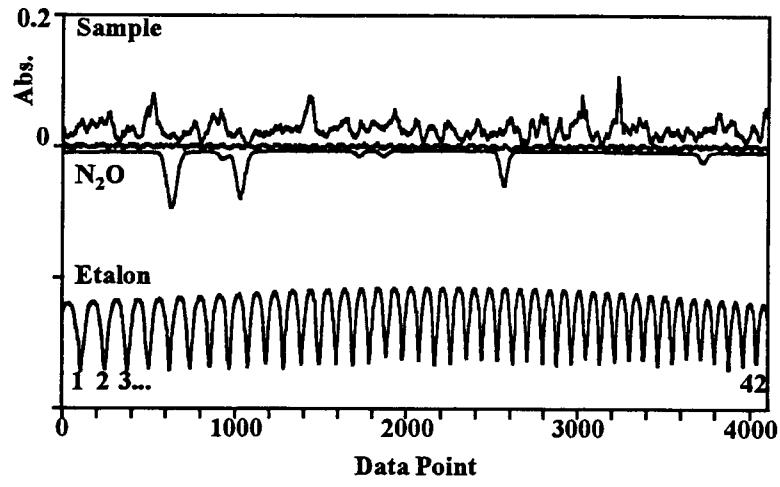

Figure B.4: The absorbance spectrum is linearized by interpolating the x axis to be linear in etalon number. The etalon trace was peak picked using a center of mass algorithm and these centers were defined as the new x increment.

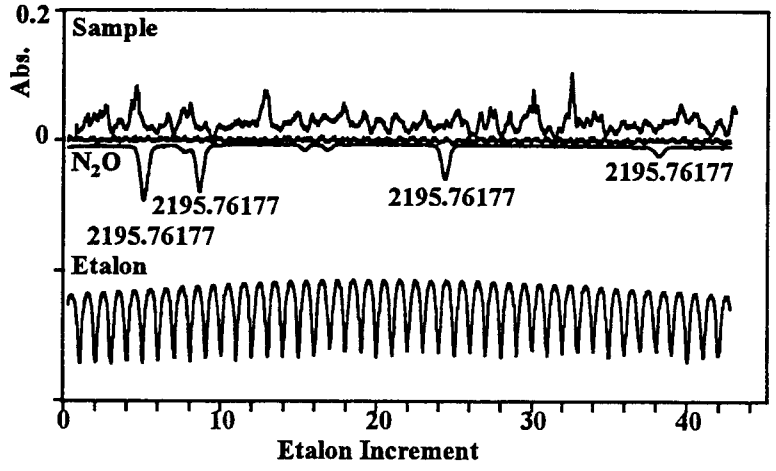

Figure B.5: Then, the spectrum was calibrated using the peak picked N_2O positions in etalon increment and the NIST N_2O spectral atlas. If there were more than two calibration peaks in a scan the x axis shift and span were optimized by least squares minimization.

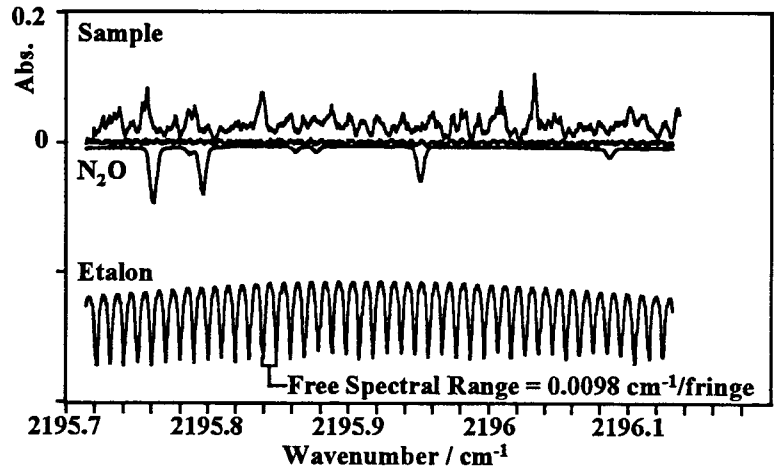

Figure B.6: The baselined, linearized, calibrated absorbance spectrum is shown and the FSR of the etalon is calculated as a check. (It was known to be ~0.01 cm^{-1}.) The calibrated spectra are stacked together in the spectral atlas and compared to the peak table and its noise free convolution.

B.4 Spectral Atlas of $Be(BH_4)_2$

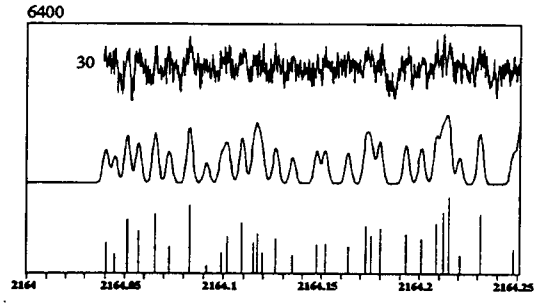

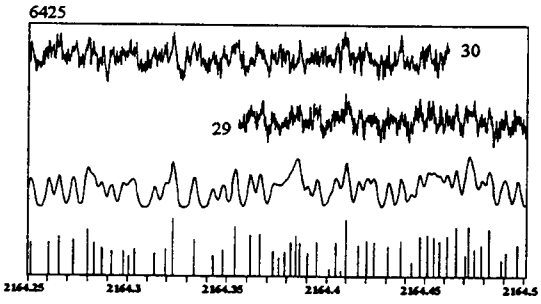

Index	6400 ω	Abs	Index	6425 ω	Abs
1	2164.04039	0.0158	31	2164.25149	0.0270
2	2164.04498	0.0124	32	2164.26057	0.0272
3	2164.05115	0.0225	33	2164.26568	0.0307
4	2164.05695	0.0191	34	2164.27280	0.0288
5	2164.06544	0.0243	35	2164.27975	0.0357
6	2164.07262	0.0147	36	2164.28285	0.0273
7	2164.08266	0.0265	37	2164.28690	0.0234
8	2164.09128	0.0092	38	2164.29165	0.0213
9	2164.09903	0.0129	39	2164.29770	0.0216
10	2164.10212	0.0177	40	2164.30088	0.0180
11	2164.10935	0.0215	41	2164.30346	0.0225
12	2164.11519	0.0159	42	2164.31369	0.0198
13	2164.11730	0.0183	43	2164.31903	0.0225
14	2164.11932	0.0128	44	2164.32289	0.0441
15	2164.12611	0.0168	45	2164.33352	0.0294
16	2164.13486	0.0121	46	2164.34282	0.0181
17	2164.14719	0.0153	47	2164.34799	0.0221
18	2164.15155	0.0154	48	2164.35401	0.0384
19	2164.16338	0.0147	49	2164.36180	0.0258
20	2164.17270	0.0206	50	2164.36659 (94)	0.0297
21	2164.17534	0.0178	51	2164.37303 (15)	0.0191
22	2164.17979	0.0198	52	2164.37603	0.0171
23	2164.19301	0.0181	53	2164.37902 (3)	0.0189
24	2164.20102	0.0169	54	2164.38183	0.0220
25	2164.20858	0.0213	55	2164.38443	0.0256
26	2164.21184	0.0245	56	2164.38639 (18)	0.0246
27	2164.21480	0.0291	57	2164.39029	0.0160
28	2164.22037	0.0122	58	2164.39512 (18)	0.0245
29	2164.23091	0.0240	59	2164.40141	0.0097
30	2164.24783	0.0139	60	2164.40458 (11)	0.0245
			61	2164.40716	0.0068
			62	2164.40985 (79)	0.0390
			63	2164.41592 (65)	0.0224
			64	2164.42014 (33)	0.0258
			65	2164.42383	0.0224
			66	2164.43135 (91)	0.0224
			67	2164.43777 (70)	0.0264
			68	2164.44286	0.0140
			69	2164.44737 (64)	0.0281
			70	2164.45151 (0)	0.0295
			71	2164.45458 (64)	0.0266
			72	2164.45773 (1)	0.0247
			73	2164.46138 (6)	0.0286
			74	2164.46583	0.0304
			75	2164.47041	0.0153
			76	2164.47241	0.0306
			77	2164.47494	0.0187
			78	2164.47866	0.0206
			79	2164.48264	0.0294
			80	2164.48875	0.0128
			81	2164.49093	0.0171
			82	2164.49674	0.0210

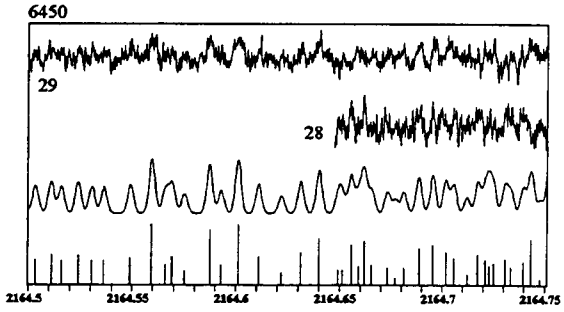

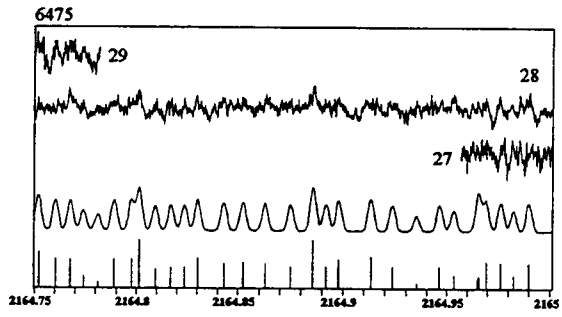

Index	6450 ω	Abs
83	2164.50348	0.0172
84	2164.51103	0.0197
85	2164.51581	0.0166
86	2164.52401	0.0193
87	2164.53059	0.0168
88	2164.53635	0.0167
89	2164.54936	0.0179
90	2164.55953	0.0345
91	2164.56599	0.0150
92	2164.56899	0.0185
93	2164.57505	0.0120
94	2164.58712	0.0313
95	2164.59277	0.0145
96	2164.60096	0.0342
97	2164.61106	0.0184
98	2164.62211	0.0110
99	2164.63137	0.0204
100	2164.64007	0.0274
101	2164.64924	0.0147
102	2164.65136 (17)	0.0136
103	2164.65540	0.0289
104	2164.65907 (13)	0.0150
105	2164.66181	0.0317
106	2164.66564	0.0145
107	2164.67298 (73)	0.0144
108	2164.67697	0.0102
109	2164.68105 (112)	0.0141
110	2164.68842 (3)	0.0247
111	2164.69542 (43)	0.0262
112	2164.70167 (182)	0.0227
113	2164.70568	0.0215
114	2164.71201 (20)	0.0111
115	2164.71729	0.0234
116	2164.72095	0.0170
117	2164.72298	0.0171
118	2164.72479 (11)	0.0164
119	2164.73038	0.0209
120	2164.73331 (18)	0.0154
121	2164.73945	0.0194
122	2164.74352	0.0271
123	2164.74769	0.0097

Index	6475 ω	Abs
124	2164.75186	0.0276
125	2164.76019	0.0239
126	2164.76768 (27)	0.0261
127	2164.77396 (18)	0.0168
128	2164.78089	0.0146
129	2164.78914	0.0286
130	2164.79750	0.0286
131	2164.80146	0.0409
132	2164.80935	0.0230
133	2164.81710	0.0237
134	2164.82380	0.0239
135	2164.83022	0.0298
136	2164.84294	0.0265
137	2164.85230	0.0271
138	2164.86278	0.0261
139	2164.87500	0.0246
140	2164.88583	0.0413
141	2164.89187	0.0246
142	2164.89806	0.0288
143	2164.91331	0.0304
144	2164.92356	0.0243
145	2164.93509	0.0143
146	2164.94629	0.0247
147	2164.95301	0.0197
148	2164.96489	0.0178
149	2164.96557 (67)	0.0187
150	2164.96890	0.0278
151	2164.97619 (85)	0.0270
152	2164.98211 (154)	0.0189
153	2164.98965 (160)	0.0262

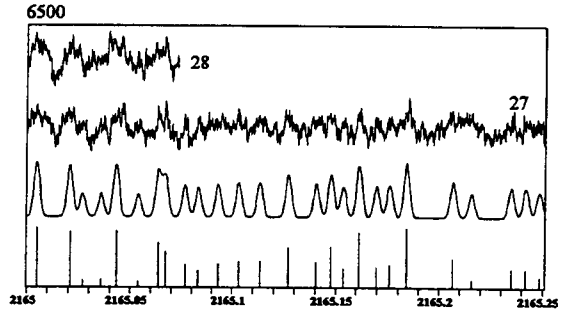

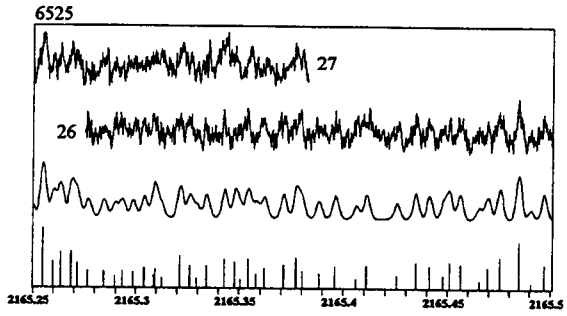

Index	6500 ω	Abs	Index	6525 ω	Abs
154	2165.00477 (2)	0.0380	180	2165.25475	0.0423
155	2165.02086 (72)	0.0364	181	2165.25979	0.0200
156	2165.02676	0.0158	182	2165.26341	0.0259
157	2165.03593	0.0164	183	2165.26845	0.0265
158	2165.04328 (137)	0.0367	184	2165.27146	0.0188
159	2165.05403	0.0154	185	2165.27652	0.0185
160	2165.06360 (8)	0.0316	186	2165.28411 (0)	0.0148
161	2165.06712 (4)	0.0280	187	2165.28963 (2)	0.0126
162	2165.07659	0.0223	188	2165.29312	0.0181
163	2165.08325	0.0203	189	2165.29864 (86)	0.0156
164	2165.09311	0.0228	190	2165.30387	0.0211
165	2165.10334	0.0237	191	2165.30853 (2)	0.0145
166	2165.11352	0.0238	192	2165.30921	0.0153
167	2165.12721	0.0296	193	2165.31219	0.0098
168	2165.14071	0.0235	194	2165.32130 (84)	0.0267
169	2165.14760	0.0300	195	2165.32602 (21)	0.0200
170	2165.15365	0.0209	196	2165.32936	0.0096
171	2165.16115	0.0362	197	2165.33402 (59)	0.0198
172	2165.16948	0.0214	198	2165.34276 (73)	0.0240
173	2165.17590	0.0224	199	2165.34783	0.0198
174	2165.18413	0.0381	200	2165.35031	0.0115
175	2165.20687	0.0252	201	2165.35437 (63)	0.0246
176	2165.21561	0.0164	202	2165.35819	0.0123
177	2165.23485	0.0208	203	2165.36214 (75)	0.0190
178	2165.24194	0.0207	204	2165.37124	0.0238
179	2165.24847	0.0174	205	2165.37755 (72)	0.0261
			206	2165.38032	0.0144
			207	2165.38850	0.0170
			208	2165.39636	0.0228
			209	2165.40617	0.0127
			210	2165.41114	0.0235
			211	2165.42562	0.0158
			212	2165.43468	0.0259
			213	2165.44123	0.0231
			214	2165.44792	0.0156
			215	2165.45101	0.0266
			216	2165.45596	0.0245
			217	2165.46535	0.0112
			218	2165.46944	0.0217
			219	2165.47524	0.0307
			220	2165.48462	0.0452
			221	2165.49044	0.0092
			222	2165.49718	0.0251

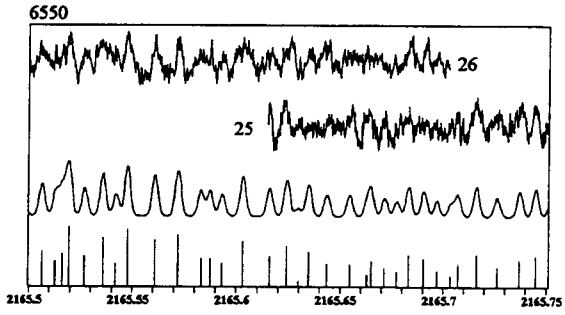

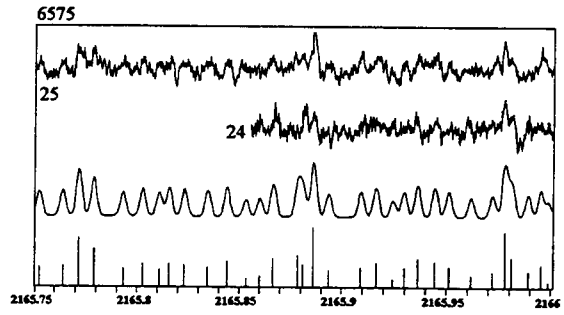

	6550			6575	
Index	ω	Abs	Index	ω	Abs
223	2165.50641	0.0338	256	2165.75228	0.0259
224	2165.51306	0.0254	257	2165.76377	0.0271
225	2165.51614	0.0314	258	2165.77140	0.0486
226	2165.51938	0.0558	259	2165.77864	0.0398
227	2165.52686	0.0295	260	2165.79305	0.0248
228	2165.53565	0.0455	261	2165.80277	0.0285
229	2165.54201	0.0230	262	2165.81080	0.0243
230	2165.54767	0.0533	263	2165.81575	0.0294
231	2165.56085	0.0436	264	2165.82309	0.0279
232	2165.57175	0.0481	265	2165.83441	0.0266
233	2165.58277	0.0274	266	2165.84395	0.0304
234	2165.58727	0.0273	267	2165.85319	0.0176
235	2165.59305	0.0236	268	2165.86007	0.0166
236	2165.60309	0.0427	269	2165.86658 (99)	0.0306
237	2165.61595 (9)	0.0361	270	2165.87873	0.0357
238	2165.62427 (100)	0.0457	271	2165.88134 (63)	0.0248
239	2165.62968	0.0115	272	2165.88620 (9)	0.0547
240	2165.63486	0.0330	273	2165.89344	0.0238
241	2165.64351 (120)	0.0242	274	2165.90924 (61)	0.0250
242	2165.65456 (105)	0.0271	275	2165.91624 (59)	0.0283
243	2165.66280 (79)	0.0182	276	2165.92424	0.0148
244	2165.66472	0.0255	277	2165.92961	0.0263
245	2165.67138	0.0274	278	2165.93638 (114)	0.0309
246	2165.67733 (149)	0.0189	279	2165.94457 (1)	0.0288
247	2165.68302 (48)	0.0355	280	2165.95107	0.0270
248	2165.69038 (67)	0.0302	281	2165.96158 (145)	0.0184
249	2165.69678 (31)	0.0185	282	2165.97201 (90)	0.0215
250	2165.70370	0.0176	283	2165.97788 (24)	0.0502
251	2165.70700	0.0326	284	2165.98122	0.0292
252	2165.71609	0.0449	285	2165.98892	0.0203
253	2165.72598	0.0283	286	2165.99506 (69)	0.0273
254	2165.73705	0.0373	287	2165.99895	0.0132
255	2165.74483	0.0421			

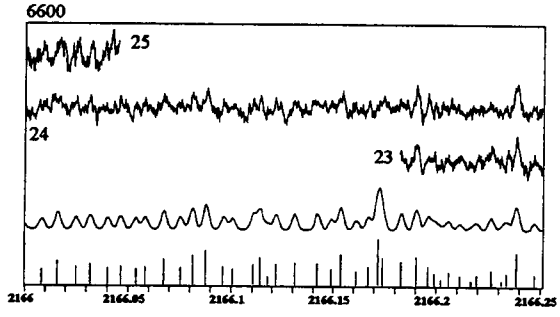

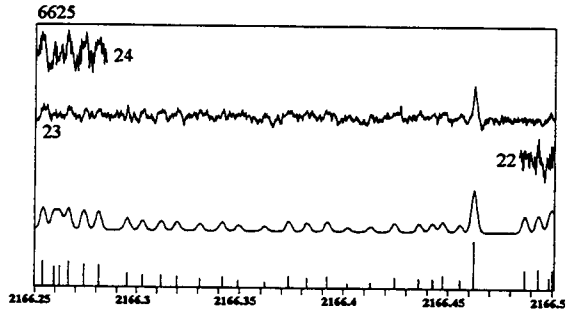

Index	6600 ω	Abs
288	2166.00837 (6)	0.0219
289	2166.01592 (72)	0.0351
290	2166.02469 (22)	0.0261
291	2166.03144 (28)	0.0294
292	2166.03994 (174)	0.0251
293	2166.04622	0.0256
294	2166.05344	0.0223
295	2166.05812	0.0241
296	2166.06722	0.0359
297	2166.07524	0.0239
298	2166.08117	0.0413
299	2166.08772	0.0486
300	2166.09610	0.0254
301	2166.10064	0.0218
302	2166.11049	0.0286
303	2166.11408	0.0389
304	2166.11763	0.0115
305	2166.12193	0.0291
306	2166.13098	0.0310
307	2166.14200	0.0304
308	2166.14898	0.0218
309	2166.15348	0.0439
310	2166.16125	0.0188
311	2166.16702	0.0257
312	2166.17388	0.0381
313	2166.18320	0.0322
314	2166.19039 (2)	0.0567
315	2166.19607 (2)	0.0350
316	2166.19914 (27)	0.0247
317	2166.20219	0.0178
318	2166.20586 (53)	0.0262
319	2166.21121	0.0313
320	2166.21664	0.0142
321	2166.21936 (53)	0.0206
322	2166.22608 (6)	0.0322
323	2166.22668	0.0109
324	2166.23121	0.0152
325	2166.23373 (69)	0.0274
326	2166.23833 (16)	0.0655
327	2166.24709 (1)	0.0226

Index	6625 ω	Abs
328	2166.25381 (85)	0.0356
329	2166.25926	0.0189
330	2166.26217	0.0192
331	2166.26628 (42)	0.0344
332	2166.27396 (64)	0.0304
333	2166.28091 (21)	0.0278
334	2166.29517	0.0336
335	2166.30285	0.0278
336	2166.31173	0.0275
337	2166.31948	0.0258
338	2166.33083	0.0200
339	2166.34153	0.0247
340	2166.34941	0.0172
341	2166.36192	0.0138
342	2166.37346	0.0277
343	2166.38263	0.0238
344	2166.39228	0.0264
345	2166.40217	0.0110
346	2166.41286	0.0142
347	2166.42443	0.0251
348	2166.43605	0.0232
349	2166.44242	0.0233
350	2166.44754	0.0299
351	2166.45556	0.0207
352	2166.46242	0.1243
353	2166.49346	0.0122
354	2166.49889	0.0259

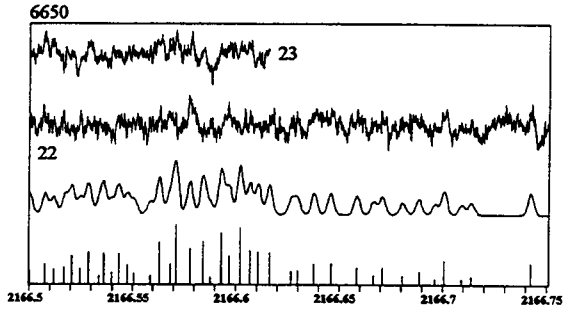

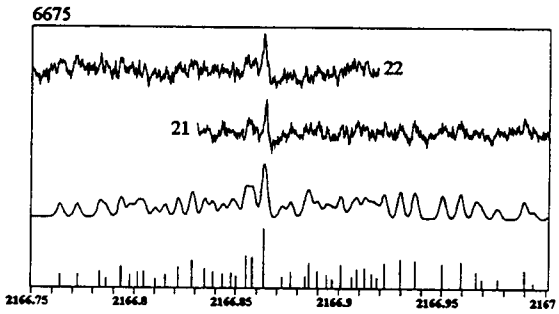

Index	6650 ω	Abs
355	2166.50023	0.0116
356	2166.50765 (37)	0.0202
357	2166.51175	0.0199
358	2166.51718 (69)	0.0190
359	2166.52039	0.0316
360	2166.52454	0.0127
361	2166.52853 (43)	0.0331
362	2166.53375 (6)	0.0113
363	2166.53588	0.0337
364	2166.53981	0.0167
365	2166.54312 (132)	0.0304
366	2166.54734	0.0236
367	2166.55071 (94)	0.0132
368	2166.55871 (63)	0.0118
369	2166.56307 (25)	0.0402
370	2166.56818	0.0153
371	2166.57098	0.0611
372	2166.57785 (105)	0.0345
373	2166.58418	0.0450
374	2166.58762	0.0082
375	2166.59302	0.0533
376	2166.59666 (28)	0.0274
377	2166.60217	0.0586
378	2166.60662 (8)	0.0332
379	2166.61074	0.0357
380	2166.61619 (67)	0.0318
381	2166.62673	0.0113
382	2166.62965	0.0118
383	2166.63778	0.0155
384	2166.64581	0.0157
385	2166.65839	0.0137
386	2166.66685	0.0095
387	2166.67097	0.0133
388	2166.68065	0.0087
389	2166.68840	0.0115
390	2166.69620	0.0075
391	2166.70074	0.0173
392	2166.70928	0.0073
393	2166.71377	0.0086
394	2166.74242	0.0160

Index	6675 ω	Abs
395	2166.76361	0.0101
396	2166.77212	0.0102
397	2166.78347	0.0119
398	2166.78636	0.0078
399	2166.79360	0.0153
400	2166.79814	0.0097
401	2166.80185	0.0117
402	2166.80473	0.0119
403	2166.81024	0.0071
404	2166.81529	0.0099
405	2166.82187	0.0150
406	2166.82871	0.0200
407	2166.83470 (86)	0.0141
408	2166.83851	0.0122
409	2166.84351 (47)	0.0104
410	2166.84772	0.0115
411	2166.85007	0.0092
412	2166.85493	0.0230
413	2166.85805 (77)	0.0217
414	2166.86376 (43)	0.0415
415	2166.87256 (14)	0.0086
416	2166.87666 (40)	0.0118
417	2166.88344 (13)	0.0090
418	2166.88573	0.0175
419	2166.88968 (39)	0.0124
420	2166.89397 (10)	0.0098
421	2166.89705	0.0074
422	2166.90088	0.0162
423	2166.90602 (43)	0.0086
424	2166.90877 (46)	0.0135
425	2166.91264 (30)	0.0143
426	2166.91585	0.0107
427	2166.91835	0.0081
428	2166.92223	0.0178
429	2166.92989	0.0201
430	2166.93705	0.0192
431	2166.95037	0.0173
432	2166.95891	0.0183
433	2166.96620	0.0117
434	2166.96889	0.0068
435	2166.97653	0.0074
436	2166.98957	0.0129
437	2166.99384	0.0050

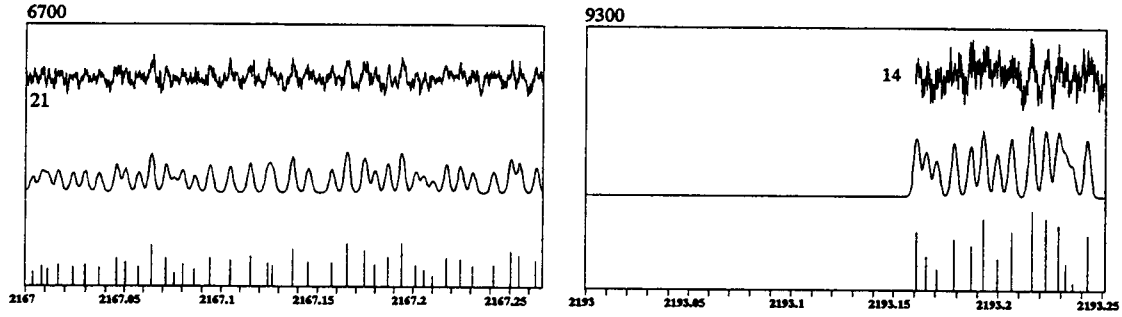

475 2167.26352 0.0142

Index	6700 ω	Abs
438	2167.00334	0.0083
439	2167.00814	0.0109
440	2167.01133	0.0093
441	2167.01643	0.0117
442	2167.02364	0.0104
443	2167.02963	0.0115
444	2167.03685	0.0105
445	2167.04586	0.0150
446	2167.05048	0.0128
447	2167.05755	0.0108
448	2167.06416	0.0213
449	2167.07168	0.0150
450	2167.07595	0.0077
451	2167.08001	0.0119
452	2167.08649	0.0093
453	2167.09430	0.0148
454	2167.10466	0.0142
455	2167.11524	0.0161
456	2167.12417	0.0125
457	2167.12681	0.0111
458	2167.13685	0.0196
459	2167.14520	0.0131
460	2167.15738	0.0127
461	2167.16523	0.0226
462	2167.17421	0.0191
463	2167.17961	0.0121
464	2167.18645	0.0159
465	2167.19392	0.0221
466	2167.20110	0.0115
467	2167.20535	0.0092
468	2167.21012	0.0066
469	2167.21728	0.0155
470	2167.22456	0.0146
471	2167.23093	0.0112
472	2167.24135	0.0116
473	2167.25020	0.0186
474	2167.25473	0.0167

Index	9300 ω	Abs
476	2193.16100	0.0294
477	2193.16563	0.0219
478	2193.17052	0.0177
479	2193.17881	0.0270
480	2193.18685	0.0251
481	2193.19295	0.0336
482	2193.19968	0.0213
483	2193.20648	0.0295
484	2193.21606	0.0361
485	2193.22288	0.0336
486	2193.22874	0.0315
487	2193.23221	0.0195
488	2193.23569	0.0137
489	2193.24278	0.0286

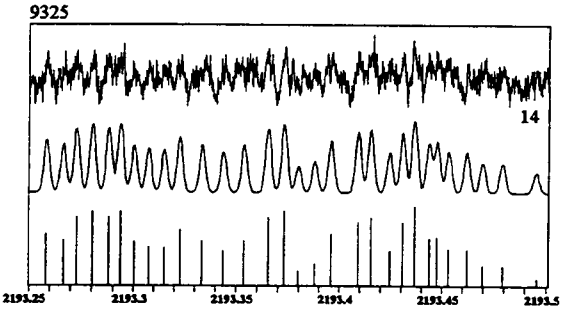

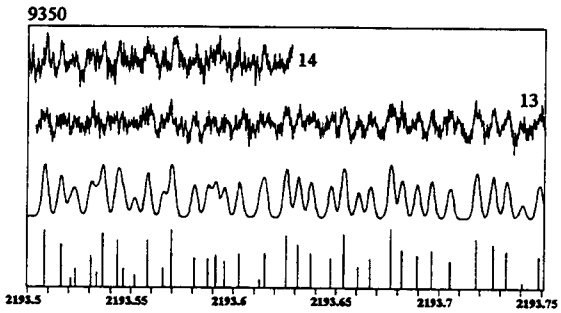

	9325			9350	
Index	ω	Abs	Index	ω	Abs
490	2193.25831	0.0211	520	2193.50824 (75)	0.0269
491	2193.26646	0.0191	521	2193.51622 (12)	0.0213
492	2193.27267	0.0258	522	2193.52085	0.0073
493	2193.28016	0.0276	523	2193.52311 (7)	0.0126
494	2193.28797	0.0259	524	2193.53050 (61)	0.0172
495	2193.29367	0.0276	525	2193.53342	0.0093
496	2193.30033	0.0188	526	2193.53633	0.0219
497	2193.30737	0.0175	527	2193.54350	0.0197
498	2193.31483	0.0171	528	2193.54610	0.0104
499	2193.32255	0.0223	529	2193.55187	0.0084
500	2193.33350	0.0190	530	2193.55820 (19)	0.0231
501	2193.34383	0.0162	531	2193.56574	0.0107
502	2193.35369	0.0190	532	2193.56986 (127)	0.0269
503	2193.36544	0.0258	533	2193.58084 (20)	0.0170
504	2193.37293	0.0278	534	2193.58742 (63)	0.0162
505	2193.37992	0.0104	535	2193.59107 (113)	0.0174
506	2193.38792	0.0124	536	2193.59536	0.0173
507	2193.39601	0.0210	537	2193.60276 (119)	0.0183
508	2193.40912	0.0244	538	2193.61289	0.0092
509	2193.41534	0.0257	539	2193.61497 (72)	0.0180
510	2193.42442	0.0163	540	2193.62574	0.0288
511	2193.43055	0.0244	541	2193.63149	0.0246
512	2193.43645	0.0291	542	2193.63764	0.0209
513	2193.44369	0.0196	543	2193.64744	0.0187
514	2193.44774	0.0201	544	2193.65375	0.0297
515	2193.45329	0.0168	545	2193.66090	0.0149
516	2193.46223	0.0166	546	2193.66678	0.0187
517	2193.46982	0.0118	547	2193.67661	0.0322
518	2193.47935	0.0117	548	2193.68194	0.0227
519	2193.49530	0.0082	549	2193.68920	0.0203
			550	2193.69621	0.0223
			551	2193.70524	0.0176
			552	2193.71830	0.0275
			553	2193.72638	0.0251
			554	2193.73297	0.0223
			555	2193.74037	0.0083
			556	2193.74873	0.0204

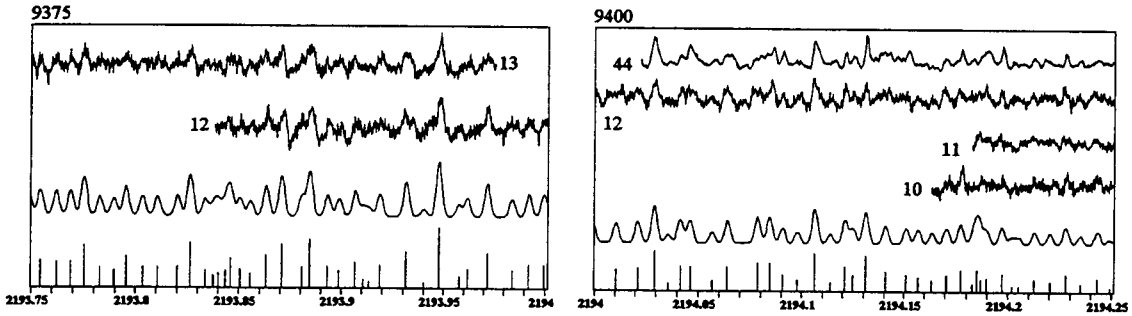

Index	9375 ω	Abs	Index	9400 ω	Abs
557	2193.75435	0.0208	594	2194.01045	0.0225
558	2193.76206	0.0199	595	2194.02093	0.0238
559	2193.76881	0.0200	596	2194.02908 (3)	0.0529
560	2193.77521	0.0316	597	2194.03560	0.0095
561	2193.78262	0.0157	598	2194.04156	0.0266
562	2193.78956	0.0136	599	2194.04624 (5)	0.0311
563	2193.79552	0.0237	600	2194.05667 (86)	0.0145
564	2193.80353	0.0157	601	2194.06392 (36)	0.0301
565	2193.81045	0.0156	602	2194.07825	0.0296
566	2193.82009	0.0163	603	2194.08432 (81)	0.0343
567	2193.82622	0.0339	604	2194.09067 (27)	0.0216
568	2193.83355	0.0139	605	2194.09795 (46)	0.0144
569	2193.83742	0.0099	606	2194.10650 (20)	0.0489
570	2193.83988	0.0119	607	2194.11408 (12)	0.0126
571	2193.84333	0.0149	608	2194.12114 (19)	0.0308
572	2193.84566	0.0223	609	2194.12508 (12)	0.0208
573	2193.85032 (45)	0.0152	610	2194.13114 (26)	0.0464
574	2193.85553 (45)	0.0124	611	2194.14057 (30)	0.0256
575	2193.86313 (49)	0.0257	612	2194.15093 (107)	0.0225
576	2193.87070 (48)	0.0334	613	2194.15668	0.0157
577	2193.88067	0.0174	614	2194.16354	0.0132
578	2193.88453 (54)	0.0378	615	2194.17036 (100)	0.0210
579	2193.89322 (66)	0.0174	616	2194.17729 (70)	0.0292
580	2193.89896 (88)	0.0144	617	2194.18283	0.0143
581	2193.90665 (72)	0.0207	618	2194.18518	0.0233
582	2193.91063	0.0075	619	2194.18665 (96)	0.0188
583	2193.91362	0.0061	620	2194.18968 (34)	0.0204
584	2193.91867 (53)	0.0183	621	2194.19691 (75)	0.0260
585	2193.93155 (14)	0.0286	622	2194.20158 (161)	0.0101
586	2193.94028	0.0058	623	2194.20503 (121)	0.0090
587	2193.94771 (10)	0.0467	624	2194.21257 (97)	0.0178
588	2193.95753	0.0101	625	2194.22026 (187)	0.0149
589	2193.96178	0.0150	626	2194.22787 (55)	0.0243
590	2193.97156 (3)	0.0274	627	2194.23477 (129)	0.0126
591	2193.98382	0.0152	628	2194.24311 (40)	0.0181
592	2193.99214	0.0197	629	2194.24893	0.0084
593	2193.99955	0.0195			

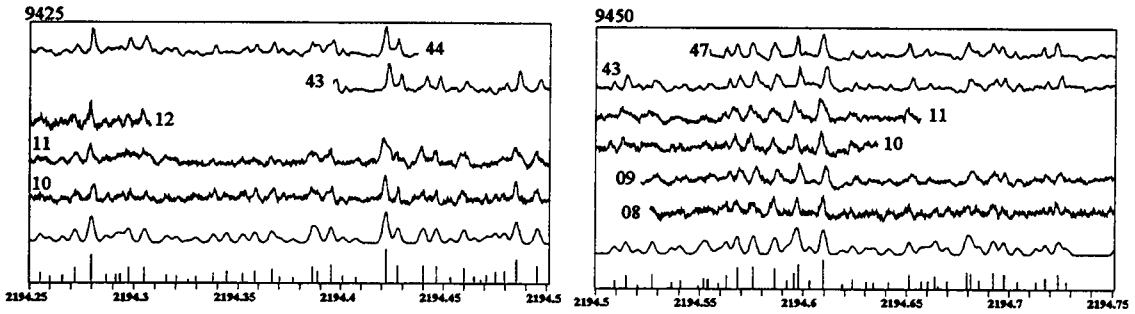

Index	9425 ω	Abs
630	2194.25519 (35)	0.0175
631	2194.25950	0.0110
632	2194.26587 (97)	0.0122
633	2194.27182 (97)	0.0265
634	2194.27953 (76)	0.0573
635	2194.28680 (83)	0.0151
636	2194.29132 (26)	0.0137
637	2194.29373 (2)	0.0181
638	2194.29746 (100)	0.0303
639	2194.30520 (87)	0.0297
640	2194.31578 (57)	0.0154
641	2194.32022 (95)	0.0129
642	2194.32583	0.0056
643	2194.32949 (0)	0.0111
644	2194.33790 (65)	0.0195
645	2194.34424	0.0210
646	2194.35241 (77)	0.0194
647	2194.35808 (60)	0.0239
648	2194.36646 (56)	0.0273
649	2194.37032 (83)	0.0111
650	2194.37662	0.0099
651	2194.38612 (44)	0.0343
652	2194.38869	0.0256
653	2194.39506 (139)	0.0381
654	2194.40096 (112)	0.0129
655	2194.40726 (105)	0.0106
656	2194.42186 (100)	0.0788
657	2194.42782 (91)	0.0372
658	2194.44002 (146)	0.0363
659	2194.44653 (151)	0.0361
660	2194.45361 (101)	0.0102
661	2194.45995 (119)	0.0325
662	2194.46482	0.0111
663	2194.46831	0.0046
664	2194.47126 (71)	0.0162
665	2194.47500	0.0231
666	2194.47952 (63)	0.0250
667	2194.48511 (135)	0.0521
668	2194.49535 (111)	0.0364

Index	9450 ω	Abs
669	2194.50893	0.0204
670	2194.51459 (141)	0.0306
671	2194.52015	0.0104
672	2194.52734 (134)	0.0282
673	2194.53671 (141)	0.0144
674	2194.54068 (115)	0.0177
675	2194.54948	0.0091
676	2194.55184 (52)	0.0235
677	2194.55393 (93)	0.0190
678	2194.55904	0.0135
679	2194.56277 (110)	0.0283
680	2194.56777 (121)	0.0434
681	2194.57558 (121)	0.0445
682	2194.58617 (113)	0.0412
683	2194.59213 (45)	0.0173
684	2194.59549	0.0363
685	2194.59731 (87)	0.0492
686	2194.60295 (175)	0.0150
687	2194.60956 (109)	0.0619
688	2194.61883 (86)	0.0090
689	2194.62412 (107)	0.0206
690	2194.63071 (90)	0.0177
691	2194.63435 (127)	0.0144
692	2194.64168 (44)	0.0128
693	2194.65145 (95)	0.0305
694	2194.65711	0.0129
695	2194.66030 (128)	0.0177
696	2194.66394	0.0213
697	2194.66524 (3)	0.0096
698	2194.66946 (69)	0.0137
699	2194.67932	0.0267
700	2194.68136 (114)	0.0324
701	2194.68534	0.0153
702	2194.69223 (59)	0.0320
703	2194.69732 (74)	0.0288
704	2194.70406 (110)	0.0162
705	2194.71316 (45)	0.0134
706	2194.71741 (115)	0.0227
707	2194.72385 (98)	0.0311
708	2194.72789	0.0125

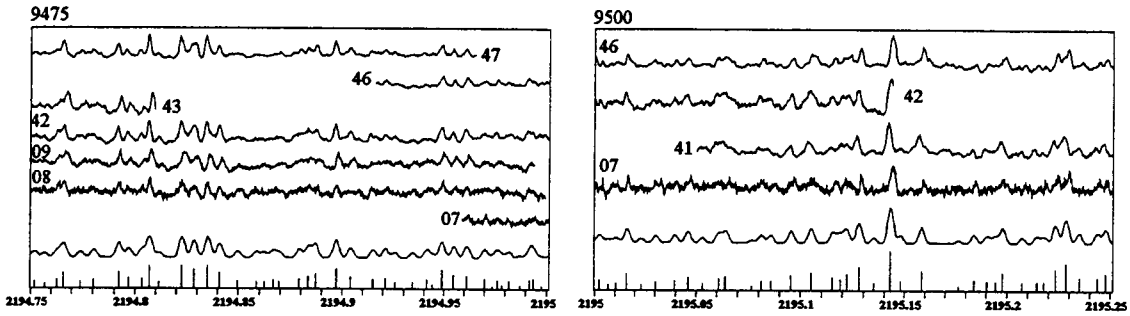

Index	9475 ω	Abs
709	2194.75170 (2)	0.0234
710	2194.75666 (77)	0.0127
711	2194.76276	0.0233
712	2194.76593 (124)	0.0413
713	2194.77383 (139)	0.0191
714	2194.78020 (106)	0.0224
715	2194.79219 (81)	0.0451
716	2194.79716 (97)	0.0273
717	2194.80340 (92)	0.0262
718	2194.80724 (76)	0.0651
719	2194.81186 (104)	0.0146
720	2194.82281 (93)	0.0619
721	2194.82863 (87)	0.0521
722	2194.83512 (89)	0.0648
723	2194.84070 (87)	0.0423
724	2194.84928 (116)	0.0167
725	2194.85847 (66)	0.0135
726	2194.86210	0.0111
727	2194.86651 (31)	0.0195
728	2194.86955 (85)	0.0139
729	2194.87927 (5)	0.0329
730	2194.88351 (39)	0.0312
731	2194.88698 (20)	0.0508
732	2194.89686 (82)	0.0545
733	2194.90402 (80)	0.0289
734	2194.91510 (98)	0.0255
735	2194.92126 (64)	0.0271
736	2194.92582 (54)	0.0200
737	2194.93446 (54)	0.0133
738	2194.94137 (132)	0.0214
739	2194.94399 (23)	0.0111
740	2194.94908 (70)	0.0498
741	2194.95491 (86)	0.0350
742	2194.96116 (70)	0.0344
743	2194.96987 (49)	0.0246
744	2194.97383 (12)	0.0049
745	2194.97599 (44)	0.0228
746	2194.97822	0.0092
747	2194.98177 (87)	0.0196
748	2194.98704 (70)	0.0067
749	2194.99176 (76)	0.0210
750	2194.99359 (63)	0.0276
751	2194.99747 (29)	0.0069

Index	9500 ω	Abs
752	2195.00244 (15)	0.0214
753	2195.00675	0.0104
754	2195.01060 (44)	0.0109
755	2195.01598 (63)	0.0316
756	2195.02271	0.0067
757	2195.03009 (69)	0.0156
758	2195.03957 (42)	0.0180
759	2195.04578 (97)	0.0254
760	2195.05301 (120)	0.0116
761	2195.06086 (135)	0.0203
762	2195.06431 (168)	0.0279
763	2195.07637	0.0066
764	2195.08095 (94)	0.0176
765	2195.08566 (178)	0.0178
766	2195.09580 (83)	0.0296
767	2195.10514 (87)	0.0365
768	2195.11552 (119)	0.0247
769	2195.11888	0.0217
770	2195.12214 (65)	0.0327
771	2195.12800 (101)	0.0483
772	2195.13495 (50)	0.0135
773	2195.14315 (86)	0.0872
774	2195.14783	0.0183
775	2195.15832 (135)	0.0369
776	2195.17616 (82)	0.0058
777	2195.18397 (88)	0.0176
778	2195.19051 (7)	0.0183
779	2195.19436	0.0185
780	2195.19793 (106)	0.0335
781	2195.20721 (175)	0.0126
782	2195.21437 (135)	0.0164
783	2195.21792 (98)	0.0143
784	2195.22348 (122)	0.0398
785	2195.22845 (126)	0.0522
786	2195.23487 (83)	0.0271
787	2195.24363 (122)	0.0229
788	2195.24772 (102)	0.0307

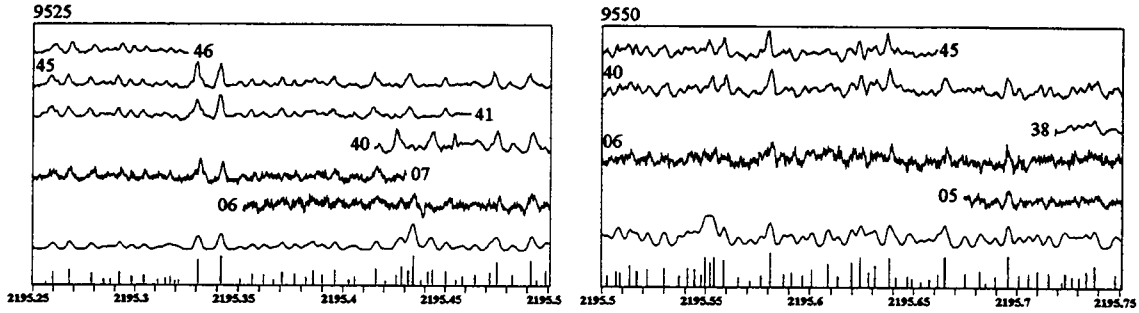

	9525	
Index	ω	Abs
789	2195.25616	0.0054
790	2195.25944 (87)	0.0310
791	2195.26786 (78)	0.0377
792	2195.27862 (116)	0.0275
793	2195.28443 (129)	0.0141
794	2195.28809 (112)	0.0134
795	2195.29254 (115)	0.0326
796	2195.29822 (84)	0.0202
797	2195.30444 (92)	0.0224
798	2195.31123 (85)	0.0108
799	2195.31491 (14)	0.0160
800	2195.31736 (1)	0.0176
801	2195.31983 (0)	0.0086
802	2195.32162	0.0107
803	2195.33082 (96)	0.0615
804	2195.34161 (82)	0.0717
805	2195.35076 (125)	0.0125
806	2195.35659 (89)	0.0212
807	2195.36263 (122)	0.0185
808	2195.36709	0.0127
809	2195.37120 (95)	0.0250
810	2195.37728 (97)	0.0197
811	2195.38242 (2)	0.0193
812	2195.38556 (59)	0.0266
813	2195.39024 (90)	0.0173
814	2195.39608 (154)	0.0279
815	2195.40290	0.0118
816	2195.40582 (30)	0.0138
817	2195.41611 (124)	0.0324
818	2195.42072 (18)	0.0076
819	2195.42592 (63)	0.0210
820	2195.42817	0.0240
821	2195.43198 (7)	0.0385
822	2195.43443	0.0393
823	2195.43804 (65)	0.0106
824	2195.44156	0.0170
825	2195.44354 (10)	0.0343
826	2195.45032 (105)	0.0291
827	2195.45537	0.0115
828	2195.45841 (96)	0.0133
829	2195.46471 (101)	0.0189
830	2195.47183	0.0166
831	2195.47514 (140)	0.0477
832	2195.48286 (167)	0.0200
833	2195.49186 (109)	0.0487
834	2195.49455	0.0126
835	2195.49897	0.0188

	9550	
Index	ω	Abs
836	2195.50259 (70)	0.0248
837	2195.50676	0.0334
838	2195.50889 (51)	0.0288
839	2195.51331 (79)	0.0337
840	2195.51676 (73)	0.0313
841	2195.52198 (86)	0.0285
842	2195.52989 (85)	0.0309
843	2195.53704 (95)	0.0207
844	2195.54109 (133)	0.0290
845	2195.54438 (112)	0.0288
846	2195.54750	0.0288
847	2195.54980	0.0287
848	2195.55190 (32)	0.0467
849	2195.55431	0.0287
850	2195.55893 (73)	0.0428
851	2195.56579 (88)	0.0192
852	2195.57123	0.0180
853	2195.57631	0.0275
854	2195.58090 (105)	0.0548
855	2195.58733 (58)	0.0226
856	2195.59109 (114)	0.0222
857	2195.59646 (58)	0.0248
858	2195.60093 (103)	0.0265
859	2195.60856 (38)	0.0329
860	2195.61324 (97)	0.0196
861	2195.61988 (116)	0.0353
862	2195.62433 (90)	0.0460
863	2195.62808 (64)	0.0300
864	2195.63144 (37)	0.0326
865	2195.63814 (116)	0.0471
866	2195.64138	0.0250
867	2195.64688	0.0264
868	2195.64907	0.0114
869	2195.65350	0.0174
870	2195.65743 (73)	0.0162
871	2195.66150	0.0309
872	2195.66516 (36)	0.0400
873	2195.67461 (66)	0.0265
874	2195.68188 (45)	0.0337
875	2195.68485	0.0071
876	2195.68913 (36)	0.0258
877	2195.69547 (40)	0.0493
878	2195.70093 (50)	0.0232
879	2195.70564	0.0323
880	2195.70986 (175)	0.0290
881	2195.71563 (123)	0.0250
882	2195.72211	0.0087
883	2195.72388	0.0327
884	2195.72721 (94)	0.0217
885	2195.73053 (21)	0.0248
886	2195.73378 (96)	0.0343
887	2195.73799 (99)	0.0387
888	2195.74796 (80)	0.0252

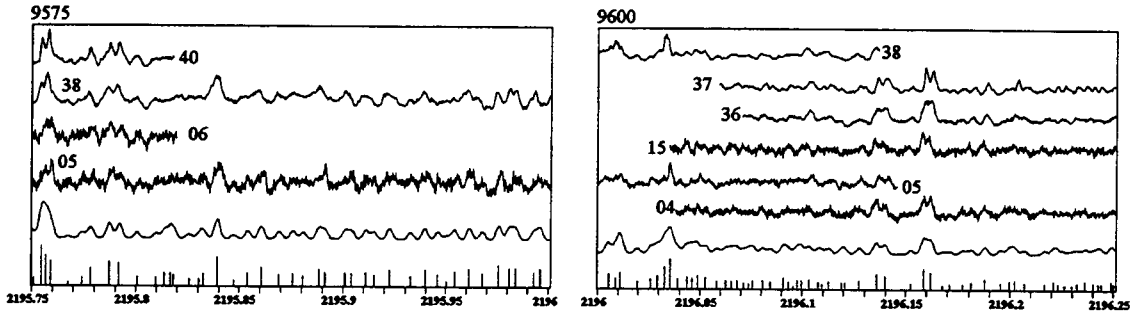

Index	9575 ω	Abs
889	2195.75066	0.0067
890	2195.75476	0.0598
891	2195.75695 (71)	0.0513
892	2195.75914 (104)	0.0307
893	2195.76742 (71)	0.0064
894	2195.77397 (72)	0.0146
895	2195.77807 (103)	0.0245
896	2195.78717 (91)	0.0332
897	2195.79207 (86)	0.0319
898	2195.80064 (102)	0.0125
899	2195.80989 (119)	0.0114
900	2195.81392	0.0107
901	2195.81664	0.0111
902	2195.81825 (74)	0.0139
903	2195.82537 (48)	0.0129
904	2195.83033	0.0138
905	2195.83255	0.0217
906	2195.83914 (73)	0.0558
907	2195.84707	0.0110
908	2195.85397	0.0224
909	2195.86060	0.0337
910	2195.86910 (80)	0.0215
911	2195.87568 (3)	0.0225
912	2195.88069	0.0180
913	2195.88827 (54)	0.0306
914	2195.89108	0.0243
915	2195.90086 (0)	0.0247
916	2195.90417	0.0221
917	2195.91086 (37)	0.0252
918	2195.91478	0.0195
919	2195.92248 (80)	0.0293
920	2195.93266 (59)	0.0187
921	2195.93962 (81)	0.0314
922	2195.94600	0.0203
923	2195.95040	0.0110
924	2195.95415	0.0263
925	2195.96109 (72)	0.0322
926	2195.96760	0.0225
927	2195.97548 (78)	0.0384
928	2195.98079	0.0360
929	2195.98400 (2)	0.0335
930	2195.99282	0.0281
931	2195.99598	0.0324

Index	9600 ω	Abs
932	2196.00510 (96)	0.0385
933	2196.00870	0.0287
934	2196.01092	0.0427
935	2196.01116	0.0213
936	2196.01940 (81)	0.0167
937	2196.02591 (85)	0.0249
938	2196.02902	0.0353
939	2196.03258 (58)	0.0647
940	2196.03534	0.0863
941	2196.03894 (91)	0.0253
942	2196.04328 (72)	0.0249
943	2196.04592	0.0257
944	2196.04863 (108)	0.0314
945	2196.05238 (122)	0.0251
946	2196.05801 (16)	0.0145
947	2196.06252	0.0157
948	2196.06551 (45)	0.0143
949	2196.06779 (48)	0.0203
950	2196.07118 (59)	0.0118
951	2196.07367 (85)	0.0108
952	2196.07572 (81)	0.0199
953	2196.08063 (85)	0.0190
954	2196.08454 (74)	0.0149
955	2196.09054	0.0275
956	2196.09311 (81)	0.0146
957	2196.09535	0.0076
958	2196.09762 (55)	0.0204
959	2196.09963	0.0151
960	2196.10321 (104)	0.0263
961	2196.10755	0.0110
962	2196.10974	0.0123
963	2196.11286 (64)	0.0176
964	2196.11901	0.0141
965	2196.12069	0.0147
966	2196.12752 (94)	0.0193
967	2196.13552 (80)	0.0401
968	2196.13967 (113)	0.0334
969	2196.15235 (103)	0.0125
970	2196.15851 (70)	0.0551
971	2196.16162 (85)	0.0485
972	2196.16725	0.0061
973	2196.17068	0.0074
974	2196.17691 (37)	0.0113
975	2196.18103 (129)	0.0150
976	2196.18770 (111)	0.0243
977	2196.19530	0.0104
978	2196.19979	0.0192
979	2196.20226 (127)	0.0247
980	2196.20671 (69)	0.0137
981	2196.21658 (157)	0.0118
982	2196.22092	0.0153
983	2196.22312 (46)	0.0147
984	2196.22599 (62)	0.0128
985	2196.22949	0.0064
986	2196.23210 (46)	0.0154
987	2196.23602 (73)	0.0195
988	2196.23974 (49)	0.0152
989	2196.24241 (40)	0.0094
990	2196.24389 (0)	0.0135
991	2196.24850 (82)	0.0147

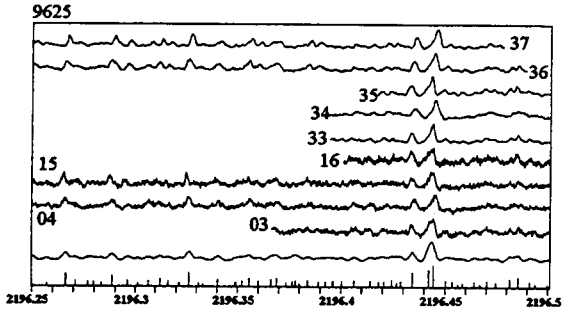

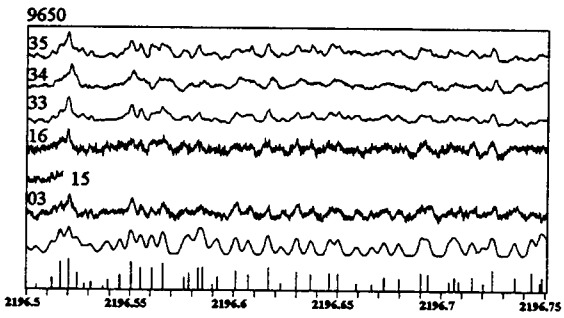

Index	9625 ω	Abs
992	2196.25005	0.0109
993	2196.25714 (52)	0.0098
994	2196.26614 (102)	0.0436
995	2196.27065 (94)	0.0174
996	2196.27683	0.0118
997	2196.27966	0.0098
998	2196.28337 (55)	0.0128
999	2196.28864 (98)	0.0386
1000	2196.29645 (109)	0.0230
1001	2196.30139	0.0073
1002	2196.30655 (121)	0.0204
1003	2196.31191 (111)	0.0271
1004	2196.31626 (97)	0.0191
1005	2196.32165 (97)	0.0105
1006	2196.32611 (99)	0.0524
1007	2196.33071 (171)	0.0118
1008	2196.33299	0.0055
1009	2196.34022 (86)	0.0249
1010	2196.34911 (76)	0.0124
1011	2196.35201 (52)	0.0156
1012	2196.35558 (56)	0.0287
1013	2196.36002 (123)	0.0205
1014	2196.36607 (124)	0.0217
1015	2196.36880 (102)	0.0277
1016	2196.37359	0.0099
1017	2196.37680	0.0118
1018	2196.37831	0.0179
1019	2196.38023	0.0098
1020	2196.38427 (73)	0.0230
1021	2196.38905 (106)	0.0180
1022	2196.39253	0.0139
1023	2196.39586 (46)	0.0156
1024	2196.40018 (27)	0.0156
1025	2196.40653 (71)	0.0198
1026	2196.41398 (102)	0.0192
1027	2196.41789	0.0114
1028	2196.42057 (105)	0.0189
1029	2196.42425 (20)	0.0203
1030	2196.42681 (61)	0.0155
1031	2196.42868 (72)	0.0155
1032	2196.43442 (92)	0.0507
1033	2196.44212 (36)	0.0653
1034	2196.44402 (95)	0.0788
1035	2196.45032 (115)	0.0265
1036	2196.45373 (28)	0.0188
1037	2196.45608	0.0098
1038	2196.45860 (103)	0.0123
1039	2196.46420 (31)	0.0162
1040	2196.46673	0.0100
1041	2196.47024 (94)	0.0215
1042	2196.47460 (80)	0.0144
1043	2196.48156 (41)	0.0274
1044	2196.48530 (59)	0.0330
1045	2196.49115 (96)	0.0178
1046	2196.49387	0.0072
1047	2196.49972	0.0073

Index	9650 ω	Abs
1048	2196.50475 (25)	0.0107
1049	2196.51188	0.0241
1050	2196.51603	0.0255
1051	2196.52015 (59)	0.0333
1052	2196.52428	0.0126
1053	2196.52775 (62)	0.0151
1054	2196.53101 (14)	0.0100
1055	2196.53679	0.0145
1056	2196.53937 (45)	0.0181
1057	2196.54502 (6)	0.0349
1058	2196.55060 (88)	0.0317
1059	2196.55511 (38)	0.0370
1060	2196.56056 (18)	0.0241
1061	2196.56600 (78)	0.0340
1062	2196.57619 (38)	0.0210
1063	2196.57858	0.0474
1064	2196.58250 (8)	0.0209
1065	2196.58505	0.0195
1066	2196.58955 (56)	0.0121
1067	2196.59215	0.0182
1068	2196.60086 (30)	0.0329
1069	2196.60695 (58)	0.0250
1070	2196.61654 (97)	0.0293
1071	2196.62286 (101)	0.0139
1072	2196.63006 (39)	0.0291
1073	2196.63703 (57)	0.0228
1074	2196.64620 (65)	0.0253
1075	2196.65028 (22)	0.0207
1076	2196.65918 (89)	0.0166
1077	2196.66669 (48)	0.0122
1078	2196.67247 (51)	0.0199
1079	2196.67945 (65)	0.0211
1080	2196.69011 (81)	0.0260
1081	2196.69339 (75)	0.0225
1082	2196.70391 (25)	0.0179
1083	2196.70596 (49)	0.0193
1084	2196.70851 (30)	0.0209
1085	2196.71489 (26)	0.0206
1086	2196.72031	0.0422
1087	2196.72467 (71)	0.0221
1088	2196.73531 (99)	0.0177
1089	2196.74364 (96)	0.0190
1090	2196.74776	0.0200

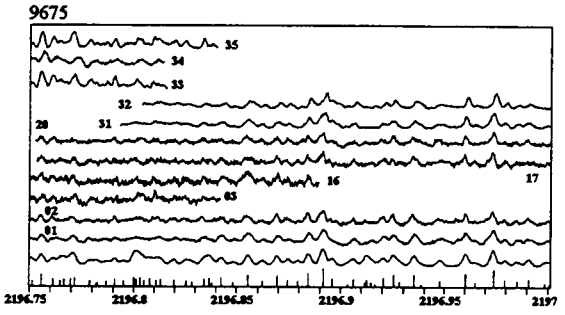

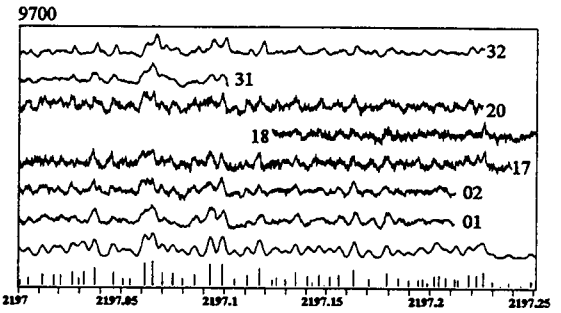

9675

Index	ω	Abs
1091	2196.75116 (36)	0.0189
1092	2196.75564 (50)	0.0447
1093	2196.76097 (79)	0.0271
1094	2196.76472 (12)	0.0190
1095	2196.76645	0.0264
1096	2196.76942	0.0307
1097	2196.77121 (82)	0.0368
1098	2196.77892 (99)	0.0197
1099	2196.78180	0.0082
1100	2196.78257	0.0131
1101	2196.78675 (67)	0.0167
1102	2196.79068 (34)	0.0266
1103	2196.79517 (108)	0.0178
1104	2196.80005	0.0308
1105	2196.80137 (9)	0.0191
1106	2196.80311 (55)	0.0352
1107	2196.80506	0.0265
1108	2196.80783	0.0248
1109	2196.81080 (105)	0.0253
1110	2196.81333	0.0225
1111	2196.81965 (93)	0.0264
1112	2196.82537 (89)	0.0231
1113	2196.82831	0.0135
1114	2196.83417 (85)	0.0303
1115	2196.83684	0.0258
1116	2196.83807	0.0148
1117	2196.84261 (93)	0.0345
1118	2196.84850 (54)	0.0165
1119	2196.85535 (108)	0.0466
1120	2196.86231 (67)	0.0214
1121	2196.86948 (73)	0.0431
1122	2196.87442 (78)	0.0276
1123	2196.87950 (65)	0.0166
1124	2196.88441 (72)	0.0582
1125	2196.89132 (79)	0.0892
1126	2196.89600 (141)	0.0336
1127	2196.90358	0.0122
1128	2196.90626 (81)	0.0324
1129	2196.91159	0.0161
1130	2196.91270	0.0271
1131	2196.91466 (39)	0.0158
1132	2196.91680	0.0118
1133	2196.92050 (70)	0.0395
1134	2196.92521 (66)	0.0534
1135	2196.92829	0.0148
1136	2196.93535 (86)	0.0529
1137	2196.93884	0.0057
1138	2196.94786 (74)	0.0275
1139	2196.96019 (69)	0.0631
1140	2196.96506 (87)	0.0152
1141	2196.97354 (72)	0.0849
1142	2196.97914 (61)	0.0287
1143	2196.98505 (63)	0.0213
1144	2196.99064 (59)	0.0325
1145	2196.99743	0.0178

9700

Index	ω	Abs
1146	2197.00079 (84)	0.0126
1147	2197.00466 (49)	0.0183
1148	2197.01182 (136)	0.0246
1149	2197.01733 (107)	0.0214
1150	2197.02086 (55)	0.0227
1151	2197.02626 (78)	0.0304
1152	2197.02958	0.0128
1153	2197.03197	0.0278
1154	2197.03713 (121)	0.0396
1155	2197.04619 (91)	0.0303
1156	2197.05108 (11)	0.0157
1157	2197.05439 (62)	0.0142
1158	2197.06147 (98)	0.0520
1159	2197.06543 (66)	0.0576
1160	2197.07016 (89)	0.0299
1161	2197.07483 (92)	0.0273
1162	2197.07963	0.0126
1163	2197.08548 (102)	0.0260
1164	2197.09320 (87)	0.0502
1165	2197.09904 (69)	0.0506
1166	2197.10498 (55)	0.0151
1167	2197.11140 (76)	0.0235
1168	2197.11727 (88)	0.0398
1169	2197.12318 (3)	0.0114
1170	2197.12563 (29)	0.0173
1171	2197.12998 (85)	0.0140
1172	2197.13487 (73)	0.0315
1173	2197.14052 (34)	0.0209
1174	2197.14276	0.0093
1175	2197.14643 (74)	0.0255
1176	2197.14902	0.0030
1177	2197.15171 (27)	0.0183
1178	2197.15627 (80)	0.0249
1179	2197.16349 (80)	0.0377
1180	2197.17073 (140)	0.0164
1181	2197.17929 (96)	0.0292
1182	2197.18491 (68)	0.0174
1183	2197.18959 (88)	0.0125
1184	2197.19429	0.0127
1185	2197.19642 (54)	0.0175
1186	2197.19879	0.0084
1187	2197.20224 (34)	0.0220
1188	2197.20443 (39)	0.0256
1189	2197.20775 (71)	0.0186
1190	2197.21193	0.0160
1191	2197.21346 (25)	0.0115
1192	2197.21850 (96)	0.0255
1193	2197.22252 (29)	0.0197
1194	2197.22522 (73)	0.0308
1195	2197.22939 (55)	0.0090
1196	2197.23372	0.0016
1197	2197.23776 (10)	0.0071
1198	2197.24365	0.0021
1199	2197.24870	0.0122

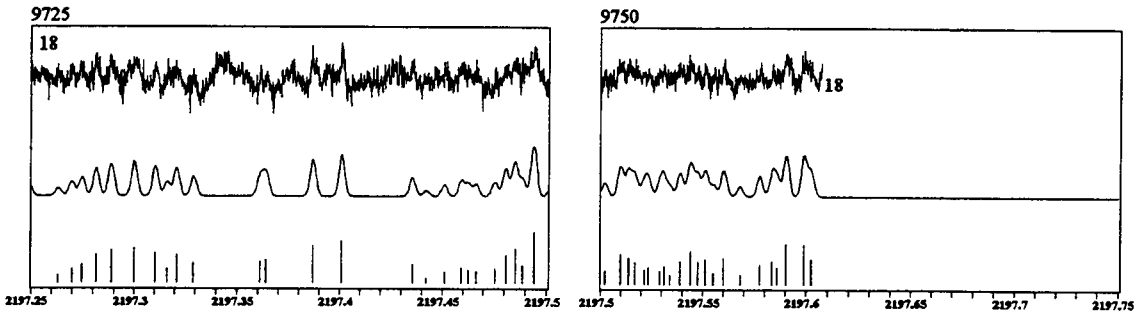

	9725			9750	
Index	ω	Abs	Index	ω	Abs
1200	2197.26329	0.0061	1225	2197.50208	0.0075
1201	2197.26972	0.0111	1226	2197.50969	0.0164
1202	2197.27459	0.0148	1227	2197.51371	0.0144
1203	2197.28152	0.0226	1228	2197.51680	0.0120
1204	2197.28878	0.0259	1229	2197.52116	0.0079
1205	2197.30014	0.0282	1230	2197.52352	0.0094
1206	2197.31030	0.0241	1231	2197.52899	0.0073
1207	2197.31605	0.0114	1232	2197.53098	0.0101
1208	2197.32069	0.0225	1233	2197.53386	0.0054
1209	2197.32903	0.0158	1234	2197.53911	0.0130
1210	2197.36108	0.0167	1235	2197.54384	0.0183
1211	2197.36412	0.0186	1236	2197.54737	0.0124
1212	2197.38688	0.0302	1237	2197.55119	0.0140
1213	2197.40120	0.0338	1238	2197.55518	0.0062
1214	2197.43547	0.0147	1239	2197.56006	0.0145
1215	2197.44204	0.0042	1240	2197.56790	0.0056
1216	2197.45095	0.0090	1241	2197.57731	0.0112
1217	2197.45916	0.0123	1242	2197.58354	0.0127
1218	2197.46258	0.0103	1243	2197.58582	0.0095
1219	2197.46652	0.0096	1244	2197.59045	0.0226
1220	2197.47550	0.0113	1245	2197.59894	0.0221
1221	2197.48072	0.0222	1246	2197.60225	0.0139
1222	2197.48522	0.0277			
1223	2197.48882	0.0137			
1224	2197.49419	0.0413			